Periodic Flow Regenerators for Supercritical CO2 Brayton Cycle

By

Jacob Fenske Hinze

A dissertation submitted in partial fulfillment of

the requirements for the degree of

Doctor of Philosophy

(Mechanical Engineering)

at the

UNIVERSITY OF WISCONSIN-MADISON

2018

Date of final oral examination: 8/13/2018

The dissertation is approved by the following members of the Final Oral Committee

Gregory Nellis, Professor, Mechanical Engineering
Sanford Klien, Professor Emeritus, Mechanical Engineering
Mark Anderson, Professor, Mechanical Engineering
Douglas Reindl, Professor, Engineering Professional Development
Bruce Beihoff, Director, M-WERC Technology Innovation
Franklin Miller, Professor, Mechanical Engineering

Abstract

The supercritical CO_2 Brayton cycle offers many advantages over conventional steam Rankine cycles such at higher efficiency and smaller footprint. One of the challenges of implementing the sCO_2 Brayton cycle is the large amount of recuperation needed, which can result in high heat exchanger costs. This thesis looks at replacing the conventional Printed Circuit Heat Exchanger with a periodic flow regenerator where heat is alternatively stored and released from a packed bed. The packed bed can be made to have a very large specific surface area by using small diameter spheres (1/8”) which leads to high effectiveness. An internally insulated pressure vessel can be used for the regenerator greatly reducing the cost of the system by allowing for low cost steel to be used in the pressure vessel. Regenerators offer the opportunity for drastically reduced costs and high effectiveness. An analytical model of the regenerator system was created that can quickly and accurately determine the performance for a regenerator. A cycle model was created that compares the Levelized Cost of Electricity for a cycle operating with either recuperators or regenerators. A 6.2% reduction in Levelized Cost of Electricity was found to be possible by switching to regenerators as compared to Printed Circuit Heat Exchangers.

Regenerators have not been tested with the combination of high temperature (550°C) and high pressure difference (17MPa) before, to verify the accuracy of the model a 10kW test facility was constructed. The test facility was able to test regenerators at up to 550°C and 3600 psi, similar conditions to a sCO_2 cycle. The facility was set up to measure effectiveness, pressure drop, and carryover for an uninsulated regenerator. In addition, a scaled down version of the insulated regenerator was tested to prove the design of the internally insulated pressure vessel. The measured effectiveness matched well to the model with an average error of 1.8%. Pressure drop was more difficult to measure because of the small pressure drop in the test section, 50% of the pressure drop data was within 20% of the model. Carryover was impossible to measure directly due to the short time it occurs

over. Instead carryover is measured using temperature and pressure data to calculate density of CO_2 in a known volume. Due to the non-linearity of temperature in the regenerator bed it is difficult to model carryover in the bed, however using a physics based correction an average error of 6.5% was achieved. A sand internally insulated regenerator was constructed and tested. One of the liners of the insulated bed developed a small crack near the high temperature end of the bed. It was hypothesized that poor packing of sand allowed the liner to experience excessive strain during pressure cycling. Better support for the liner was proposed to prevent further failures. The regenerator system was found to be a valid replacement for the current state of the art printed circuit heat exchanger and showed advantages in cost.

Acknowledgements

There are many people that have helped me during my time in grad school. First my family for being so supportive of my education, and encouraging me to continue onto my Ph.D. Without your help and support I would not be where I am today.

I also need to thank my advisors Greg Nellis, Mark Anderson, and Sandy Klein who first gave me an opportunity to continue with my PhD studies. My weekly meetings always provided new insight into the project and without you I'm it would have been impossible.

I also want to thank the other students in the SEL for so readily helping on any problems from homework to experimental testing. I truly enjoyed getting to know all of you and hope we will stay in touch.

Contents

List of Figures

List of Tables

Introduction

There has been increased focus on creating power more efficiently and with lower carbon emissions. The ideal efficiency for a power cycle is defined by the Carnot efficiency which is the highest possible efficiency with which a power cycle can convert heat from a high temperature source at T_H to work using T_C as heat sink. The formula is given by [1] in equation (0.1).

$$\eta_C = \frac{T_H - T_C}{T_H} \tag{0.1}$$

Equation 1.1 indicates that larger temperature differences between the high and low temperature heat sources will lead to higher efficiencies. In many cases, the low temperature is essentially set by the wet bulb temperature of the environment so the only way to increase efficiency is to increase the heat source temperature. For many years the energy industry has used coal and natural gas fired steam cycles operating at relatively moderate temperatures (565°C) due to corrosion with current materials at higher temperature that achieve efficiencies on the order of 35-40 percent [2,3]. Recent advances in materials have relaxed this limitation. For example, the ASME Boiler Pressure Vessel Code (BPVC) has certified Inconel 740 which is a nickel alloy with code cases up to almost 800°C [4]. Such advancements have allowed the development of higher temperature steam cycles such as the Ultra SuperCritical (USC) and Advanced Ultra SuperCritical (AUSC) cycles that operate at higher temperatures and pressures than conventional steam cycles. USC and AUSC cycles have efficiencies on the order of 45% and are based on tested and proven steam power plant designs, making them well understood and readily accepted by industry [5]. Rankine cycles are able to reach relatively high thermal efficiencies because they have a very low back work ratio, which is defined in equation (0.2).

$$r_b = \frac{\dot{W}_{comp}}{\dot{W}_{turb}} \tag{0.2}$$

where $\dot{W}_{comp}$ is the compressor (or pump) power in and $\dot{W}_{turb}$ is the turbine power out. The minimum possible specific work for an isentropic compressor can be approximated by equation (0.3) if the compressibility effects are ignored [1].

$$W_{comp} = \Delta P V \tag{0.3}$$

where ΔP is the pressure increase over the compressor, V is the specific volume of the fluid and W_{comp} is the compressor specific work. The pump in a Rankine cycle works with liquid water that has a very low specific volume resulting in a small value for the compressor power (usually only about 3 percent of the turbine power) [6]. However, steam plants face several obstacles that prevent them from achieving efficiency greater than 50 percent. One issue is condensation in the turbine that can lead to blade erosion; care must be taken to ensure the fluid will be single phase throughout the turbine [7]. To obtain higher efficiency, the plant must become larger and more complicated with more feed water heaters and turbine sections needed, increasing costs and complicating operation [8]. Also, steam cycles are generally quite large due to the large pressure ratio that necessitates many stages of turbines in order to efficiently expand the steam [7]. The solution to achieving higher efficiencies is to further increase the temperature at the inlet of the turbine; however this option is not economical in a Rankine cycle due to the corrosiveness of water at high temperatures and the high pressures needed [5]. As a result the upper limit on the efficiency for a steam is cycle about 45% with a turbine inlet around 700°C [9], [5].

With the recent increase in fracking, the cost of natural gas in the United States has dropped drastically leading to many new natural gas combined cycle (NGCC) plants. These NGCC plants use a natural gas-fired open Brayton cycle paired with a Rankine cycle to create power with an overall efficiency of around 60 percent [3,6]. This combined cycle achieves high efficiencies by having a high turbine inlet temperature, in excess of 1200°C [6]. The exhaust of the turbine is at approximately 550°C, which is used to provide heat to a bottoming Rankine cycle [6]. The high heat source temperature is

made possible by cooling the walls of the pressure vessels and the blades in the turbine, which allows the wall temperatures to be lower than the fluid temperatures [6]. Also, the air in the Brayton cycle is much less corrosive than the water in the Rankine cycle. The NGCC cycle configuration has impressive efficiency and it is possible to push the turbine inlet temperature to more than 1500°C with advanced materials [6]. However, at these temperatures, the exhaust gas would be too hot to directly heat a steam Rankine cycle. Gas turbines have a high back work ratio, with about 50% of the energy from the turbine being used to power the compressor. The high back work ratio is a product of the high specific volume of air entering the compressor, however the cycle is still very efficient because it can operate at high temperature.

Open Brayton cycles like the NGCC rely on combustion to obtain their high temperature inlet conditions where the walls and blades can be actively cooled. Reaching the same temperatures with a closed Brayton cycle would be impossible since there are no code-qualified materials available [10]. A heat exchanger in a closed Brayton cycle must operate at a maximum temperature that is less than 800°C so that ASME BVPC materials can be used. Therefore, while air Brayton cycles can work well with high temperature combustion they are generally incompatible with renewable heat sources such as solar, nuclear, or geothermal where the lower heat source temperatures mean lower efficiency.

It is possible to obtain high efficiency closed Brayton cycles by using a supercritical fluid. A fluid is considered supercritical when the temperature and pressure are above the critical temperature and pressure [11]. The critical temperature and pressure are defined as the temperature and pressure at which the first and second derivatives of pressure are zero with respect to volume at constant temperature, this is the location of the critical point [1]. The specific heat of the fluid goes to infinity at the critical point [7].

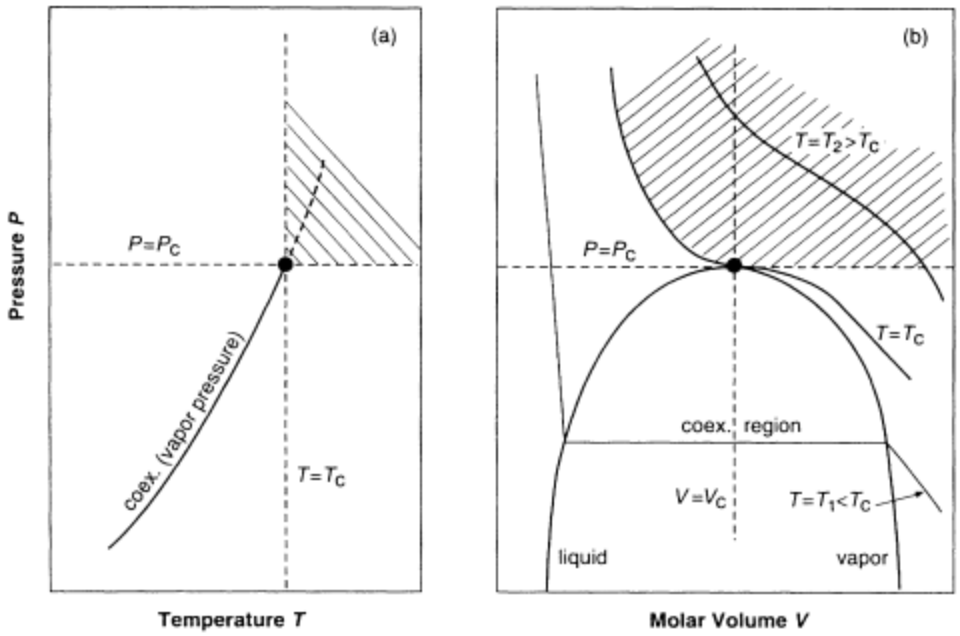

Figure 1 Pressure vs Temperature and Pressure Vs Volume for a generic supercritical fluid. From [11].

Figure 1 shows pressure vs temperature, and pressure vs volume plots of generic fluids, illustrating the critical point. The critical point is located at the very top of the vapor dome. Here, the fluid experiences isothermal heat addition at constant pressure, infinitely large specific heat, just like a fluid boiling in the vapor dome. A fluid is supercritical when both the temperature and pressure are above the supercritical temperatures and pressure [11]. In the supercritical region the fluid has properties between those of liquid and gas; the fluid is usually dense like a liquid but has similar transport properties to a gas [12]. Near the critical point the fluid will exhibit a large change in specific volume with a small change in temperature [12] which means with relatively little cooling the fluid can be made very dense resulting in lower compressor power. Compressor specific work is approximated by equation (0.3) so a more dense fluid means less compressor work. A supercritical Brayton cycle improves on the air Brayton cycle by reducing the back work ratio from 50% to about 35% [7,13,14]. In addition to the large density change near the critical point, there is also a large increase in the specific heat capacity near the critical point as illustrated in Figure 2.

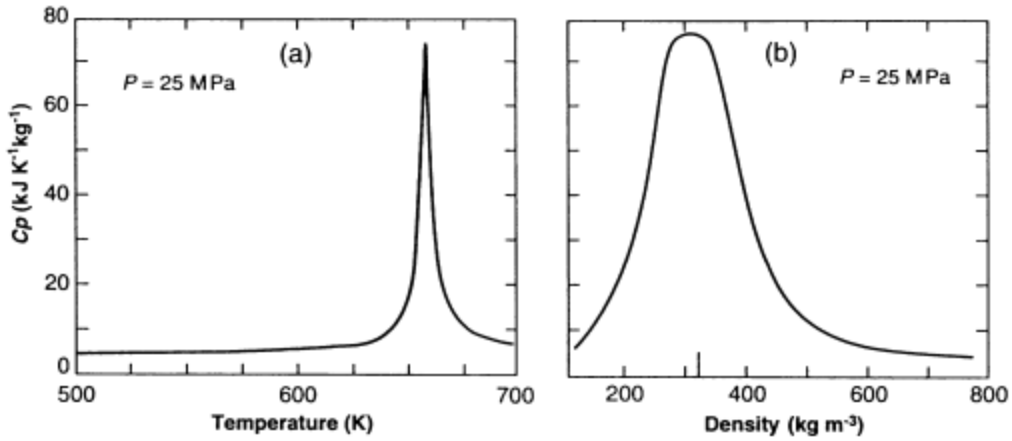

Figure 2 Specific heat capacity vs temperature and density for a generic supercritical fluid. From [11].

The high specific heat capacity without being condensing (isothermal) means that supercritical fluids can avoid the pinch point issues in the feedwater heater as in the Rankine cycle [12]. The net result is that the supercritical Brayton cycle can operate more efficiently than an air Brayton cycle or a steam Rankine cycle.

A supercritical fluid has the potential to operate in a more efficient cycle, however the fluid needs to be chosen carefully to ensure it can be used safely and efficiently. The critical temperature needs to be near the heat rejection temperature of the cycle in order to take advantage of the high density near the critical point [15]. Also, since the cycle needs to operate above the critical pressure, the critical pressure should be low to eliminate the need for expensive pressure containment [15]. The fluid also must be thermally stable at high temperature and not corrode the components or seals [15]. Supercritical water was the initial choice for such cycles, but as mentioned above water is highly corrosive at the high temperatures needed [16]. Ammonia was another option for a supercritical working fluid, however it is toxic and corrosive at high temperature. Carbon dioxide was the obvious choice since it has relatively moderate supercritical conditions (7.37 MPa, and 31 C [17]), as well as being low cost, non-toxic, and non-corrosive [7].

Supercritical CO_2 Cycles

Supercritical carbon dioxide (sCO_2) cycles require high amounts of recuperation in order for them to reach very high efficiencies [7] [8]. The single phase nature of the flow also eliminates any risk of condensation in the turbine which prevents damage to the turbine blades [7]. A lower pressure ratio than a steam cycles means fewer turbine and compressors stages are needed to achieve the desired pressure drop [7,13]. Work has also shown that sCO_2 turbomachinery will be significantly more compact (10 times) than a Rankine cycle [14]. However, in order to be efficient the sCO_2 Brayton cycle requires high effectiveness recuperation and without it, it would be better to use a Rankine cycle [7]. Additionally in order to achieve efficiencies near 50%, more complex cycles must be used similar to those used in large Rankine cycles [18].

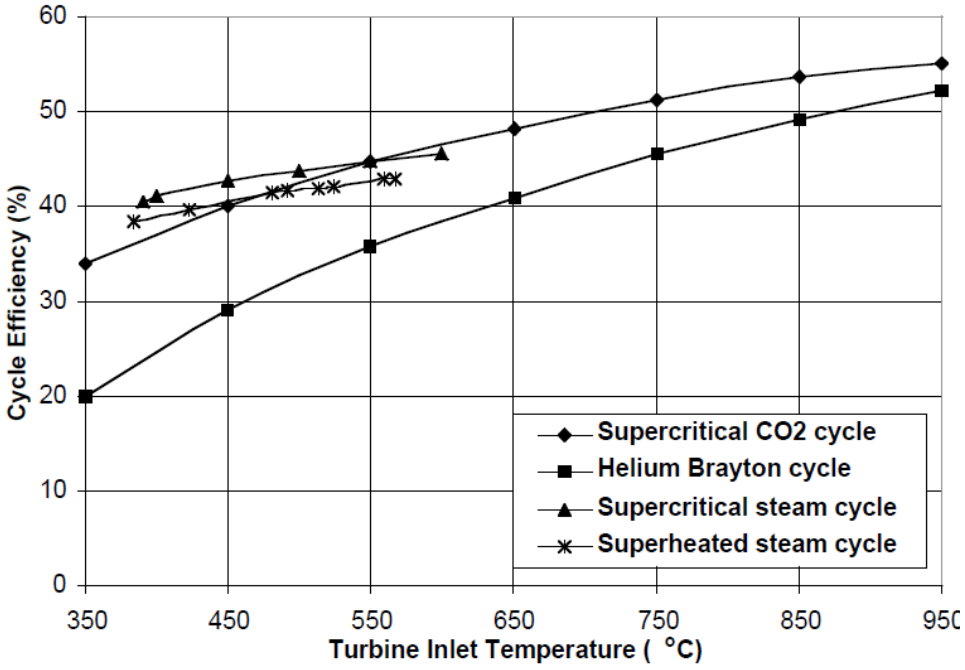

Figure 3 Cycle efficiency vs turbine inlet temperature for various cycle configurations. From [9]

Figure 3 shows the cycle efficiency as a function of the turbine inlet temperature for various cycles. The steam cycles shown limit temperature to about 600°C and an efficiency of 45% but sCO_2 and helium

cycles can go to much higher temperatures. After the turbine inlet temperature increases to greater than 550°C the sCO_2 cycle is more efficient than the steam cycles and continues to increase with increasing turbine inlet temperature. The maximum temperature that a sCO_2 cycle can reach is dependent on the materials of construction. A direct fired sCO_2 cycle could reach turbine inlet temperatures greater than 1100°C, similar to advanced air Brayton cycles [6]. Figure 3 shows why it is desirable to push the turbine inlet temperature as high as possible for sCO_2 cycles.

Supercritical CO_2 cycles are not a new idea and papers were published in the late 1960s that discussed supercritical power cycles. Researchers then were interested in a power conversion cycle that could work with higher temperature nuclear heat sources. One researcher even began design on a 150 kWe test loop, but it was never completed as a production model [15]. There were researchers from the United States, the Soviet Union, and Italy [7], [19], [8,18] who have proposed use of supercritical carbon-dioxide cycles. Most of this work looked at cycle configurations for various heat sources and compared the cycle configurations to each other based on different metrics. Depending on the cycle configuration, the performance can be drastically changed. There are two main types of cycles under consideration today: the simple cycle that uses a single recuperator and the recompression cycle which has two recuperators and two compressors. The simple cycle is the most basic cycle and has the fewest components but also the lowest efficiency, it is shown in Figure 4.

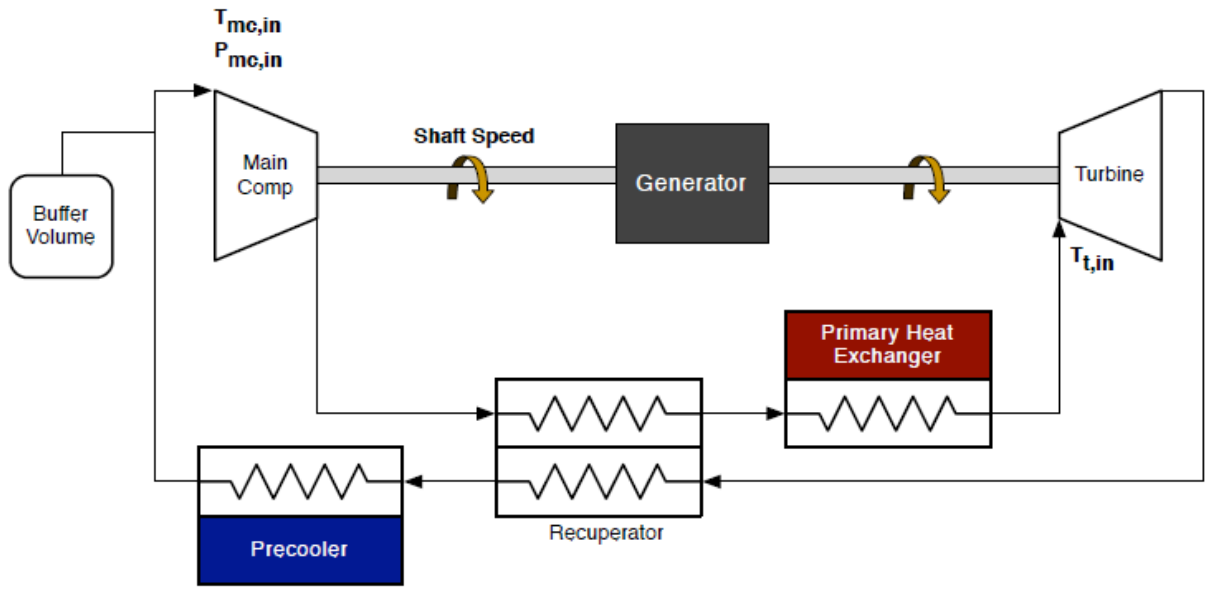

Figure 4 Flow diagram of Simple Closed Brayton Cycle (SCBC) from [20]

The recompression cycle shown in Figure 5 adds an additional recuperator and compressor to the simple sCO_2 cycle. The flow is split after the low temperature recuperator and about 30 percent is sent to the recompressor where it is compressed and rejoins the main flow at the inlet of the high temperature recuperator. The advantage of this cycle configuration is that it balances the capacitance rates for each of the streams in the recuperator. At low temperature the specific heat of the low pressure fluid is higher than the high pressure fluid since it is closer to the critical point. Even for a high effectiveness recuperator in the simple cycle, more heat can be recovered if a recompression cycle is used where the capacitance rates are about the same for both fluids streams (i.e., balanced) in both recuperators [21]. Balanced flows result in more heat being recovered and a higher thermal efficiency.

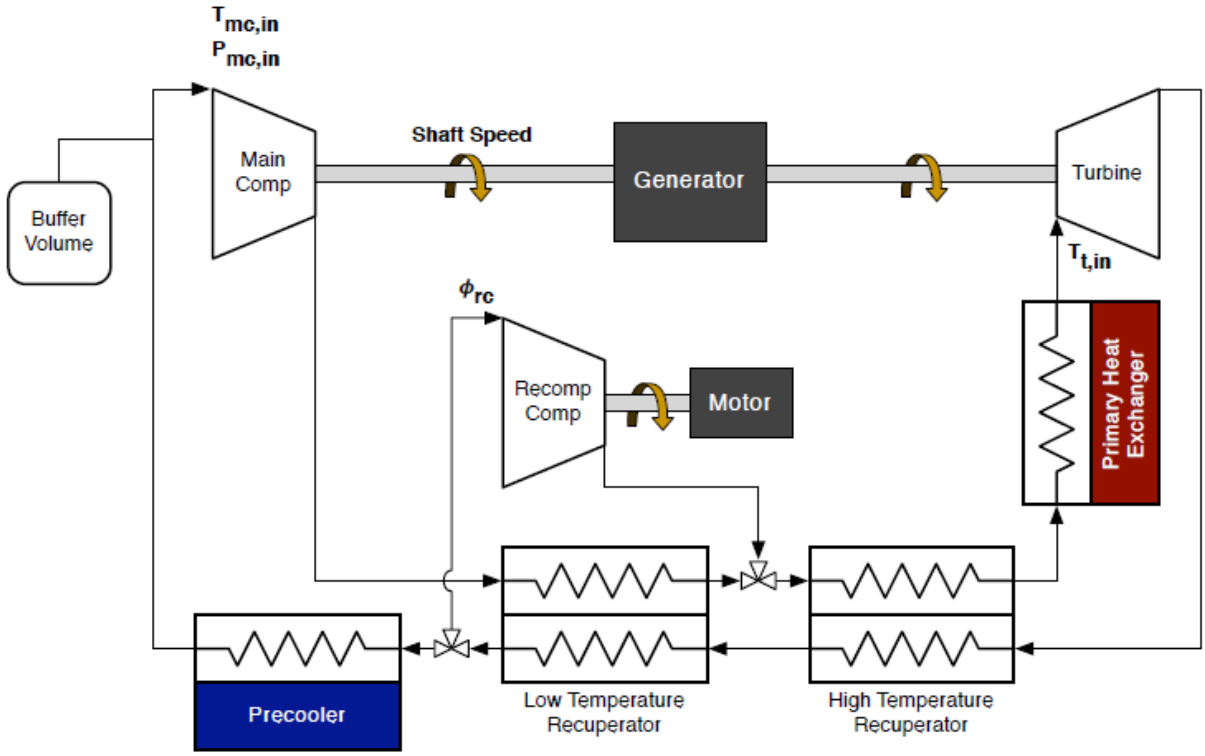

Figure 5 Flow diagram of sCO_2 Recompression Closed Brayton Cycle (RCBC) from [20]

The recompression cycle is being used by the Department of Energy (DOE) in its Supercritical Transformational Electric Program (STEP) initiative which seeks to create a 10 MWe sCO_2 pilot plant in order to test this technology. The DOE has released money to pay for studies into the cost and design of building and testing the test facility. As such, the design goal of this project was set using the STEP facility as a baseline for cycle performance and configuration. Any results obtained will be directly comparable to those from the 10 MWe STEP facility. Because of competition between component suppliers, the cost numbers for the 10MW components have not been released and therefore it will not be possible to compare the regenerator costs to these devices in this thesis.

As in steam plants, performance can be improved by providing reheat to the turbine, and by providing intercooling in the compressor. The reheat in the turbine allows more power to be extracted for a given pressure differential by changing the expansion to be more isothermal than isentropic [6].

Equation (0.3), which has been used to estimate the work extracted from a turbine, shows that a larger specific volume in the turbine will lead to more work extracted. Reheat adds heat to fluid that has been partially expanded and therefore has had its temperature reduced (reducing its specific volume). Reheating increases the specific volume of the working fluid resulting in an increase in the power extracted from the turbine. Likewise, the intercooling in the compressor decreases the specific volume, decreasing the amount of power needed for compression. Both options have the ability to increase the efficiency of the cycle but at the cost of cycle complexity and capital costs. For each stage of reheat or intercooling, a new heat exchanger and turbine/compressor will need to be added. Additionally, the control of the cycle becomes more difficult with more compressors and turbines to control.

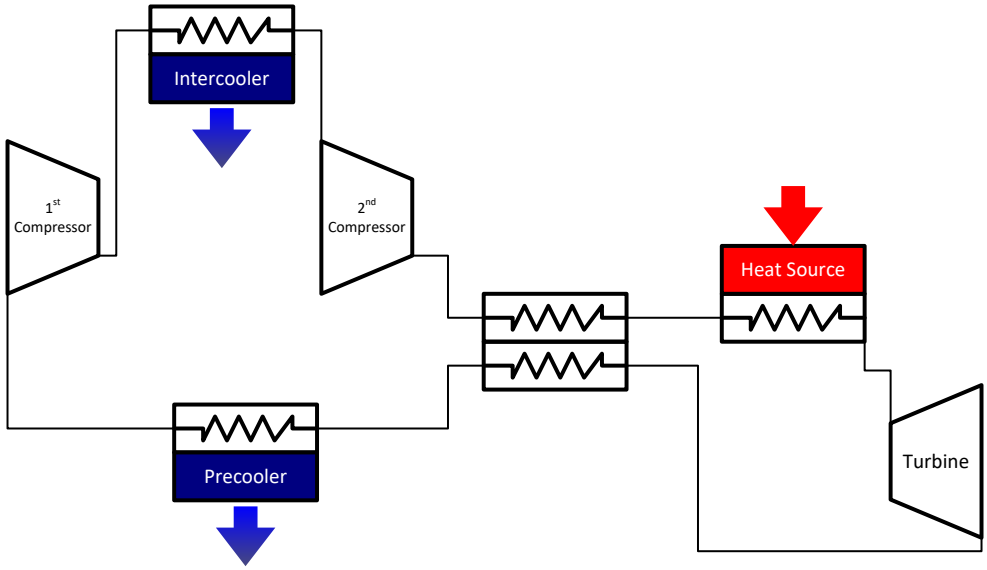

(a)

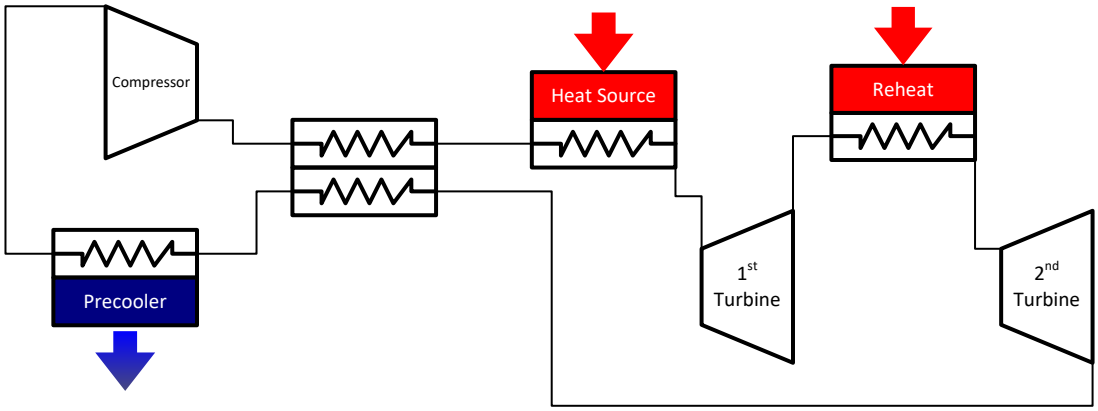

(b)

Figure 6 Flow diagram of SCBC cycles with (a) intercooling and (b) reheat

Novel sCO_2 cycles have been proposed, such as the Allam cycle which seeks to create a direct fired sCO_2 Brayton cycle. This cycle cryogenically separates air into nitrogen and oxygen and uses just

the oxygen to combust with coal or natural gas in the primary heater section of the cycle [22]. The CO_2 plus combustion products are cleaned and the water is separated, and pure CO_2 is fed back through a recuperator. The CO_2 is then cooled and some of the CO_2 is removed to make up for the CO_2 added to the cycle through combustion. This CO_2 can be sold or stored making it carbon neutral. The advantage of this design is that it allows for high turbine inlet temperatures, up to 1000°C, which means the efficiency is quite high: 59% when using natural gas as a fuel and 51% when using coal as a fuel [22]. This cycle is a good option as it allows for on demand power production and stores carbon dioxide much more efficiently than current coal fired Rankine cycles with carbon capture [22].

SCO_2 seems to be a good option for many renewable heat sources in addition to nuclear. Since the desire for new generation nuclear plants is to achieve higher efficiencies (at lower cost), a new power conversion cycle is needed that can reach these higher temperatures. CO_2 has already been used in some nuclear power plants for cooling and the low temperature difference in the primary heat exchangers makes it a good match with a nuclear power source which are designed for a small temperature change, but these designs do not reach the supercritical region [13,15]. A second promising heat source for sCO_2 is from Concentrating Solar Power (CSP). CSP takes energy from the sun and focuses it on a heat exchanger using mirrors. The heat is usually transferred to a molten salt or thermal oil and then to a power conversion cycle. The heat transfer fluid allows thermal energy to be stored allowing the power plant to produce power even when the sun is down or a cloud is passing overhead [23]. It is also possible to use fossil fuel as a heat source. Natural gas is already used in the combined cycle with high efficiency, but it may be possible with newer high temperature gas turbine designs that the turbine exit temperature could increase enough to justify using a sCO_2 Brayton cycle instead of a steam Rankine cycle. Coal can also be used, and at high enough temperature it could also produce energy efficiently although with the consequence of higher carbon emissions.

There have been several studies that have looked at which sCO_2 cycle configuration might be best for a given heat source, and how those cycles compare to traditional Rankine cycles. One study looked at a nuclear power plant with a relatively low temperature heat source of about 300°C. A comparison of SuperCritical Brayton Cycle (SCBC), Recompression Brayton Cycle (RCBC), and RCBC with reheat was conducted and found that the efficiency of the RCBC reheat cycle was similar to that of a Rankine cycle while the mass of components was reduced 40 percent [24]. The authors also pointed out that the simplicity of the cycle would lead to faster assembly times since there are fewer components to connect [24]. A study was also conducted looking at the optimal sCO_2 configuration for CSP applications [14]. It was found that a partial cooling cycle, which adds an additional pre-cooler and compressor to the recompression cycle, would work best at lower levels of recuperation while a RCBC would perform better with larger recuperators [14]. It was also shown that either cycle would offer an improvement over the Rankine cycle in performance [14].

Schroder [25] optimized many different configurations of the sCO_2 cycle for efficiency. A model of a sCO_2 cycle was created with the ability to change the number of recuperators, compressors, and turbines as well as cycle parameters such as pressure, temperature, and recompression fraction. Optimization was conducted with a maximum turbine inlet temperature of 650°C, a minimum compressor inlet temperature of 47°C and a maximum pressure of 30 MPa [25]. It was found that an optimal cycle would have at least three compressors (two stages of main compression and one recompressor), two recuperators, and two turbines with reheat [25]. The result is a cycle with an efficiency of 49.6 percent with the ability to go higher with lower heat rejection temperatures [25]. This was similar to the results presented by Dyreby on the design point optimization of sCO_2 cycles [26].

Current Recuperator Research

One of the key requirements of the sCO_2 cycle is large amounts of recuperation; there is a need to transfer heat internally at a rate that is many times larger than the rate of heat transfer to the cycle from the heat source. This challenge is the focus of this project. Currently there are several options for sCO_2 heat exchangers; shell in tube, plate, Printed Circuit Heat Exchangers (PCHE), micro tube, as well as some more exotic options. Each of these technologies could work in theory at the temperatures and pressures of a sCO_2 cycle, but there remains concerns about each [27]. The shell in tube heat exchangers are well understood as they have been used extensively in the steam Rankine cycles [27]. They are easy to manufacture and can be designed to handle large thermal stresses. However, shell in tube heat exchangers have relatively poor thermal performance, and are large due to their low surface area to volume ratio [27]. Additionally, due to the large shell and tube sizes, the pressure containment wall needs to be quite thick in order to be used in a sCO_2 cycle where pressures can be in excess of 20 MPa. As a result, conventional shell in tube heat exchangers are not considered to be a good option for sCO_2 cycles.

The plate heat exchanger consists of many formed plates that have flow paths stamped into them. The plates are stacked and bolted together with support and headers/manifolds added to each end. These heat exchangers can be made very cheaply because there is no need to weld or bond the plates together [28]. However, there can be issues with sealing the plates against each other, particularly at high pressures. These plate type heat exchangers could be a good option for components in the sCO_2 cycle where temperature and pressure are low, such as in the precooler where the pressure is about 8MPa and the temperature is below 200°C. However, it is unlikely that a plate heat exchanger can be constructed to withstand the greater than 20 MPa needed for a recuperator.

A PCHE has similar geometry to a plate heat exchanger. The PCHE is made by stacking plates with channels machined/etched into them that are then diffusion bonded together in a vacuum oven using heat and pressure. The diffusion bond that is created is nearly as strong as the base metal itself. The channels can be created by stamping, laser, or by chemically etching a pattern in a plate [12]. The result is a heat exchanger that has channels with very small hydraulic diameter which leads to a large surface area to volume ratio. Additionally, the small channel size means that the walls do not have to be as thick to contain the pressure. For 20 MPa pressure, the PCHE can have a porosity of about 40 percent [29]. Effectiveness also is improved by the small channel size and PCHE's have the ability to reach high effectiveness (90%) at a reasonable cost [30]. PCHE heat exchangers have been used extensively in the oil and gas industry over the last 25 years, but have not found wide spread use in the power industry [31]. One of the most pressing issues is the thermally-induced strain caused by the large temperature difference across the heat exchanger and the daily cycling of temperature if the power plant is not run continuously [27,29]. The concern is that, over the life of the plant, the pressure containment could fail and there could be a leak. If there is an internal leak between the two streams the headers would have to be cut off to make the repairs which would be costly and time consuming. Additionally, fixing the leak would mean plugging some of the flow channel so the overall effectiveness of the heat exchangers would be reduced. Additionally, with some header designs repairing a PCHE can be difficult or impossible. Current work on PCHEs will be discussed later, but they are currently the best choice for recuperative heat exchangers in a sCO_2 Brayton cycle.

Similar to a PCHE, Sandia National Labs have been developing a Cast Metal Heat Exchanger (CMHE) which seeks to replicate the small channel size and excellent heat transfer of the PCHE at a lower cost [29]. The idea behind the CMHE is to create cores of out polymer sand and stack them in a similar configuration to a PCHE and then cast the metal around the cores. Casting would eliminate many of the problems associated with using nickel alloys that are hard to machine and weld [29]. Sandia

estimates that it would be possible to create a comparable CMHE at 1/5 of the cost of a PCHE [29]. It would also be possible to create a similar heat exchanger using 3d printing of powdered metals; however, this would require much more development work as powdered metals do not have the same density and therefore strength and conductivity as conventionally cast metals. Additionally, there is currently no code case for the 3d printed pressure vessels which would be associated with a 3d printed heat exchanger. CMHEs are not currently used and it is assumed that significant work is needed to develop CMHEs for sCO_2 cycles.

Microtube heat exchangers are made from many small diameter tubes (less than 0.1") laid out in a similar manner as a shell and tube heat exchanger. Small tubes can withstand high pressures and provide good surface area for heat transfer making them a significant improvement over a conventional shell and tube heat exchanger. The main problem with microtube heat exchangers is the construction of the headers. The flat tube sheet gets very thick at sCO_2 cycle pressures (25 MPa) and it becomes difficult to manufacture. Additionally, thermal expansion of the tubes needs to be considered in the design which can necessitate the use of a sliding seal. MezzoTech, a leader in microtube heat exchangers have been working on adapting their technology to sCO_2 applications [32].

A more novel heat exchanger design uses ceramics to create solid block heat exchangers that can withstand high pressures and have acceptable effectiveness. Solid block heat exchangers are created by laser cutting ceramic sheets with a specific flow pattern and header design, and then stacking the plates much like a PCHE [33]. The plates are placed into an oven to cure and the final result is similar to a PCHE except with ceramic material instead of metal. The ceramic heat exchangers have much the same issues as PCHEs associated with cleaning and thermal stress. However, the cost could be lower than a PCHE due to the low cost material and simple manufacturing process. A major unknown with this type of heat exchanger is whether it can withstand the harsh environment of the sCO_2 cycle over the lifetime of the power cycle, which can be in excess of 20 years. While ceramic heat exchangers show

promise, they are much further down the technology readiness scale compared to the other options that have been described.

Cermet, has recently received some research interest for use in sCO_2 heat exchangers. There are many different kinds of Cermet, two of those being looked at for sCO_2 are tungsten carbide (WC) and zirconium carbide (ZrC) which has good thermal properties and strength. Starting with a porous block of WC researchers were able to machine out complex shapes such as those needed for a heat exchanger. Preforms are then immersed in molten Zr_2Cu which fills in the porosity of the WC preform [34]. The resulting matrix a very strong and capable of withstanding high pressures without being brittle. Numerical modeling of a primary heat exchanger for a sCO_2 cycle (using molten salt as the heat transfer fluid) has been conducted to see its viability in the sCO_2 cycle [35].

The current focus of the sCO_2 recuperator research has been on PCHEs, and since they are the current best option, the state of the art for PCHEs will be examined. There have been many different studies modeling the performance of PCHEs. In particular, work at the University of Wisconsin has looked at different channel geometries and their effect on the performance of the heat exchanger [12] [36] [37]. Carlson compared straight channels, zig-zag channels, and air foil shaped fins in PCHEs [12]. A test facility was constructed that could measure the thermal and hydraulic performance of each of these different designs. Instead of bonding the layers of the heat exchanger together, the etched plates were simply bolted together, which allowed for different channels to be tested in the same test facility easily. The heat transfer was measured by rejecting heat to cooling blocks along the length of the heat exchanger, as shown in Figure 7.

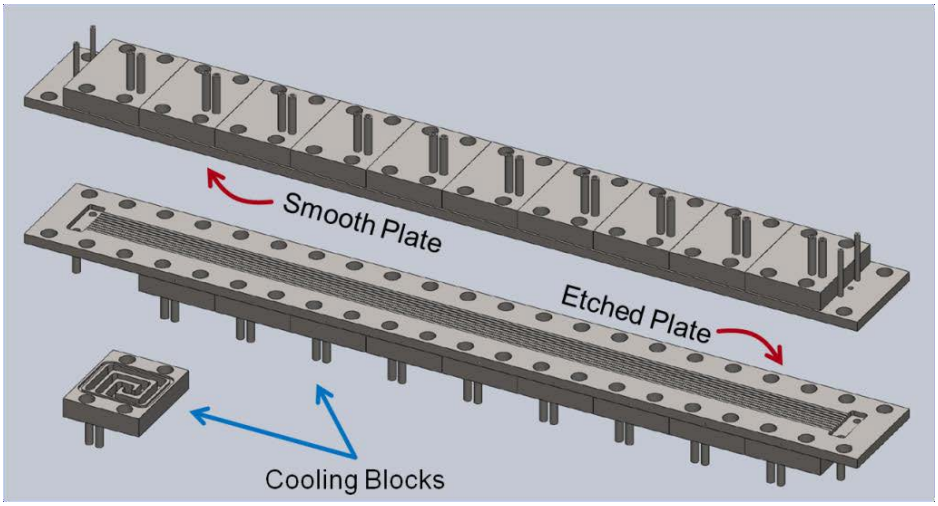

Figure 7 Test section used by Carlson to test performance of different channel types. From [12]

The cooling blocks allowed the measurement of the local heat transfer and from that the local heat transfer coefficient. Using this information, the results could be compared to models and the heat transfer coefficient predictions can be used to more accurately model PCHEs. The results showed that the air foil channels had much better thermal performance than the discrete channels (strait or zig-zag) [12]. However, there was uncertainty about wall thickness calculations of the air foil geometry since the wall thickness calculations were intended for discrete channels, this could result in higher costs if it is found that more material is needed. The research also showed there was an approximately 30% geometric deviation between the designed and actual etched specimens [12]. More recent work at UW has focused on experimental testing of PCHEs under sCO_2 conditions [37]. Additionally, researchers at UW have been working on a program to test PCHEs and qualify them for use in a nuclear power plant [38].

Carlson also developed a tool that can be used to automatically design a PCHE for a given temperature, pressure, and fluid called SEARCH [39]. The model uses a sub-heat exchanger method described in [40] to capture the effects of property non-linearity which can be significant in CO_2 near the critical point. The model was developed in Engineering Equation Solver (EES) [17] which was also used to

determine the properties of the fluid. The model uses the ASME BPVC to determine the spacing of the channels and the amount of material that is needed for pressure containment [10]. A model of a PCHE that was tested at Sandia National Lab was created in order to compare the results from the model to experimental results [39]. The SEARCH program was found to under-predict the effectiveness of the PCHE by about 10 percent [39]. The goal for the program is that more results will improve the fidelity of the model so that the program can be used to obtain results with an acceptable design margin [39].

Sandia National Lab has a test loop operating at Barber Nichols that has been used to test various components of a sCO_2 system [41]. The cycle is designed for temperatures of 540°C and pressures of 17 MPa [42]. The test facility is designed to understand and demonstrate the performance of the compressors, turbines, and heat exchangers that will be used in scaled up sCO_2 systems. Additionally, the test loop is being used to test control strategies for a sCO_2 cycle. The initial heat exchanger results from the Sandia demonstrator seem promising, with heat exchangers transferring 1.7 times the heat input into the cycle (which is expected of a highly effective recuperator [42] [43]). It was also found that the thermal transient associated with the recuperator was fast, on the order of 60 seconds, making it possible for the cycle to rapidly adjust to changing conditions [42].

Additional testing of PCHE performance has occurred at the Tokyo Institute of technology. A PCHE from Heatric was tested with CO_2 at 280 -300°C and 2.2 to 3.2 MPa at the hot side, and 90-108°C and 6.5 to 10.5MPa on the cold side [44]. These temperatures are lower than what is expected for a sCO_2 Brayton cycle, but the results can be extrapolated to the conditions of interest. A zig-zag channel configuration was used and an effectiveness of 99 percent was measured for some of the test conditions [44]. While this high effectiveness likely means that the heat exchangers were grossly oversized for the given conditions, it does show that high effectiveness is possible for PCHEs. The researchers also measured values for the heat transfer coefficients in the channels that ranged from 300-650 W/m2-K, and compactness (surface area/volume) values of about 1000 [44]. The researchers went on to create

an experimental model of the heat exchanger using CFD in order to compare results [45]. The model was used to determine the heat transfer coefficients and pressure drop for zig-zag and airfoil geometries [45]. It was found that, for similar Reynolds number, the Nusselt number was about 25 percent larger than the zig-zag channels, while the pressure drop was 4-5 times less [45]. A CFD model was also created for S-channels in a PCHE and a correlation for the Nusselt number was obtained for various inlet temperatures [46]. The temperatures were chosen to be near the critical point of CO_2 and the expected error was determined to be about 3 percent [46]. The results were compared to experimental results and matched within 5 percent [46]. This study showed that CO_2 heat exchangers can be modeled accurately using CFD even near the critical point.

More recently research has focused on airfoils for use as the fins in PCHEs. The goal is to have the same conductance but with less pressure drop. The airfoils prevent separation of the flow, reducing form drag while maintaining relatively high surface area for good heat transfer. Some studies have suggested that it is more important to reduce the pressure drop than it is to increase the effectiveness in order to improve the performance of a sCO_2 cycle and one research group has worked to optimize the airfoil fins to do that [47]. In this effort, new fins are proposed that have slightly better pressure drop performance with the same heat transfer rate.

Other work has been done relative to optimizing channel designs for different nuclear heat sources. It was found that PCHEs with an S-shaped or airfoil geometry had the best thermal-hydraulic performance; however, the straight or zig-zag channels actually performed better when looking at the system as a whole due to laminar flow in the strait or zig-zag channels resulting in lower pressure drops [48].

A group at the Korea Advanced Institute of Science and Technology (KAIST) has done significant work on CFD modeling and experimental testing of PCHEs. They have used CFD to predict the Nusselt

number for CO_2 flows over a range of conditions, including those expected in a sCO_2 Brayton cycle. They have confirmed these results through experimental testing with helium and CO_2 [49][50][51][52] [53][54].

One of the oldest manufacturers of PCHEs is Heatric, a company that has over 1000 units sold over the last 25 plus years [31]. Heatric has found some important solutions to the issues faced by PCHEs. One of these issues is in the header design, the small channels in the heat exchanger block reduces the need for thick pressure containment [31]. However, in the headers the flow diameters can get quite large and as a result the header walls end up being very thick [31]. To reduce this problem Heatric has designs that incorporate the header into the block of the heat exchanger in order to eliminate the need for welding on larger headers. A much smaller pipe can be welded on instead [31]. While this provides an advantage in manufacturability, it hinders maintenance of PCHEs since the header cannot be cut off to make repairs to the flow channels.

Past Regenerator Experimental Testing

Regenerators are not a new technology and have been used in many different applications because of their low cost and ability to effectively recover heat [6,55]. Regenerators operate by alternatively storing and releasing heat from a packed bed. All experimental testing and modeling until now has focused on drastically different conditions compared to those experienced by a regenerator in an sCO_2 cycle. There are four main applications where regenerators are used that have been extensively studied; Gifford McMahon (GM), cryogenic Stirling, high temperature Stirling, rotary, and pebble bed. Regenerators used in GM cryocoolers have a rotary valve that directs flow into and out of a packed bed. GM regenerators operate at very low temperatures (down to 4K) and can have very fast switching times (1 Hz). GM cryocoolers usually operate at rather low pressures as well (2 MPa), another difference from the sCO_2 regenerator [56–58]. Cryogenic Stirling cycles use the power from a compression piston to

produce an expansion in a colder piston which leads to a cooling load; the Stirling system is a moving piston device [55]. Using a regenerator in the chamber increases the performance of the cycle. However, these regenerators are much different from an sCO_2 regenerator because they do not have any valves. Switching for Stirling cycles is very fast (60 Hz) and they operate at low temperatures (less than 100K) and pressures on the order of a MPa [59–62]. Stirling cycles can also be used to generate power by applying heat to one end and recovering the energy from the motion of the piston. Stirling cycles are a good option to use with dish solar systems because of their compact size and good efficiency at a small scale [6]. Significant testing has been done at very high temperatures (up to 1500°C) and moderate pressure (4 MPa) with switching times reaching up to 50 Hz [6,63–65]. Rotary regenerators operate by rotating the heated regenerator bed into the cold stream without the use of valves. Rotary regenerators have found use in air Brayton cycles as well as HVAC applications. Sliding seals are used to prevent leakage from the high pressure stream to the low pressure stream. These seals work well even at the high temperatures seen in the air Brayton cycle (in excess of 1000°C), however the air Brayton cycle operates at low pressure (around 6 bar) [66–70]. In an sCO_2 cycle where the pressure differential between the streams is 17 MPa, sliding seals would result in excessive leakage. Pebble bed regenerators are used for heat recovery mainly from processes with waste heat. Hot air is passed over a packed bed of a low cost energy storage material (rocks or similar) which stores the energy for later use. Pebble bed regenerators can have switching times on the order of minutes and can operate at high temperatures (greater than 1000°C). However, they also operate at low pressure (1 bar) making them significantly different than sCO_2 regenerators [71–73]. This research fills a gap in current research by testing a switched bed regenerator operating at moderate switching time (45s), moderate temperature (560°C), and high pressure (25 MPa). One main difference is the effect of carryover (where fluid is trapped in the bed due to the pressure differential) drastically impacts the cycle due to the high pressure differential which is less important in the other regenerator types.

A sCO_2 power cycle could be much more efficient than current steam cycles, but it will never be used if the initial cost is too large. Currently, the sCO_2 cycle is more expensive from an initial cost standpoint compared to a steam Rankine cycle [2]. After considering the additional cost of financing a sCO_2 cycle, the Levelized Cost of Electricity (LCoE) for a sCO_2 and steam Rankine cycle are similar [2]. A Rankine cycle has much less risk since it is a technology that has been used for decades and is the current power system choice. However, if the LCoE for the sCO_2 cycle could be lowered then there would be an economic driver to change to a sCO_2 cycle even with the increased risk. It has been shown that PCHEs have the potential to have high heat transfer coefficients, even if the lifespan of these devices is still a concern. However, studies have shown that the recuperation for sCO_2 cycles could account for 16-34 percent of the total power block cost in cases with two recuperators [13,23]. The goal of this research project is to study the advantages and disadvantages of using a periodic regenerator to replace PCHE recuperators in a sCO_2 cycle in order to reduce the capital cost associated with the on recuperation while maintaining or improving the performance of the cycle. An analytical model has been developed and integrated into a cycle model of a RCBC in order to analyze the cost savings of switching to regenerators. Experimental testing is conducted to validate the regenerator model at the design conditions and to ensure the regenerator design can withstand the harsh environment of an sCO_2 cycle. The final result is a verified regenerator model that can be implemented into an overall cycle model to quickly model cycle performance and optimize the cycle design.

Regenerator Operation

A regenerator actually consists of 2 packed beds to allow continuous flow on the high pressure and low pressure sides of the cycle. The flow through the beds are controlled with a system of 8 valves. There are four steps in one complete cycle of regenerator operation as illustrated in Figure 8.

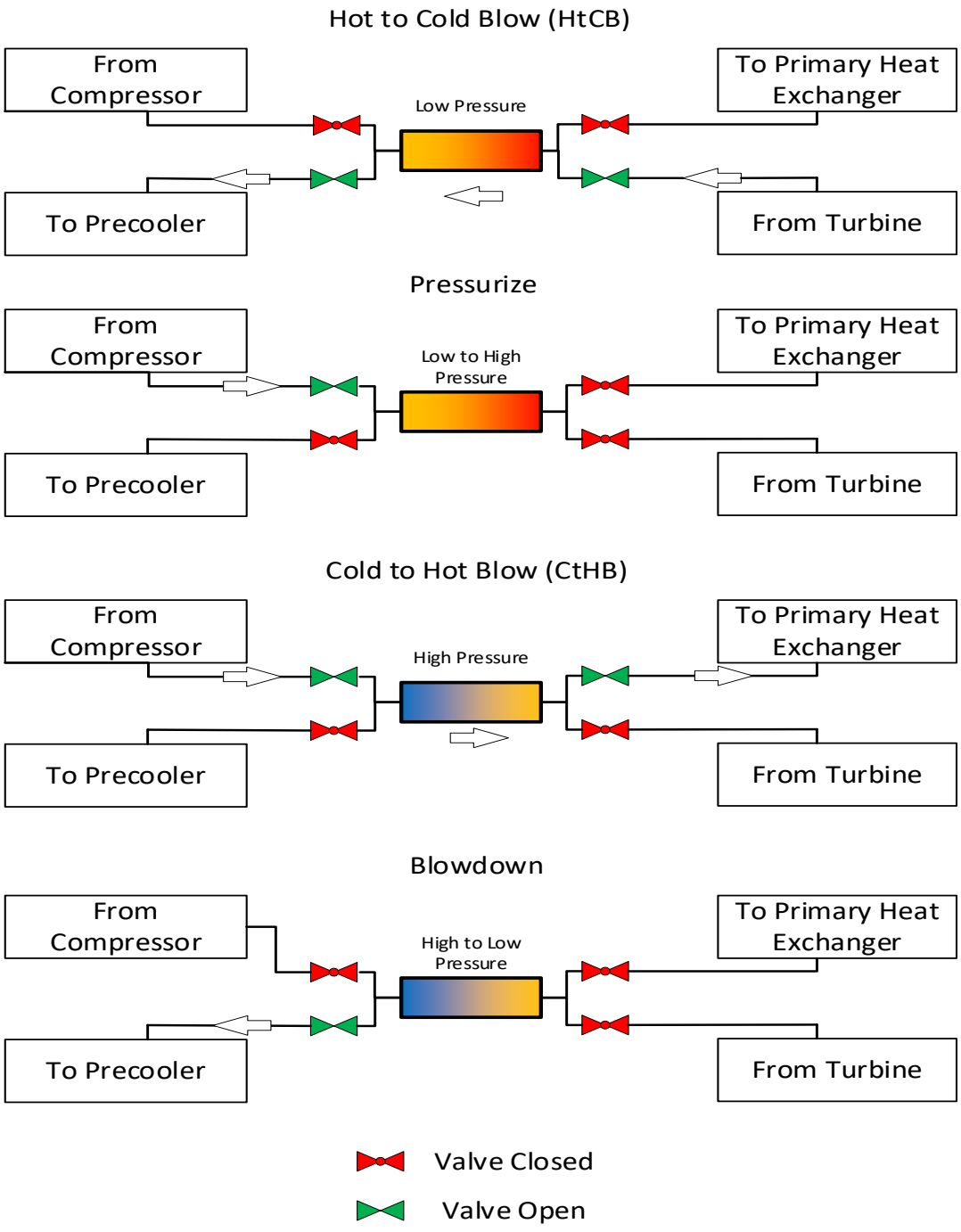

Figure 8 Four steps of regenerator operation, a second bed operating 180° out of phase is needed for steady operation

First is the Hot to Cold Blow (HtCB) where hot, low pressure fluid coming from the turbine is passed over the bed where energy has been previously stored. Second, the bed is pressurized so it is ready for the next step. Third, the Cold to Hot Blow (CtHB) occurs where energy is removed from the bed

and heats the CO2 before it reaches the primary heat exchanger. Finally, blowdown occur where the excess CO2 in the bed is removed so the HtCB can occur again at low pressure. A second bed would be operating 180° out of phase with the bed shown to allow continuous operation. This process is repeated for many cycles and the regenerators reach a quasi-steady state where they behave similar to a recuperator.

Due to the transient nature of regenerator operation, the temperature of the fluid leaving the regenerator is not constant throughout the cycle as illustrated in Figure 9.

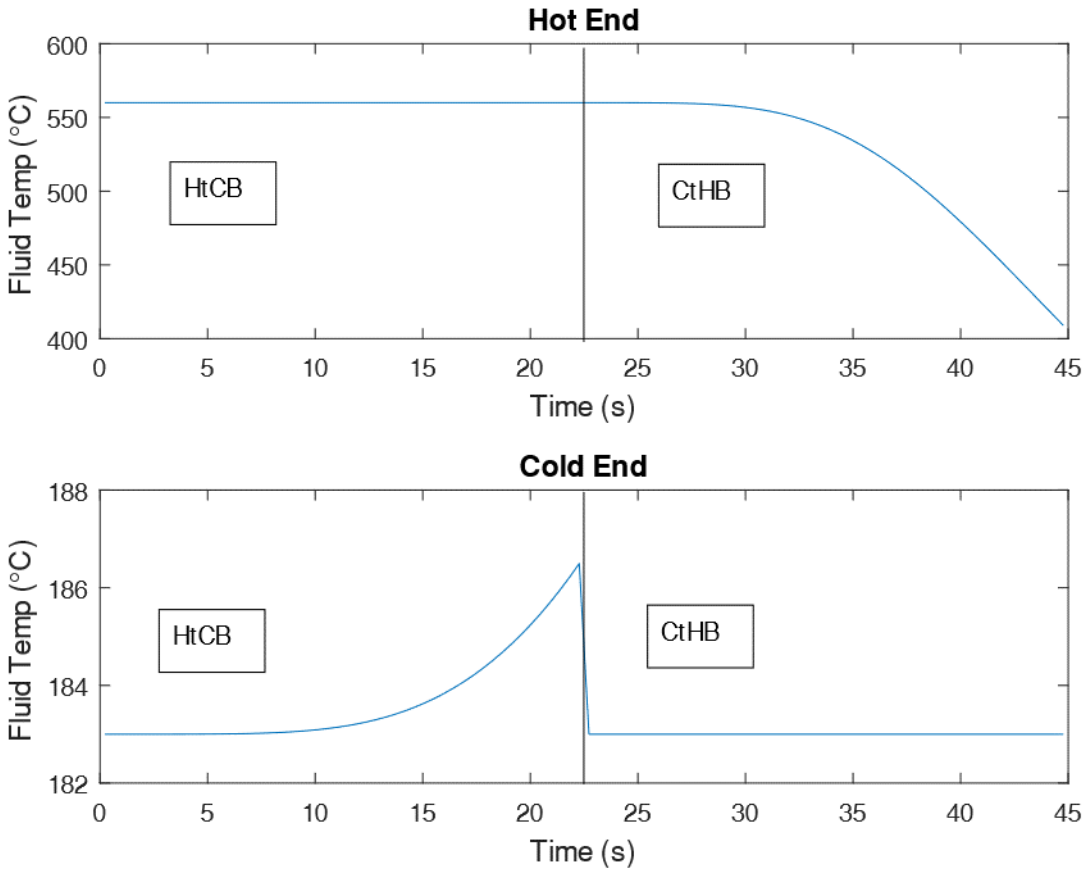

Figure 9 Bed inlet and exit temperatures of representative sCO_2 regenerator

Since the time scale of the temperature change in the regenerator (seconds) is much shorter than the time scale of the power cycle fluctuations (minutes) a mass flow averaged temperature can be used in the calculations. With sufficient buffer volume, and thermal mass of the components it is not unreasonable to think the temperatures the other components actually see would be much more constant. Other participants on the project have been working on transient modeling of the cycle and have shown that a modestly sized thermal transient reducer (packed bed similar to regenerator) can reduce the transients to an acceptable level [74].

The differentiating feature between a regenerator and a recuperator is the presence of carryover. Carryover is any fluid that has been compressed but is not expanded through the turbine, resulting in higher compressor work. A plot of mass in the regenerator bed can be used to illustrate carryover as shown in Figure 10.

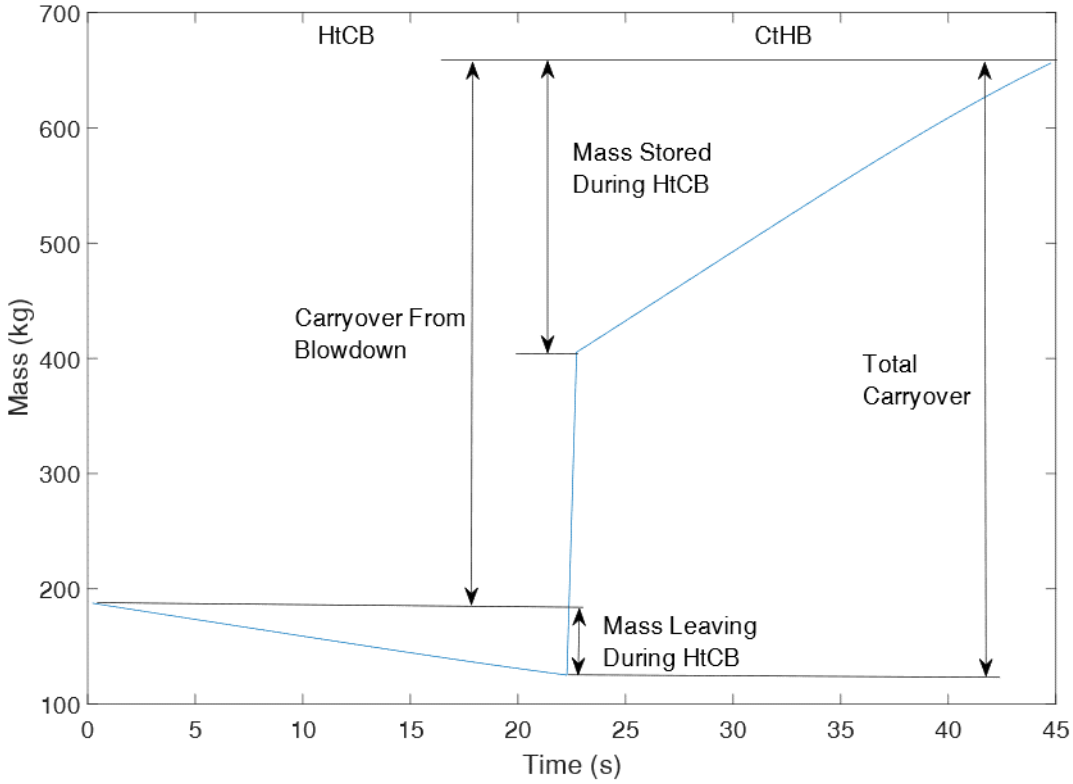

Figure 10 mass in regenerator bed for a representative regenerator cycle

In extreme cases carryover can increase the mass flow through the compressors by 25%. Carryover is highly temperature dependent, at low temperature where CO_2 is denser carryover is higher. Temperature dependence leads to an interesting scenario where making the low temperature regenerator larger has a much smaller performance impact than increasing the size of the high temperature regenerator. There are two sources of carryover in the bed, one is from the pressure change during the pressurization and blowdown steps. The other source of carryover is from the temperature change of the fluid in the bed because of the temperature change in the bed. During the CtHB the bed is cooling, and density is increasing so mass is being stored in the bed. During the HtCB the bed is heating, and mass is being removed from the bed due to the density change. Both sources of

carryover need to be considered because both will cause an increase in compressor mass flow. The easiest way to visualize carryover is to plot the mass of CO_2 in the regenerator as a function of time and take the difference between the maximum and minimum point. The different contributions to carryover are illustrated in Figure 10.

To get an idea of how much the temperature changes in the bed and how that can affect the mass stored, the temperature in the bed for a representative cycle is shown in Figure 11.

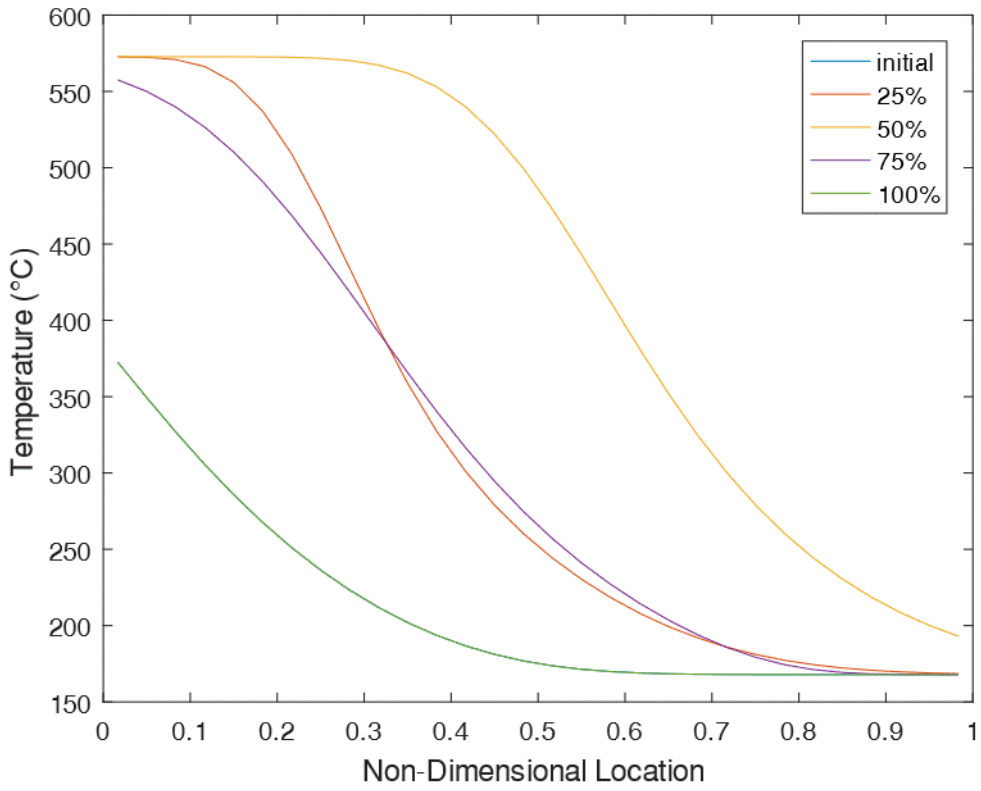

Figure 11 Temperature profile in bed at various completion percentages of cycle

Figure 11 shows temperature as a function of non-dimensional location at different percentages of completion of one cycle. In this case the cycle starts with the HtCB at 0% and ends the HtCB at 50%, at which point the CtHB starts and continues to 100% completion. At 100% the temperature profile is the same as 0% since regenerators are a cyclic device.

Regenerator Model

A model is needed to predict the performance of the regenerator, so it can be used for an economic analysis of the regenerator system. This model should be able to solve quickly and provide reasonably accurate results, so it can be used for optimizing the design of a regenerator in a power block. For this reason, a model based on two dimensionless parameters similar to the effectiveness-NTU model for heat exchangers was used which is defined in [55]. The model takes inputs of Number of Transfer Units (NTU) and matrix capacity ratio (C_m) and uses them to determine the effectiveness of the regenerator. NTU and C_m are defined as follows.

$$NTU = \frac{UA}{\dot{C}_{\min}} \tag{1.1}$$

$$C_m = \frac{m_b c_b}{P_0 \dot{C}_{\min}} \tag{1.2}$$

where *UA* is the conductance of the regenerator, $\dot{C}_{\min}$ is the minimum capacitance rate of the two streams, m_b is the mass of the energy storage media in the packed beds, c_b is the heat capacity of the bed material, and P_0 is the switching time. The definition for NTU is the same for a conventional heat exchanger, which is the dimensionless size of the heat exchanger. C_m can be thought of as the ratio of energy the bed can store compared to the amount passing through the bed, the larger the C_m the more energy the bed can store. The model is given a bed length, diameter, mass flow, inlet pressures, and inlet temperatures which are used to calculate *NTU* and C_m. The bed is assumed to consist of randomly packed spheres. The heat transfer coefficient of the bed was calculated from experimental data presented by Kays and London and programed in EES [17,75]. The properties of the bed can vary drastically based on the void fraction which is defined at the volume of free space in the bed compared to the total volume of the bed. For a randomly packed bed of uniform spheres this varies between 0.32

and 0.37 [40]. During construction of the regenerators a packing fraction of 0.37 was measured and used in the model. It is important to remember that the regenerator flow is not balanced, meaning the capacitance rate of the hot and cold fluids are not the same which causes a pinch point at one end of the regenerator. Since all of the correlations for effectiveness of a regenerator are based on balanced flow, the *NTU* and C_m need to be corrected the correction method from [55] is shown below.

$$NTU_e = \frac{2C_R NTU}{1+C_R} \tag{1.3}$$

$$C_{m,e} = \frac{2C_R C_m}{1+C_R} \tag{1.4}$$

Where C_R is the capacitance rate ratio (maximum capacitance rate over minimum capacitance rate). NTU_e and $C_{m,e}$ are used to interpolate a lookup table created from an analytical regenerator model to determine effectiveness. Contours of constant effectiveness as a function of *NTU* and C_m are shown in Figure 12.

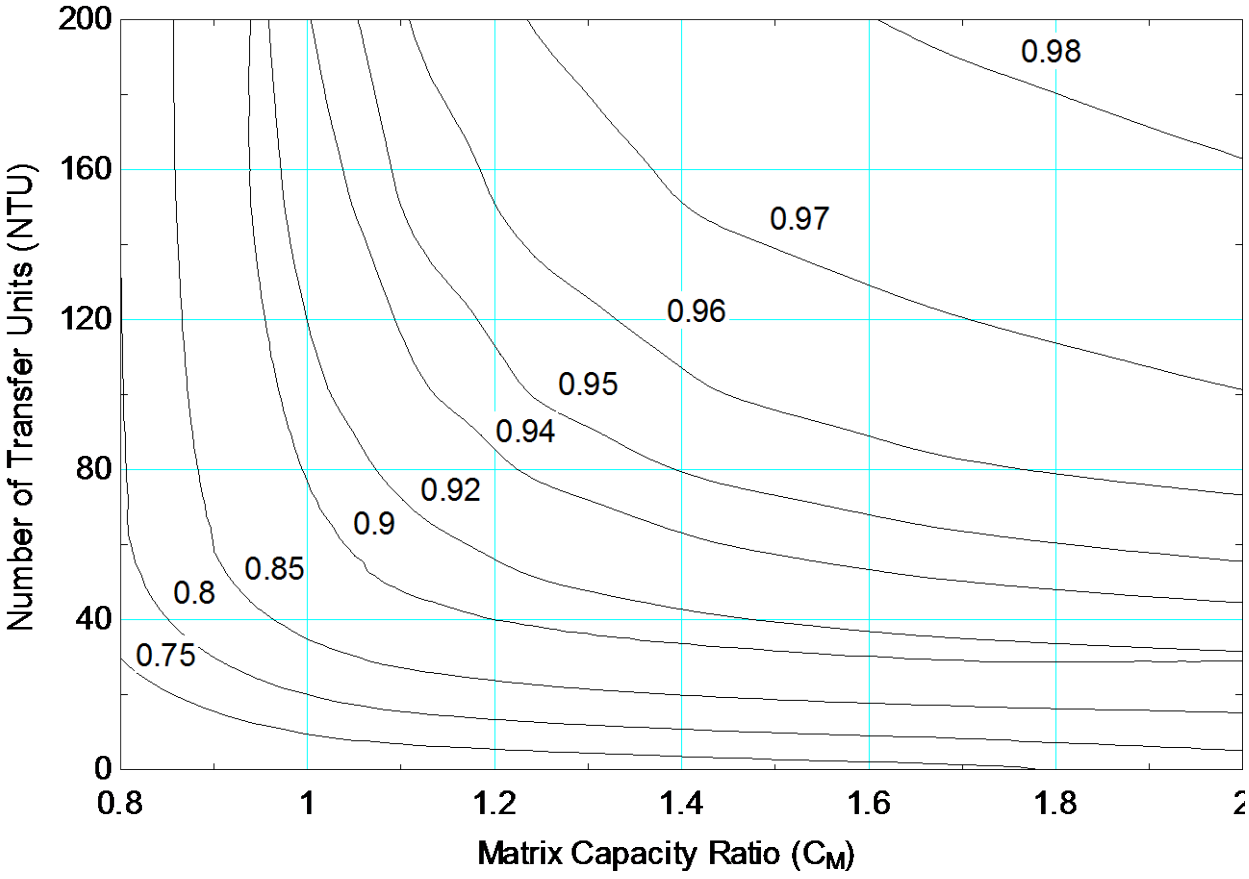

Figure 12 Contours of constant effectiveness as a function of NTU and matrix capacity ratio

The effectiveness returned by the interpolation also must be corrected to account for flow imbalance. The corrections are shown below.

$$X = \left(\frac{1-C_R^2}{2C_R}\right)\left(\frac{\varepsilon}{1-\varepsilon}\right) \tag{1.5}$$

$$\varepsilon_{cor} = \frac{1-e^{-X}}{1-C_R e^{-X}} \tag{1.6}$$

where ε is the effectiveness returned by the interpolation and ε_{cor} is the effectiveness corrected for unbalanced flow. Effectiveness can then be used to determine the heat transfer rate in the regenerator, shown in equation (1.7).

$$\varepsilon_{cor} = \frac{\dot{Q}}{\dot{Q}_{\max}} \tag{1.7}$$

where $\dot{Q}_{\max}$ is the maximum possible heat transfer rate calculated by determining the heat transfer in a perfectly effective heat exchanger operating with the same conditions as the regenerator (inlet temperatures, pressures, and mass flow rates). $\dot{Q}_{\max}$ is solved using the counter flow heat sub-heat exchanger module written by Dyreby for EES [26]. This module breaks the heat exchanger into many sub heat exchangers, all with the same conductance. The advantage of the sub-heat exchanger method is that the capacitance rate can be calculated for each sub-heat exchanger using the local properties. Using the sub-heat exchanger method is especially important near the critical point where the properties of CO_2 can change drastically as a function of temperature.

In addition to calculating effectiveness, the model also calculates pressure drop in the packed bed. Past work has looked extensively at pressure drop through a randomly packed bed of spheres and the most common pressure drop equation used is the Ergun equation [76]. However it was found the Fahiem-Schriver correlation did a better job at predicting pressure drop in the Reynolds number of interest [77]. The equations used to solve for pressure drop in the Fahiem-Schriver correlation are given in equations (1.8) - (1.15) [77].

$$\Delta P = \frac{f_p \rho V^2 L}{d_p} \tag{1.8}$$

$$f_p = \left(q \frac{f_{1L}}{\mathrm{Re}_m} + (1-q)\left(f_2 + \frac{f_{1T}}{\mathrm{Re}_m} \right) \right) \frac{(1-\phi)}{\phi^3} \tag{1.9}$$

$$q = \exp\left(-\frac{\phi^2 (1-\phi)}{12.6} \mathrm{Re}_m \right) \tag{1.10}$$

$$f_{1L} = \frac{136}{(1-\phi)^{0.38}} \tag{1.11}$$

$$f_{1T} = \frac{29}{(1-\phi)^{1.45}\phi^2} \tag{1.12}$$

$$f_2 = \frac{1.87\phi^{0.75}}{(1-\phi)^{0.26}} \tag{1.13}$$

$$\mathrm{Re} = \frac{d_p \rho V}{\mu} \tag{1.14}$$

$$\mathrm{Re}_m = \frac{\mathrm{Re}}{(1-\phi)} \tag{1.15}$$

The definition of the parameters used in the equation is shown in Table 1.

Table 1 Definition of parameters used in Fahiem-Schriver correlation

ρ	Density of fluid in bed [kg/m3]
V	Velocity of fluid in bed [m/s]
L	Length of bed [m]
d_p	Diameter of spheres [m]
$\mathrm{Re_m}$	Modified Reynolds number
ϕ	Void fraction
μ	Viscosity of fluid (average) [Pa-s]

Since the model does not resolve the local conditions in the bed, the pressure drop was calculated using properties calculated at the average temperature and pressure of the CO_2 in the bed.

Regenerator carryover model

To get an accurate measure of carryover, the spatial temperatures in the bed must be well known. The effectiveness-NTU-C_m model cannot determine the actual temperature in the bed at the end of the

CTHB but rather returns the average temperature. The actual temperatures (obtained from a numerical model of the regenerator) in the bed compared to the model temperatures are shown in Figure 13.

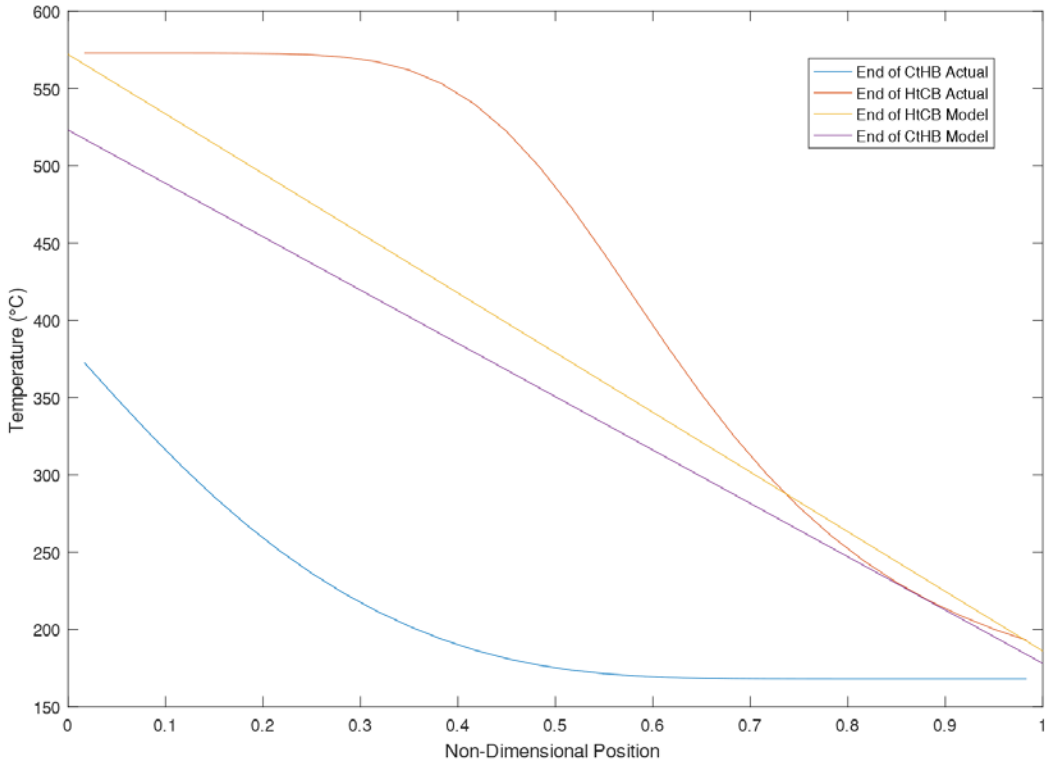

Figure 13 Temperature comparison of numerical model to effectiveness-NTU-C_m model at minimum and maximum mass in bed conditions

The model temperature profile in the bed is much different than the actual temperature distribution seen in the bed, see Figure 13. A correction will be discussed in the Test Results section. Using the temperature profiles given in Figure 13 and the operating pressures, the carryover mass in the bed can be calculated by integrating the fluid density throughout the length of the regenerator, as given in equation (1.16).

$$m_c = \int_{x=0}^{x=L} \frac{\pi D^2}{4} e_v \left[\rho(T(x), P_H) - \rho(T(x), P_L)\right] dx \tag{1.16}$$

where D is the inner diameter of the regenerator vessel, e_v is the void volume fraction of the packed bed (e_v = 0.37 for a randomly packed bed of spheres), and $\rho(T(x),P_H)$ and $\rho(T(x),P_L)$ are the densities of the fluid at location x in at the time that the CTHB and HTCB flow processes are complete, respectively.

Since there are two regenerator beds this mass of fluid is carried over to the compressor twice every cycle. This carryover mass is quantified as a mass flow rate according to equation (1.17) and treated as a leakage in the system from the high pressure inlet to the low pressure exit of the regenerator since this is where the valving forces the fluid to go.

$$\dot{m}_c = \frac{2m_c}{P_0} \tag{1.17}$$

Regenerator BPVC Design

In order to accurately determine the cost of the regenerator, the outer shell must be sized correctly using ASME Boiler and Pressure Vessel Code (BPVC) [10]. Initially, the shell design was based on Section VIII Division 2 Chapter 4 of the BPVC , which specifies a design based on rules [10]. However, one of the stipulations to using Chapter 4 of the BPVC is that there cannot be stress in excess of 10^6 cycles which the regenerator design exceeds. The regenerator, by definition, requires pressure cycling in order to properly operate and therefore the pressure vessel must be designed to meet the BPVC requirements for stress cycling. BPVC allows a pressure vessel with cyclic loading to be designed using Chapter 4 (design by rule) as long as it passes the test for stress cycling that is specified in Chapter 5 (design by analysis) [10]. The stress cycling can be caused either by mechanical stresses associated with changes in internal pressure or by thermal stresses associated with time varying temperature gradients in the shell. While the regenerator bed itself experiences significant temperature changes during each cycle, the regenerator pressure vessel can be designed to maintain a nearly constant temperature that is significantly lower than the regenerator bed or the outer wall of a similarly configured recuperator. An

internal insulation is added to the pressure vessel, separating the packed bed from the wall of the regenerator. An insulated regenerator design eliminates the thermal transients in the wall, additionally the lower temperature allows for thinner walls made of a less expensive material which reduces cost. Insertion of an insulating material between the bed and the pressure vessel wall also limits the corrosion by the sCO2 fluid on the pressure vessel walls. This concept is illustrated in Figure 14.

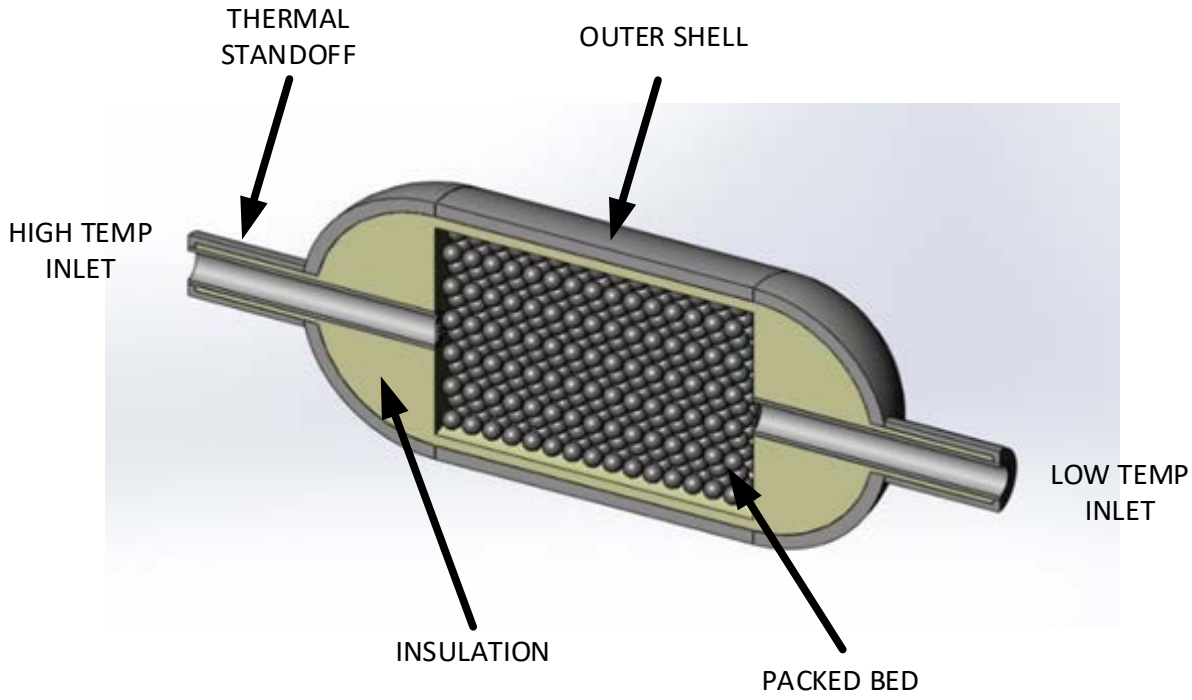

Figure 14 Concept drawing of insulated regenerator pressure vessel

BPVC specifies the maximum allowable stress of materials based on the temperature at which they are used; as temperature increases, the allowable stress for the material is decreased. A plot of the maximum allowable stress vs temperature for various materials is shown in Figure 15.

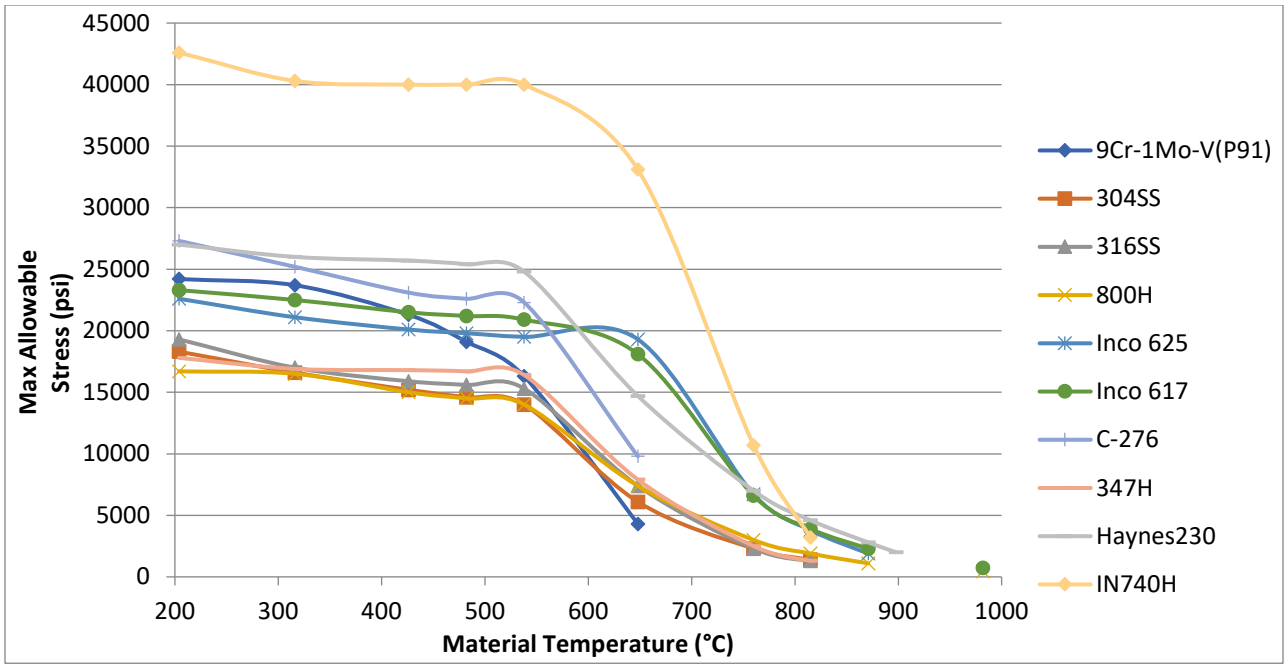

Figure 15 Max allowable stress vs temperature for various materials according to Tables 1A and 1B in [10]

Type 91 steel is a good choice for this application due to its low cost, high strength, and proven corrosion resistance to CO_2. Type 91 steel experiences a loss in allowable stress above 375°C, and its allowable stress falls drastically above 500°C [10]. 375°C was set as the upper limit the wall can reach under normal operating conditions. Insulating a pressure vessel is not a new idea, the most similar application that currently exists in the market are the pressure vessels used in Fluidized Catalytic Crackers (FCCs) [78] in the oil and gas industry to refine fuel. FCCs have an outer pressure vessel shell in which the internal surface is lined with a castable refractory insulation and can be quite large, usually 2-3 meters in diameter and up to 10 meters long [79]. At a 10MW scale the regenerator beds are estimated to be approximately 1 meter in both length and diameter. Communication with an FCC supplier suggest that it would be possible to make a similarly lined pressure vessel at regenerator conditions, and even provided samples of insulation for testing [80]. Therefor it this technology was assumed to be proven.

There are several properties that the refractory insulation must have to fit for service in a regenerator. First, the insulation needs to have a low conductivity so that the thickness of insulation required is not too large, which would make the vessel diameter large. Second, the insulation must be able to withstand the large, rapid pressure changes that the regenerator will experience on a cyclic basis. Third, the insulation cannot create excessive dust that could cause damage to turbomachinery. Fourth, the insulation cannot be excessively porous as any CO_2 that migrates into and out of the insulation pore volume on a cyclic basis will result in an increase in carryover. Several castable insulations and pourable insulations were analyzed as part of the study.

The initial insulation sizing was conducted utilizing a one dimensional (discretized radially) steady state model with information from the manufacturer's material data sheets used to estimate the conductivity of the candidate insulation materials. Initial testing of the refractory insulation shows that the conductivity of the insulation will increase by approximately 100 percent when it is filled with CO_2 and this effect was accounted for in these results. It was found that approximately 2" of insulation was needed, assuming a conductivity of 1W/m-K. ANSYS was used to create a 2-D, axisymmetric model of the regenerator shell and insulation using this information. The sizing of the wall of the regenerator used in the model is described in the following section. The temperature dependent material properties of the insulation and wall were programed into ANSYS along with the bed temperature and heat transfer coefficient obtained from the numerical model. The outside of the regenerator was allowed to convect to an ambient temperature of 32°C, with the heat transfer coefficient calculated assuming natural convection [40]. Radiation from the wall was not considered but would only act to further reduce the wall temperature. The inlet and outlet nozzles of the regenerator were included in the model and are assumed to have the same temperature as the bed at the nearest point. The heat transfer coefficient in the nozzles was calculated assuming forced convection in a pipe [40]. The entire model was initialized at a constant temperature and successive substitution was used to solve for the steady state temperature

of the bed under quasi-steady state conditions. Additionally, a thermal stand-off has been added which isolates the shell from the fluid flow. The design was modeled in ANSYS and using the temperature profile of the fluid in the bed, the result at the end of the HTCB is shown in Figure *16*.

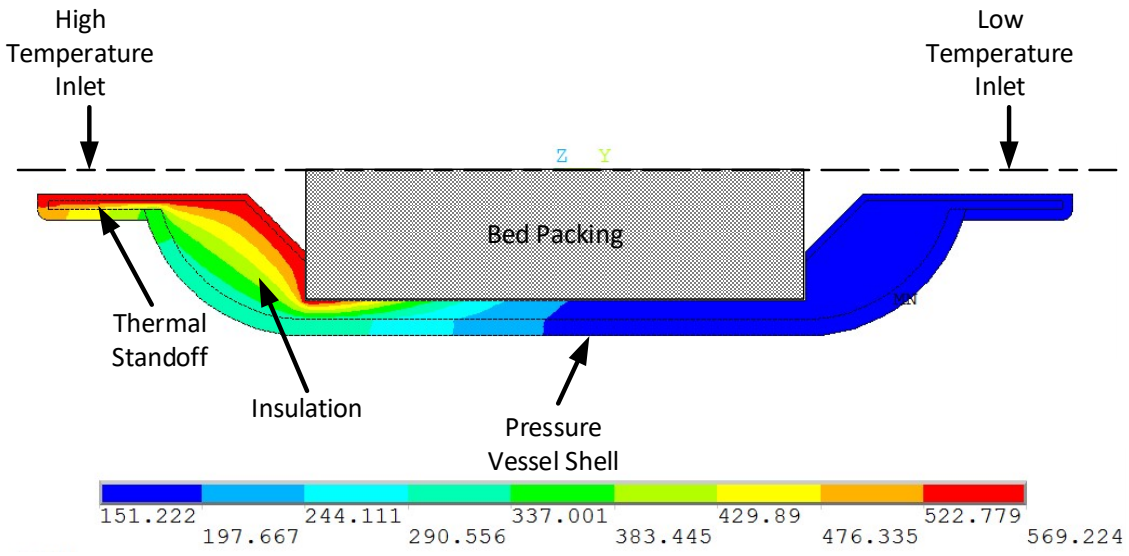

Figure 16. Temperature (°C) distribution in wall and insulation of regenerator with a thermal standoff, results are shown at the end of the HTCB process.

The thickness of the thermal standoff required was determined by calculating the insulation thickness needed to maintain a shell temperature of less than 375°C while the outer tube of the standoff is experiencing natural convection to 32°C air. The heat lost to the cooling of the outer pipe is insignificant compared to the heat transfer occurring within the pipe. The stress due to the thermal strain is small (about 5 MPa at the maximum temperature gradient) and due to the high conductivity and high heat capacity of the wall and the insulation, the wall temperature does not change significantly over the cycle.

Since the effect of temperature on stress cycling has been eliminated in the larger diameter portion of the pressure vessel using the thermal standoff design, Chapter 5 of BPVC Section VIII Division 2 can be employed to determine the wall thickness needed for the required pressure-based stress cycling. Chapter 5 defines a limit on the number of cycles for a given stress amplitude. The stress amplitude in the BPVC must be estimated using a model of the entire pressure vessel simulated throughout the entire stress cycle. This model takes into account stress from pressure, structural loading, and thermal sources. A full finite element analysis is impractical for this high level study where the goal is to obtain a reasonable estimate of the cost of a regenerator; the model must be able to rapidly iterate on the regenerator size. The solution instead used analytical methods to determine a pressure vessel size that will approximately pass the BPVC. The analytical solution does not include thermal stresses in the stress amplitude; these thermal stresses have an insignificant variation over each cycle. The stress amplitude due to the pressure variation has a maximum value at the point where the largest absolute stress exists; this value can be determined using stress equations for a cylindrical pressure vessel experiencing internal pressure. Chapter 5 of the BPVC provides a lookup table for the allowable stress amplitude as a function of the number of cycles that the vessel must withstand. The lookup table was programed into the design model along with the stress amplitude calculations in order to automate the process of selecting the vessel dimensions. The stress amplitude was found using cylindrical shell stress equations and the minimum stress was calculated for an internal pressure of 8 MPa while the maximum stress was found with an internal pressure of 25 MPa [81]. The diameter of the pressure vessel was determined by the regenerator model, taking into account the additional thickness needed for the insulation. The number of cycles in the life of the system is calculated using the lifetime of the power plant (30 years), the daily number of hours of operation (10 hours), and the switching time (45 seconds); these conditions are consistent with the objectives of the Department of Energy APOLLO project. For these conditions there will be 8.76 million cycles during the lifetime of the regenerator. To account for startup and other

pressure cycling events, the total number of cycles is increased by 20 percent to 10.5 million cycles for the design basis. Using this total number of cycles, the allowable stress amplitude can be determined using the lookup table provided by the BPVC Chapter 5.

In order to check the results of the analytical model used to predict the pressure stress in the design model, a 2-D axisymmetric ANSYS model was created [82]. The predicted results for the pressure vessel experiencing 8 MPa and 25 MPa of internal pressure are listed in Table 2. The ANSYS model predicts a stress amplitude of 74.6 MPa whereas the analytical cylindrical shell stress equations predict a stress amplitude of 79.74 MPa; this suggests that the analytical method provides a slightly conservative estimate of the stress amplitude. The stress amplitude corresponds to 31.6×10^6 allowable cycles according to BPVC, which is much more than what is required and therefore, the shell passes the BVPC [10].

Table 2. Maximum shell stress under minimum and maximum loading calculated using ANSYS model and with the analytical method that is integrated with the design model.

	ANSYS predicted maximum stress (MPa)	**Analytically predicted maximum stress (MPa)**
8 (MPa)	69.9	69.8
25 (MPa)	219	229
Stress Amplitude (MPa)	74.6	79.6

The BVPC has strict design limits for reinforcement necessary for the protrusions and penetrations into the end caps of pressure vessels. The size of the openings that are needed was determined from the thermal analysis of the wall. It was assumed that the material that would be used for the outer pipe is either 316 SS or IN740 due to its good corrosion resistance and strength at high temperature. Chapter 4 of the BPVC includes a section that specifically addresses nozzles in the heads of pressure vessels. The procedure involves calculating an effective force applied to the nozzle and an effective area that the force is being applied to. The resulting stress is compared to the allowable stress associated with the

material making up the nozzle. 316 stainless steel has an allowable stress of 92.8 MPa at 375°C, the maximum temperature experienced in the shell. Using a nozzle configured from a 10 inch schedule 160 pipe leads to an effective stress of 111.9 MPa; this passes the BPVC which requires that the effective stress be below 1.5 times the allowable stress of the material. If the nozzle were made of IN740 then a significantly thinner wall could be used.

In conclusion, an appropriate pressure vessel that meets the BPVC uses a design that employs a thermal standoff at the hot end of the vessel and refractory insulation on its inner surface in order to eliminate thermal transients in the outer wall of the vessel and reduce the wall temperature, respectively. The vessel wall is then sized to reduce the stress amplitude associated with the pressure load to below the allowable limit given the anticipated number of cycles. The pressure vessel dimensions for a 10MW power plant are listed in Table 3.

Table 3. Regenerator dimensions for 10MW power plant

Dimension	Low Temp Regenerator	High Temp Regenerator
Length	1.10 m (43.3 in)	0.90 m (35.4 in)
Reqd. Diameter	0.97 m (38.2 in)	1.05 m (41.3 in)
Wall thickness	55.3 mm (2.18 in)	58.0 mm (2.28 in)
Reqd. Number of Beds	4	4

Insulation testing

The insulation is one of the components of the regenerator design that is the least known. In order to separate the pressure boundary from the thermal boundary the insulation needs to be located inside of the pressure vessel. A search of similar pressure vessels revealed that the oil and gas industry was using a similar design for their Fluidized Catalytic Crackers (FCC), which are used to refine petroleum. FCC's are large pressure vessels 2-3 meters in diameter and up to 10 meters long. The inside is lined with a cast refractory and they are operated at around two bar of pressure [78]. Two bar is much

less than the 250 bar that the regenerators need to withstand, however the FCC design provides a good baseline for the regenerator. A fabricator of FCCs provided several recommendations for insulation that are used in FCCs and may also work for regenerators. There are two options for the insulation design, the first is directly exposing the insulation to the CO_2 similar to an FCC. The insulation needs to withstand many cycles of CO_2 entering and exiting the insulation matrix without degradation if directly exposed to CO_2. The other option is having a stainless steel liner between the packed bed and the insulation. Under this scenario the insulation needs to transmit the pressure force from the liner to the outer pressure vessel wall. Some proof of concept tests were developed to test both options.

There are several properties that the insulation must have in order to withstand the rigors associated with use inside of a regenerator especially when used without a liner. First, the insulation needs to have a low conductivity so that the thickness of insulation required is not too large (making the vessel diameter large). Second, it needs to be able to withstand the large, rapid pressure changes that the regenerator will experience on a cyclic basis. Third, the refractory cannot create excessive dust that could cause damage to turbomachinery. Fourth, the refractory cannot be excessively porous as any CO_2 volume in the insulation will result in an increase in carryover. Finally, the refractory needs to withstand erosion from the packed bed being in contact with the refractory. Four different insulation options were analyzed to determine which would meet all of these requirements for use in a regenerator without a liner. The first was Pyrogel, a silica aerogel formed into a flexible sheet. In addition to the flexible Pyrogel there were also three castable type insulations that could be mixed with water and poured into the shell and cured. Two were products recommended by Refractories West, a company that provides refractory and refractory services to the FCC industry. The first product recommended was Grefcon-98, which is 50 percent alumina refractory and is fairly porous. The second product recommended was Express-27 which is a very hard refractory made of almost all alumina. The final insulation being considered is Ziralcast-95 which is another alumina refractory. Ziralcast-95 has the additional advantage

of being filled with hollow alumina spheres which greatly cuts down on the void volume in the insulation. An image of each insulation and the reported conductivity of each of the insulations is listed in Figure 17 at a temperature of 450°C, the average temperature of the insulation in the high temperature regenerator.

k = 0.05 [W/m-K] [83]

(a)

k = 1.16 [W/m-K] [80]

(b)

k = 2.84 [W/m-K] [80]

(c)

k = 0.70 [W/m-K] [84]

(d)

Figure 17 Pictures of insulation samples before testing. (a) Pyrogel, (b) Grefcon-98, (c) Express-27, (d) Ziralcast-95

In order to test how the insulation will hold up to the conditions seen in a regenerator, a cylindrical sample of each was placed in pressure vessel and the pressure was cycled using industrial grade nitrogen gas. Figure 18 shows a picture of the test facility.

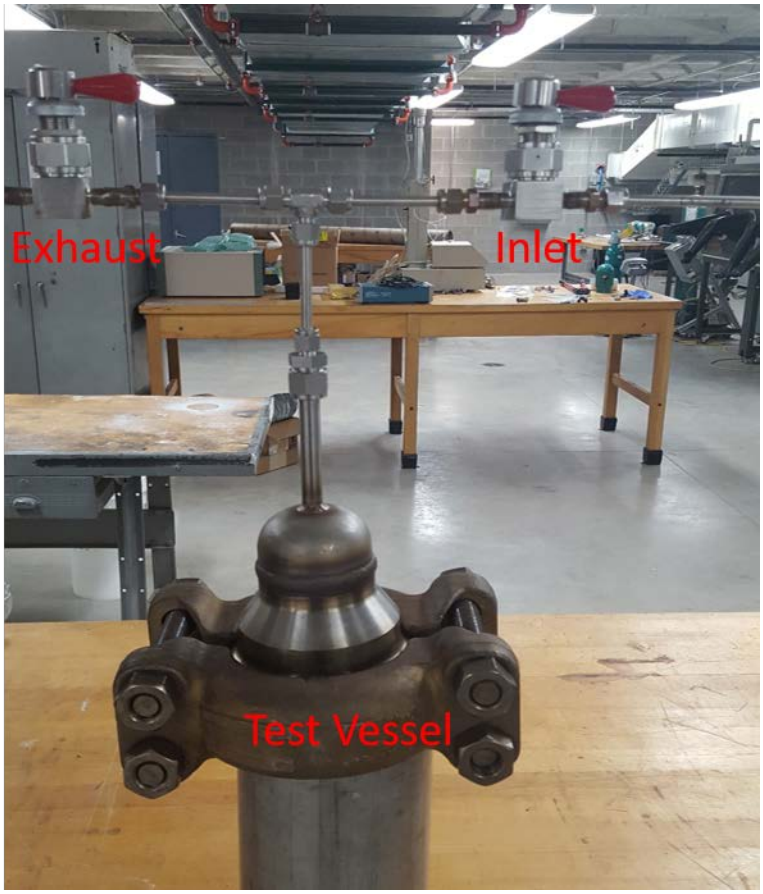

Figure 18 Pressure cycling test facility

Nitrogen was used for these initial tests since it has very similar properties at room temperature as CO_2 does at the operating conditions of the regenerators. The Pyrogel was cycled for 290 cycles with a maximum cycling pressure of 10.3 MPa. The three castable samples were cycled for 60 cycles under a maximum pressure change of 6.9 MPa. The samples were removed at regular intervals, so they could be inspected for damage and weighed to determine the weight loss of the sample. None of the samples experienced any cracking or loss of integrity from testing. The Pyrogel, Grefcon-98, and Ziralcast-95 all experienced low levels of initial dusting but it appeared that most of the dusting was caused by the

handling of the samples rather than from the pressure cycling. Express-27 did not experience any dusting. The weight loss after all of the pressure cycling is reported in Table 4.

Table 4 Conductivity for various insulations at an average temperature of 450°C and weight loss from pressure cycling

	Conductivity (W/m-K)	**Weight Loss Percent**
Pyrogel	0.05	0.78%
Grefcon-98	1.16	0.06%
Express-27	2.84	N/A
Ziralcast-95	0.85	0.11%

All of the samples with the exception of Express-27 created some amount of dust meaning that the insulation will need to be isolated from the CO_2 flow to prevent dust from reaching places where it could cause damage, such as bearings and valve seats. As a result, the insulated regenerator design will require some barrier between the inner packed bed and insulation.

Having a barrier between the bed and insulation means that there will be a pressure difference between the bed and insulation meaning the insulation will have to transmit the pressure force from the bed to the outer shell. Pyrogel has no structure and will readily collapse under any force thus, pyrogel cannot be used for insulation even though it has the lowest conductivity. The castable insulations generally have a high cold crushing strength (6,300 psi for Grefcon-98, 13,000 psi for Express-27) high enough to withstand the pressure exerted by the fluid (3,600 psi maximum) [85,86]. However, it was unknow how the insulation would behave under the cyclic load exerted by the changing pressure in the regenerator bed. Javier Martinez conducted a simple test to determine applicability which will be outlined below. Each refractory was cast into a thin walled stainless steel tube and caps welded on, sealing the tube. The new test samples were placed in the same test facility that was used for the pressure cycling as shown in Figure 18. All three of the refractory samples did not rupture proving they could work as insulation. For more information please see Martinez's thesis [87].

While designing the insulated regenerator there were significant concerns about thermal expansion and the stresses that would cause failure of the insulation. Since the outer wall will be kept significantly cooler than the inner liner the difference in expansion will be significant. One concern was that the castable insulation would not allow adequate expansion for the inner liner and bed. An alternative to the castable insulation was using a flowable insulation media that could still support the pressure force from the fluid. Evacuated particles are used as an insulation at low temperatures, and the same principle was applied to regenerators [55]. Sand was a good option since it can withstand high temperatures, has good strength, and relatively low conductivity. The first step to choosing an adequate sand was identifying a sand that could withstand the force of the fluid pressure without breaking down. Shawn Aakre used a hydraulic press to determine the stress-strain curves for six sand compositions, the test rig is shown in Figure 19.

(a) (b)

Figure 19 (a) Hydraulic press used to measure stress-strain of sand mixtures and (b) test cylinder filled with sand to be tested

The stress strain curve for the different sands are shown in Figure 20. Each sand was tested for 4-6 cycles of pressurizing to 11,000-14,000 psi then back to 0 psi. The final pressurization run for each is shown in Figure 20.

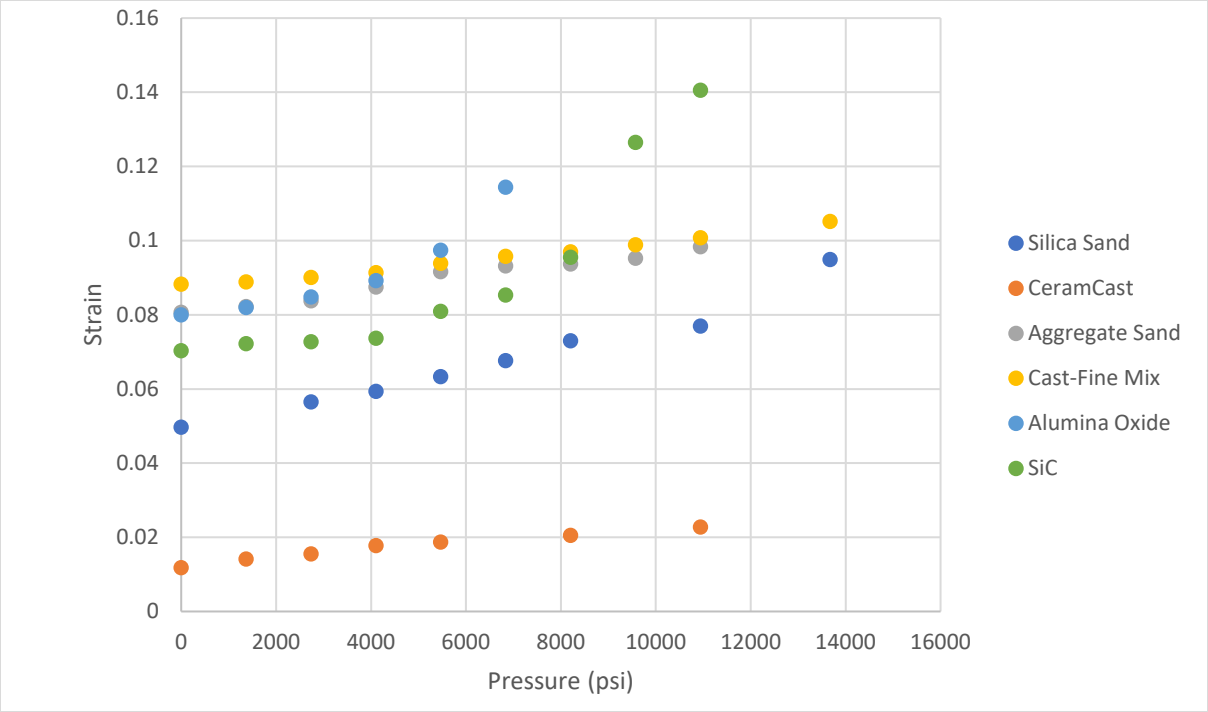

Figure 20 Strain vs stress for six different sand mixtures.

CeramCast sand held up the best to the pressure cycling due to its highly spherical particles which do not fracture when compressed. CeramCast is a casting sand and the thermal conductivity is not reported. Knowing the thermal conductivity is critically important to designing the regenerator because it specifies how thick the insulation must be. A simple test was set up by Paul Brooks to measure the conductivity of the CeramCast sand at elevated temperatures at atmospheric pressure and under vacuum. A cartridge heater was inserted into 1” x 0.120” tube and capped, the 1” tube was then inserted into a 2” pipe. The gap between the two tubes was welded closed and filled through a 3/8” port with CeramCast. Thermocouples were inserted at both the inner wall of the heater tube and the inner wall of the outside wall to measure the temperature difference. The temperature difference, geometry and known heater power is used to calculate the conductivity of the sand. A diagram of the test section and a picture of the inside construction is shown in Figure 21.

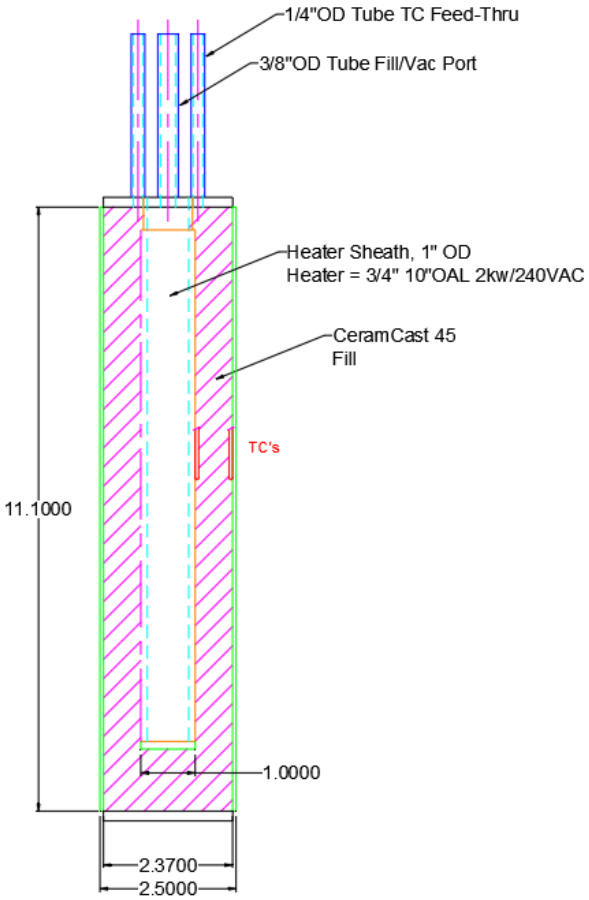

(a) (b)

Figure 21 (a) diagram of sand conductivity test section. (b) look at inside of constructed conductivity test section

The conductivity was measured with the sand at atmospheric pressure and under vacuum at an internal temperature of 500°C. The conductivity is listed in Table 5.

Table 5 Conductivity of sand at atmospheric pressure and under vacuum

Pressure	**Conductivity (W/m-K)**
1 Bar	0.8
Vacuum	0.2

The vacuum is important because it reduces the convection heat transfer between the sand particles. Without air to transfer heat, the only mechanisms for heat transfer are conduction between the particles and radiation between the particles. Point contact between the sand particles means conductivity between the particles is poor. For particles under cryogenic conditions the conductivity of the particles as a function of vacuum is shown in Figure 22.

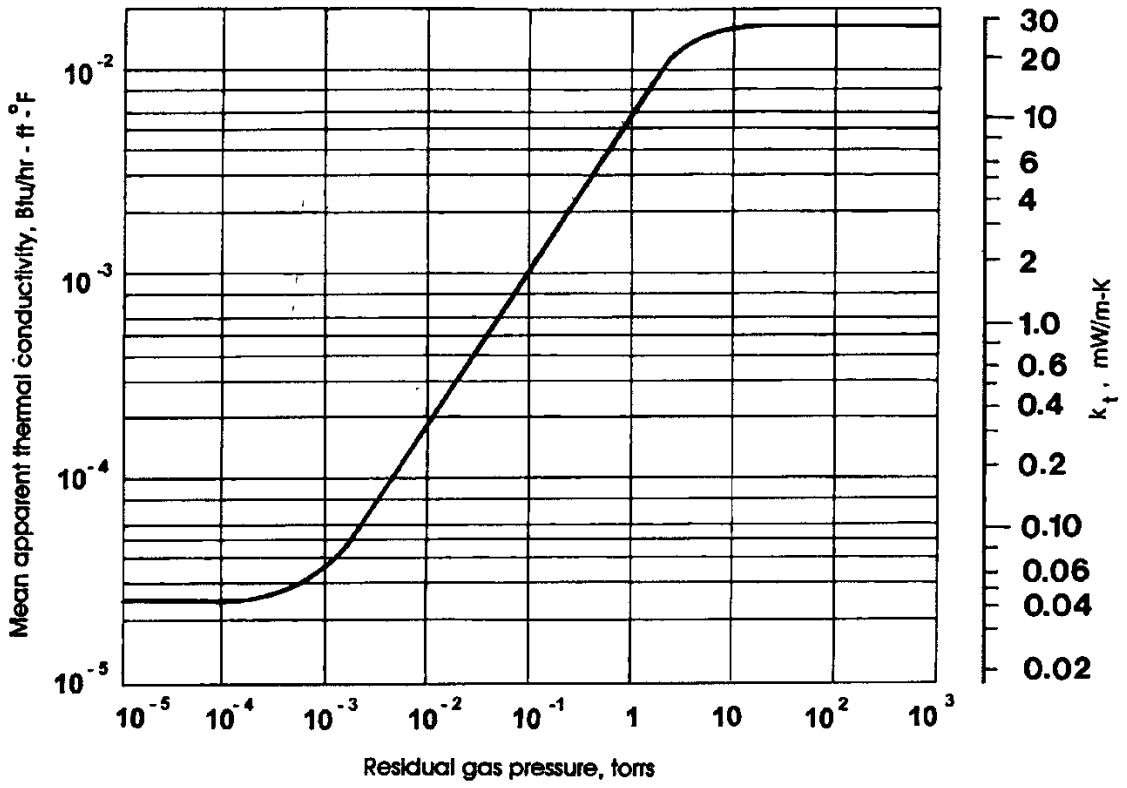

Figure 22 Conductivity vs gas pressure for an evacuated powder (30 to 80 mesh perlite) with nitrogen gas from [55]

Assuming a conductivity of 0.2 W/m-K the thickness of sand insulation needed is only approximately 1” in order to keep the wall below 375°C, the limit for type 91 steel [10]. Before a test regenerator was created at a 10kW size, a smaller test section was made in order to test the sand insulated design before significant time was invested in creating the 10kW regenerator. A small test

section was designed to be representative of the 10kW test, the design and pictures are shown in Figure 23.

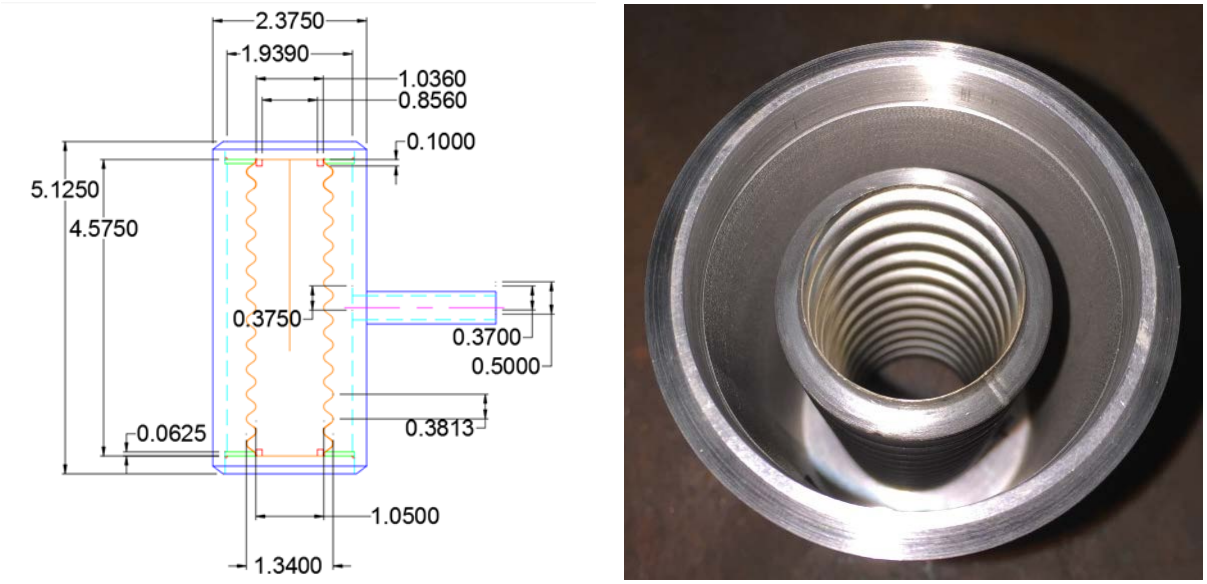

(a) (b)

Figure 23 (a) Sand insulation realistic test section design, (b) picture of inside of test section showing bellows wall and outer shell.

An inner vacuum tube is used to hold the packed bed, which allows for thermal expansion of the bed without causing excessive thermal strain. The inner bed is welded to a plate that separates the sand from the fluid in the cap. A hydrostatic tester was used to pressurize the inner bed up to 3500 psi. A pressure gage in the sand was used to indicate if the bed had broken. The test section was cycled 150 times at various pressures as listed in Table 6.

Table 6 Pressure range and number of cycles for sand insulation test section

Pressure Range (psi)	Number of Cycles
500-1000	10
1000-1500	10
1500-2000	10
2000-3000	10
2000-3500	10
1000-3500	50
0-3500	50

In addition to the pressure cycling the pressure was held at 3500 psi for 30 mins to ensure a leak would not form. Throughout all of the tests the test section did not leak, proving that the sand was able to effectively transmit the force from the inner shell to the outer wall. Combined with the testing done on the thermal conductivity, sand insulation seemed like the best option since it allowed for expansion and contraction of the inner shell, separate from the outer shell, while keeping the outer wall cool. The sand insulated design was chosen for use and incorporated into the cycle model and used for experimental testing. More information about the insulation used in our 10kW regenerator will be described in the Experimental Regenerator Design section.

10MW Cycle Model

A model was created of a regenerator that can determine the effectiveness, pressure drop, and carryover for a specific design, however it does not directly provide insight into how a regenerator might compare to a PCHE. A regenerator and a recuperator operating at the same effectiveness will have a significantly different effect on the system because of carryover in the regenerator. Regenerators also use many valves, which can represent a large portion of the system costs and need to be considered [13,88]. A complete cycle model is needed that can compare the thermodynamic performance and economics of regenerators vs recuperators.

At the start of this project, the 10MW STEP facility was in its early bidding phase, and it provided a good baseline design for the sCO_2 cycle. The STEP facility was designed to provide 10MW of electrical power with a thermal efficiency of approximately 50% operating using the RCBC configuration. The STEP cycle was modeled in EES assuming steady state operation [17]. Fluid properties for CO_2 were obtained using FIT [89]. An overview of the cycle along with values used for various components is shown in Figure 24.

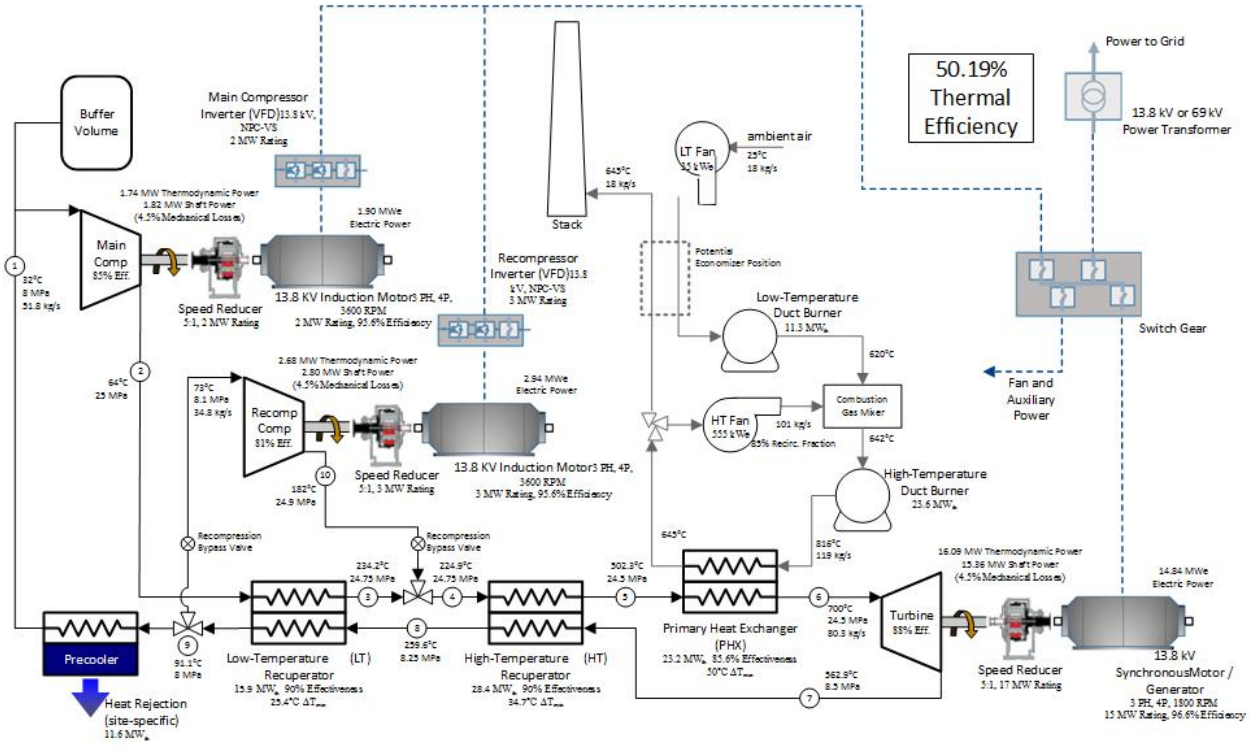

Figure 24 Operating conditions and component specifications of 10MW STEP facility from

Since the goal of this model was to determine the steady state cost savings of operating the cycle at the design point, simple 0-d isentropic efficiency models were incorporated for the turbomachinery. Isentropic efficiencies of the turbomachinery were chosen to be representative of a n-th of a kind cycle as recommended by [90]. The main compressor and recompressor isentropic efficiency was 88%, while the turbine isentropic efficiency was 92%. It was assumed that there were no losses in the power conversion equipment. The recuperators were modeled using a sub-heat exchanger model

described in [40] and implemented for EES by [26]. The primary heat exchanger and pre-cooler were not modeled, and instead were assumed to be adequately sized to always provide a constant specified exit temperature. A constant 20MW of heat input was assumed. An economic model of the 10MW cycle was created using costing data provided by Sandia [20,88]. Sandia reported cost per unit of cycle power for each component in the cycle; heater, recuperation, cooling, compression, and expansion. It was assumed that between the recuperator and regenerator cycle the balance of plant costs would be the same and only the recuperation costs would change. Sandia reported the costs on a per kWe basis, for the case of the recompression cycle the costs (excluding recuperation) was 1171 $/kWe [88]. Sandia specified a thermal efficiency of 46% for their cycle. For all costing calculations the cycle was assumed to have a thermal efficiency of 46%, otherwise an optimization could push the cycle to non-realistic operating points. For 20MW of thermal heat input the cost of the power block, with the exception of the recuperation, would be 10,773 k$ and would be constant no matter cycle thermal efficiency. Estimated recuperator costs were provided by project partner CompRex as a function of recuperator conductance (UA), the function is shown in Figure 25.

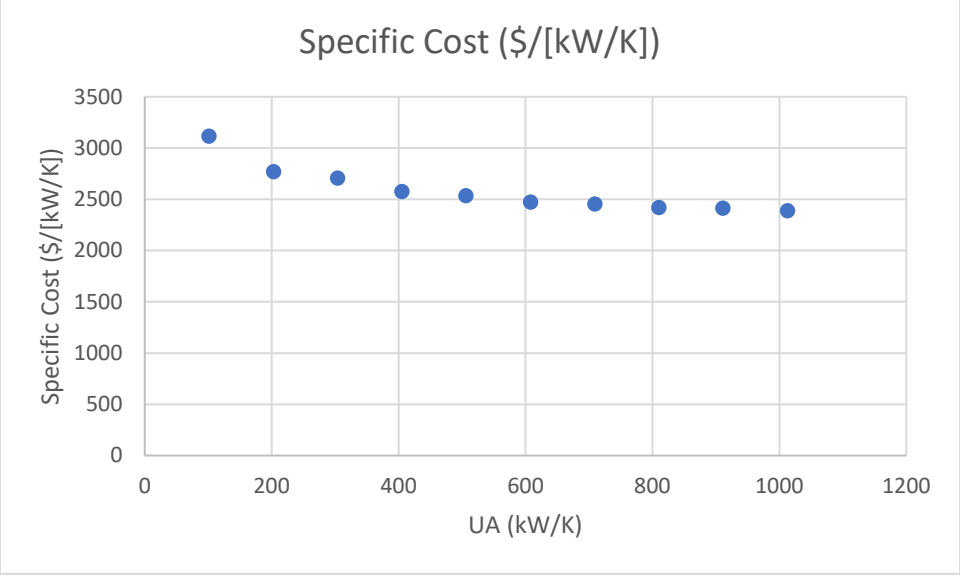

Figure 25 Specific cost of recuperators as a function of conductance from CompRex

The regenerator costs were calculated based on the size of the packed bed and using a rough estimate of the manufacturing costs. The mass of the packed bed material was determined from the model outlined in the Regenerator Model section and was assumed to be made of 304 stainless steel. The mass of the wall was calculated based on the BPVC requirements, it was assumed that the end caps would be hemispherical with the same thickness as the wall of the cylindrical section which leads to a conservative estimate of mass. Type 91 steel was used for the pressure vessel wall. Similarly, the mass of sand insulation needed was calculated from the size of the pressure vessel and the thickness of insulation needed, a conservative estimate being 50mm. The required mass of each component needed was multiplied by the specific cost. Costs for 304 and type 91 steel were determined using Design For Manufacture (DFM) a program that gives cost estimates for manufactured parts [91]. Insulation costs were determined using costs provided by the suppliers of CeramCast [92]. All of the costs are listed in Table 7.

Table 7 Specific costs of regenerator components

Material	Cost ($/kg)
304 Stainless Steel	4.17
Type 91	1.43
CeramCast	1.55

An additional 10% was added to the costs to account for any extra costs that might arise. A cost of manufacturing the shell was also calculated using DFM [91]. Since the size of the regenerators is approximately constant for all cases (due to the switching time being set as short as possible which will be discussed below) a constant manufacturing cost per bed is used. There are three costs to consider; the cost of casting the outer shell, welding the outer shell together, and finally creating the stainless liner between the insulation and packed bed. Costs for one bed are listed in Table 8.

Table 8 Construction cost estimates for single regenerator bed

Process	Cost per bed ($)
Casting Shell	18181.87
Welding Shell	2509.54
Insulation Liner	1201.68

The model can then calculate a rough order of magnitude cost for the regenerator beds based on their size.

One large unknown left out of the model is the heat source. It is modeled as a constant input at a constant temperature, however different heat sources have very different economics. Fossil energy has low capital costs, but a recurring fuel cost. Nuclear energy has very large capital costs and rather large operation and maintenance (O&M) expenses. Solar energy also has large capital costs, but has relatively small O&M costs [6]. The configuration of the solar field and associated thermal energy storage can drastically change how the power block is operated, from base load power to peaker plant. The goal of this research was to specifically look at the advantages of using a regenerator rather than a recuperator, making the choice of a heat source outside the scope of the project. Instead of conducting a more rigorous economic analysis such as the Integrated Rate of Return (IRR) a simple Levelized Cost of Electricity (LCoE) analysis was chosen instead. To make the analysis heat source neutral, the LCoE of only the power block was analyzed not considering the capital cost of the heat source or any ongoing O&M or fuel costs. The equation for LCoE is given in equation (1.18).

$$LCoE = \frac{TLCC}{\sum_{n=1}^{N} \frac{Q_n}{(1+d)^n}} \tag{1.18}$$

Where *TLCC* is the total lifecycle cost of the plant, in this case this is only the capital cost of the power block (balance of plant costs plus recuperation costs which depend on which type of heat exchanger is

modeled). Q_n is the amount of power produced in year *n*, this model assumed that the power output was constant year to year. *N* is the number of years of service for the plant, the standard length of time for a solar power plant is 30 year which was used [93]. *d* is the discount rate, 8.66% was used because it was the value given in the SunShot System Advisor Model [93]. This LCoE analysis in effect spreads the initial capital costs of the power block over the total amount of electricity produced in the lifetime of the plant, discounted to put the value of the electricity in today's dollars.

Cycle Parameters

There are many inputs to the model that need to be adjusted in order to determine the optimal design for the regenerator system. The objective statement is the lowest possible LCoE when subject to reasonable constraints for the optimization parameters. There are two types of parameters that need to be optimized, monotonic and non-monotonic. Monotonic parameters are those that will always cause LCoE to decrease over the range, for example the LCoE will always be lower when increasing the turbine inlet temperature. Monotonic parameters must be constrained to a reasonable value. All of the possible parameters are shown in Table 9.

Table 9 Independent variables in 10MW cycle model

Monotonic Parameters	**Non-Monotonic Parameters**
Compressor Discharge Pressure	Regenerator Effectiveness
Compressor Inlet Temperature	Compressor Inlet Pressure
Bed Switching Time	Recompression Fraction
Bed Sphere Size	Regenerator Pressure Drop
Void Fraction	
Turbine Inlet Temperature	

These parameters are inputs to the model, and the model returns the cycle costs, thermal efficiency, and LCoE. To see the effect the parameters, have on LCoE and thermal efficiency, the LCOE corresponding to each parameter is plotted over a reasonable range to show their effect on the cycle. These plots cannot be used to find the optimal regenerator design point because all parameters must be optimized simultaneously to determine the optimal regenerator design. However, the plots provide insight into how each parameter effects thermal efficiency and LCoE. For each plot a parameter will be varied which will change the cost of the regenerator and thermal efficiency of the cycle. Figure 26 shows the LCoE and thermal efficiency as a function of the compressor discharge pressure.

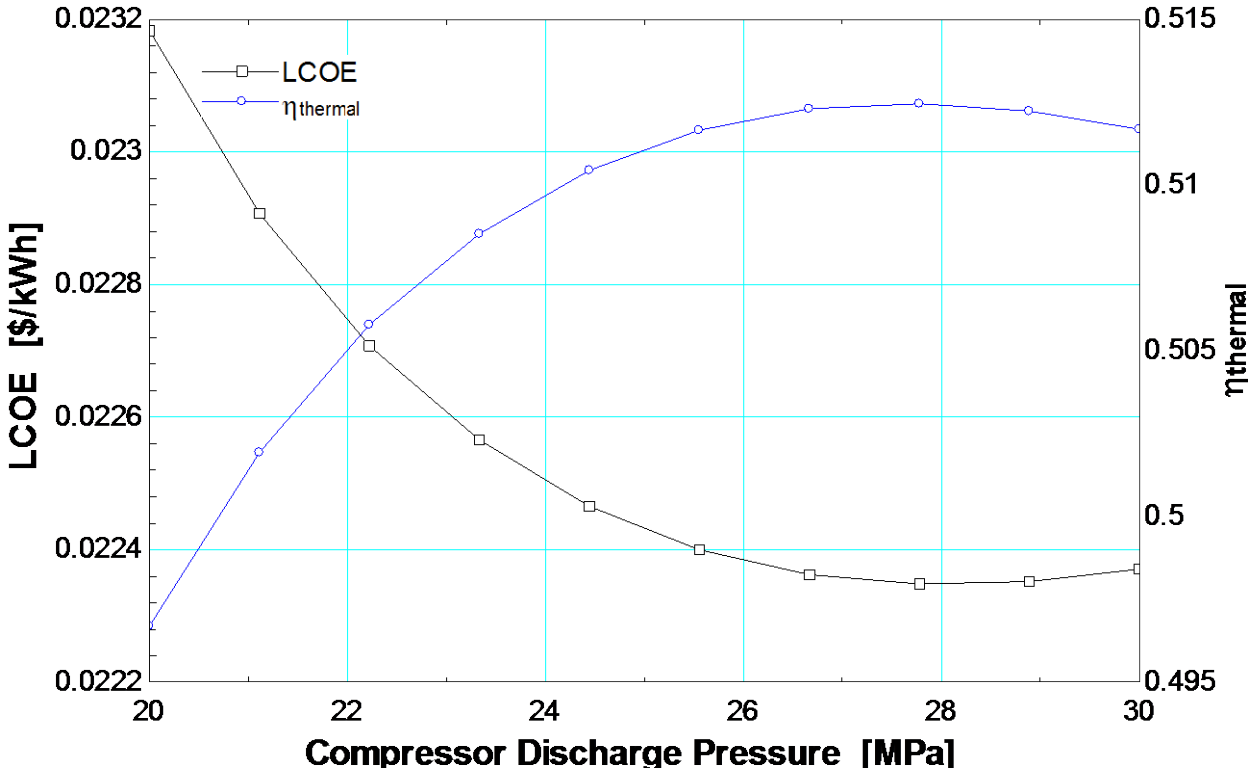

Figure 26 LCoE and thermal efficiency of the cycle as a function of compressor discharge pressure.

Figure 26 clearly shows that as discharge pressure increases, the thermal efficiency also increases to a maximum near 29MPa. At higher pressure ratios, more energy is produced in the turbine, increasing thermal efficiency. LCoE shows a decreasing trend with higher discharge pressure, due mainly to the fact

that the cycle is becoming more efficient and there is little increase in cost (apart from the thickness of the regenerator wall). One of the problems with this analysis is that it does not consider the additional costs that would be incurred by operating at higher pressure. In particular, the piping and turbo-machinery will have to be significantly larger to survive at these high pressures. The widely accepted limit for the discharge pressure is about 25MPa which is about the limit for currently available piping materials [20,88]. As a result, the model was limited to a 25MPa discharge pressure at all times.

The compressor inlet temperature has a drastic impact on efficiency of the cycle. A lower inlet temperature to the compressor will decrease the amount of work needed for compression because less energy is needed to compress denser fluids. However, more recuperation is needed to make up for the additional heat rejection. A plot of LCoE and thermal efficiency as a function of compressor inlet temperature is shown in Figure 27.

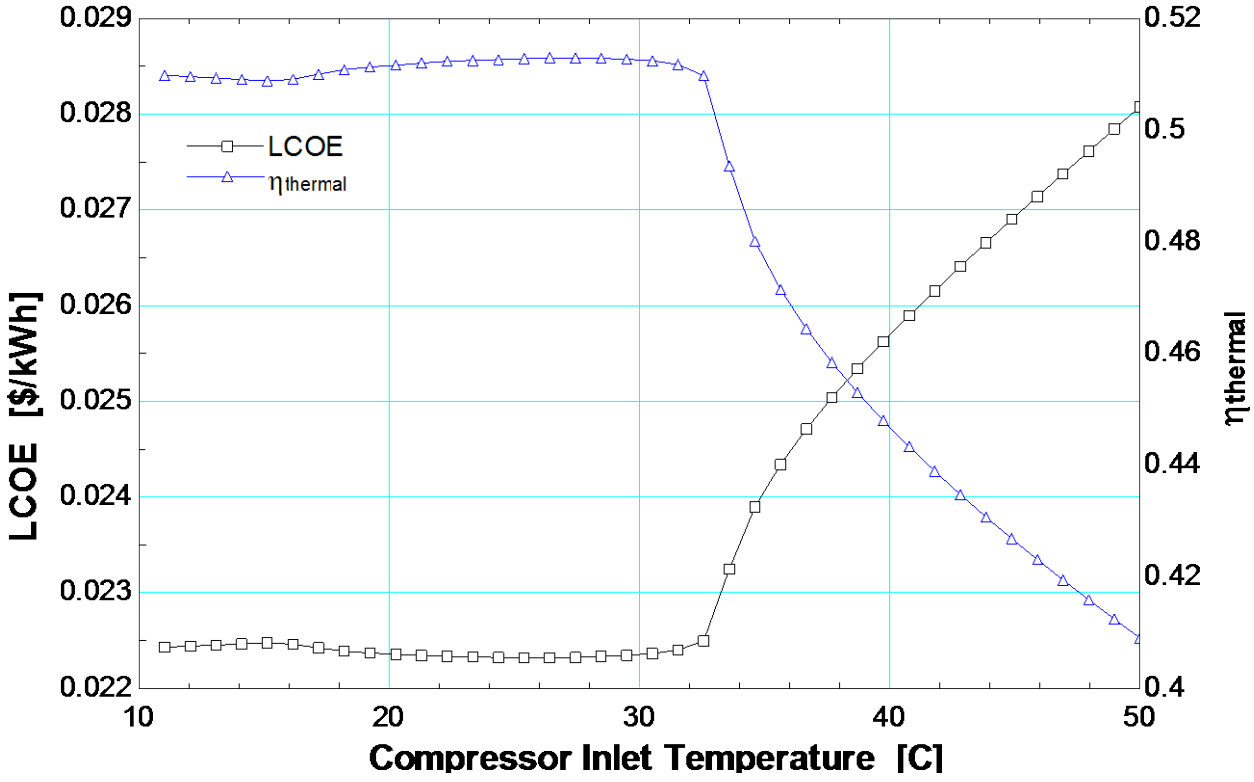

Figure 27 LCoE and thermal efficiency as a function of compressor inlet temperature

Below 32°C the thermal efficiency is relatively constant, above 32°C the thermal efficiency decreases because of the decreased density. This curve changes drastically when the inlet pressure is changed since the cycle operates best when the inlet to the compressor is near the pseudo-critical point. A lower limit is set on temperature of 32°C since this was the temperature specified by the SunShot model [93].

Switching time is important because it controls how large the regenerator beds need to be. The shorter the switching time the smaller the bed can be. However, a very short switching time can also lead to excessive wear on the valves, as well as a thicker wall needed to account for the increased number of stress cycles. A plot of LCoE and thermal efficiency as a function of switching time is shown in Figure 28.

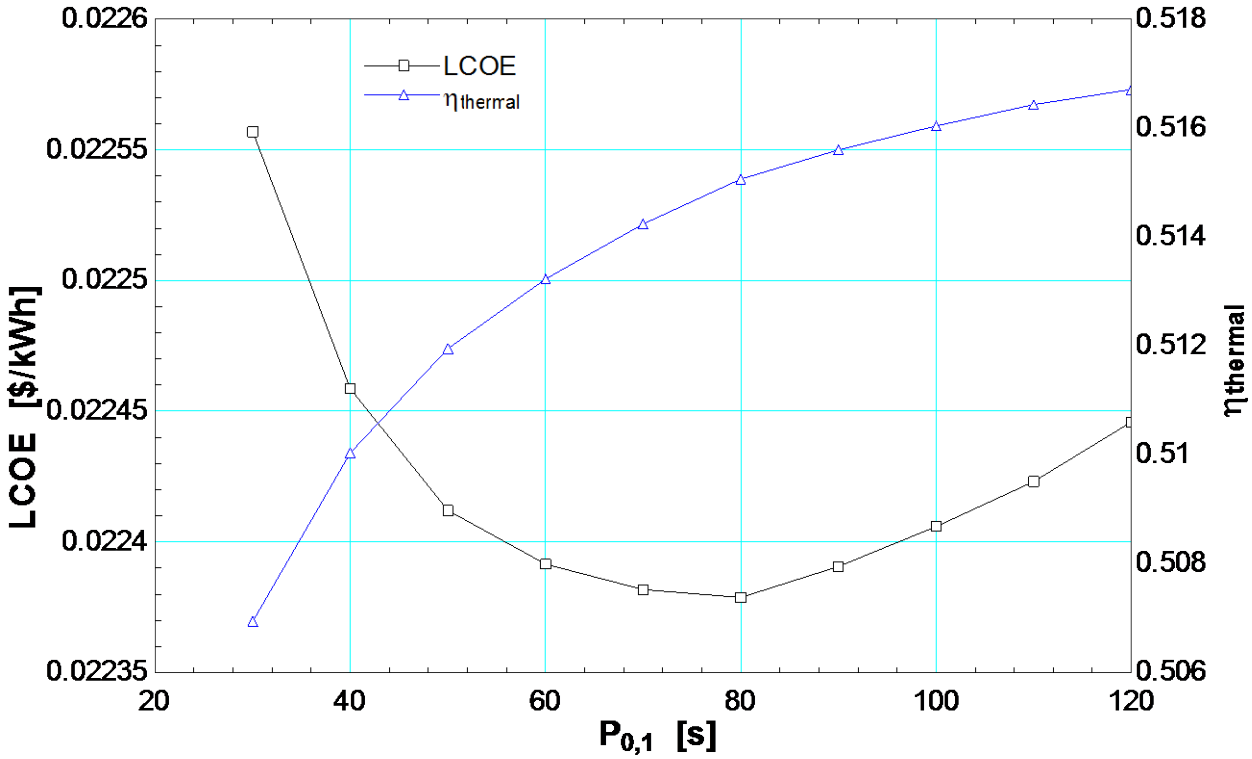

Figure 28 LCoE and thermal efficiency as a function of switching time

Figure 28 shows an interesting behavior in that thermal efficiency decreases even as LCoE decreases when going to shorter switching times. What this means is the cost savings of having a smaller bed is

more important the thermal efficiency loss from increased carryover. There is a set volume in the headers of the regenerators that contributes to carryover that is independent of regenerator size. As a result, at short switching times there is more carryover. The valves for the 10MW plant will be large and take a significant amount of time to actuate. The switching time needs to be much longer than the valve actuation time. A lower limit for switching time was set at 45 seconds as this was considered the minimum amount of time needed for the cycle to operate properly.

The regenerator packing sphere diameter can also be optimized, up to a point. Changing the sphere diameter dramatically affects both the pressure drop and NTU of the regenerator. Generally, the smaller the sphere diameter the higher the surface area and heat transfer coefficient, which increases NTU and thus effectiveness. However, when the hydraulic diameter of the passages in the bed get too small the pressure drop for constant mass flux can be very high. The regenerator model will size the bed to a specified pressure drop, meaning that for very small sphere diameter the bed has a small aspect ratio (length/diameter) in order to achieve the proper pressure drop. A bed with a large diameter requires more wall material and insulation, which increases the cost. Having a very small aspect ratio also invites issues with jetting through the bed, where the bed mass near the wall is not fully participating in the heat transfer process. A plot of LCOE and thermal efficiency as a function of sphere diameter is shown in Figure 29.

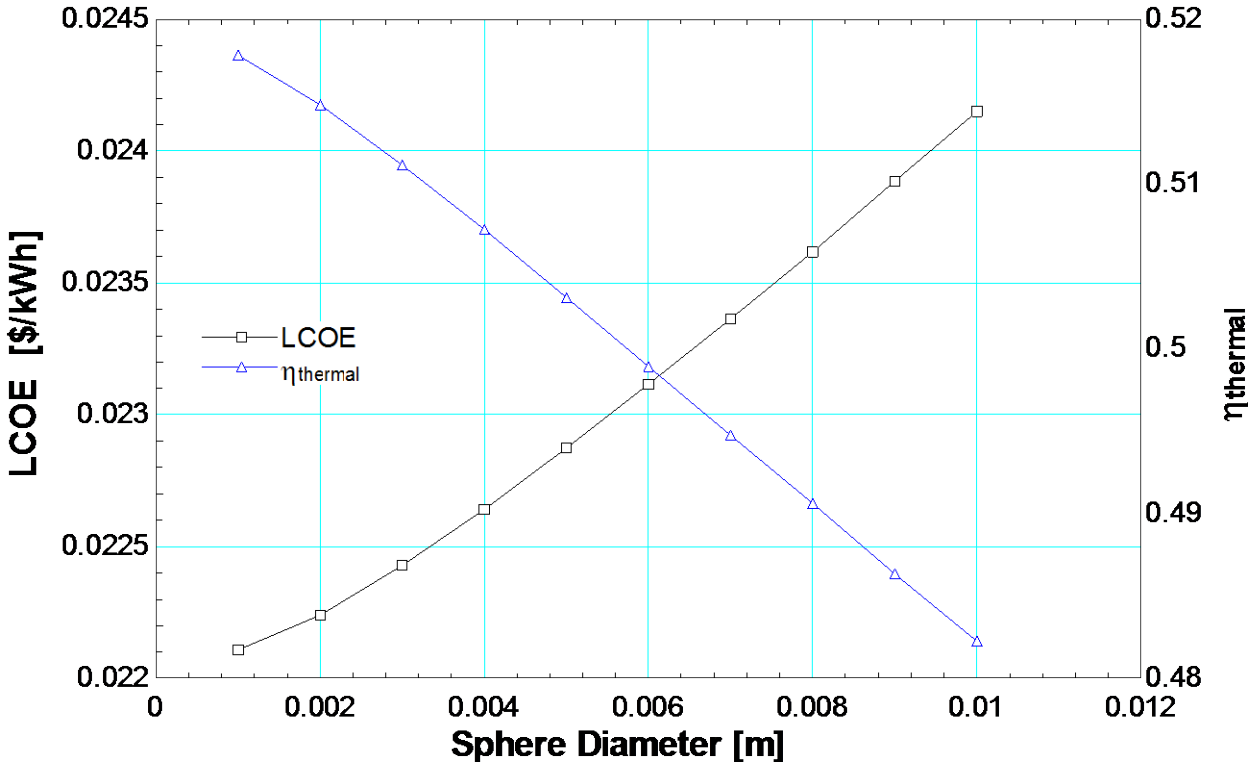

Figure 29 LCoE and thermal efficiency as a function of sphere diameter

It is clear that going to smaller sphere diameter is universally favored, even if it leads to some impractical aspect ratios. A lower limit was set at 3mm (approximately 1/8”) as this limited the aspect ratio to reasonable values (around 1) and were readily attainable.

Changing the void fraction by adjusting the fill geometry is an attractive optimization parameter since carryover is highly dependent on the void volume in the bed. The lower the void volume the lower the amount of carryover in the bed, increasing cycle efficiency. Additionally, the pressure vessels can be smaller at lower void volume because the same amount of packed bed mass can be stored in the same volume. A plot showing LCoE and thermal efficiency as a function of void fraction is shown in Figure 30.

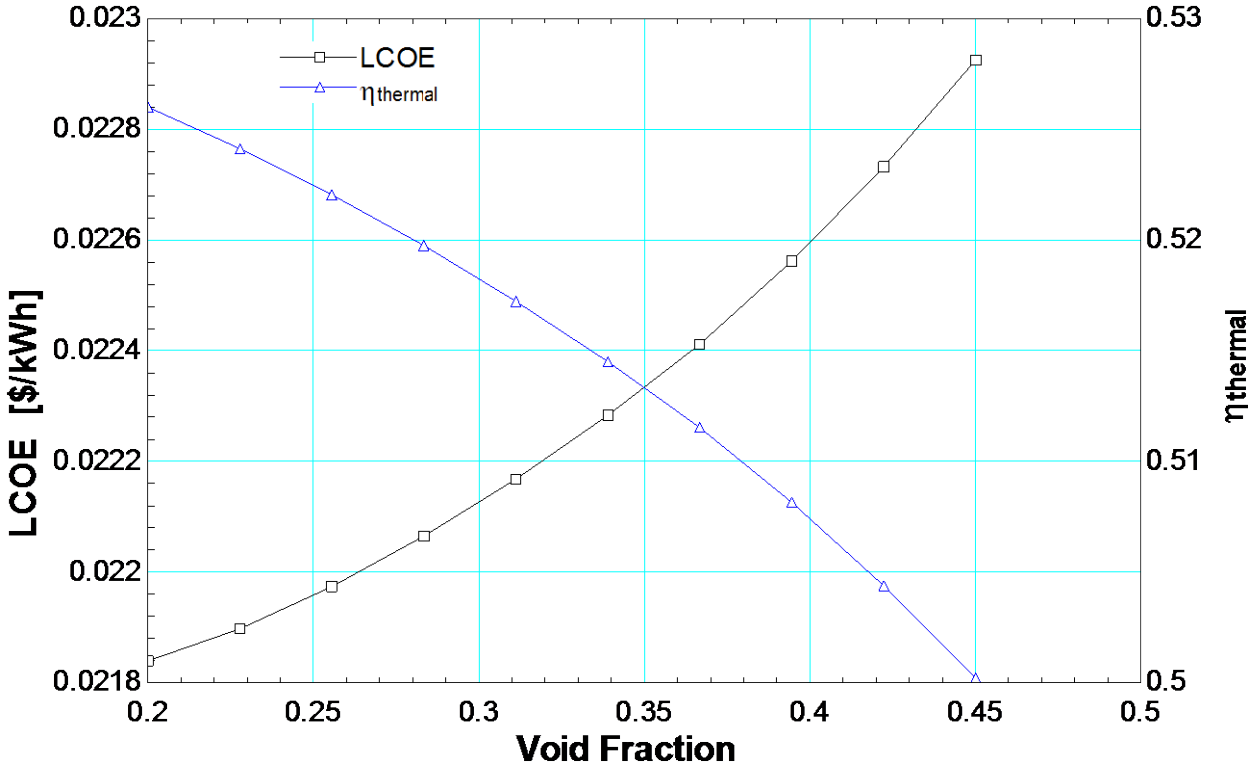

Figure 30 LCoE and thermal efficiency as a function of void fraction

Figure 30 clearly shows that lower void fractions are favored, however there is a lower limit on void fraction for packed spheres. Ideally packed spheres can have a void fraction of 26% [94]. It is difficult to reach 26% void fraction. For randomly packed spheres the void fraction is in the range of 37% which was measured from experimental testing. One option to have a lower void fraction would be to have a binary system of spheres which can reach void fractions of 20% [94]. Binary packing was briefly explored and is discussed in the Future Work section; however it was not chosen because of the lack of models available for pressure drop and heat transfer coefficients. For this model a single sphere size with 37% void fraction will be used.

Finally, the Turbine Inlet Temperature (TIT) is also a monotonic parameter, any increase will result in more power output without any additional costs. This is illustrated in Figure 31.

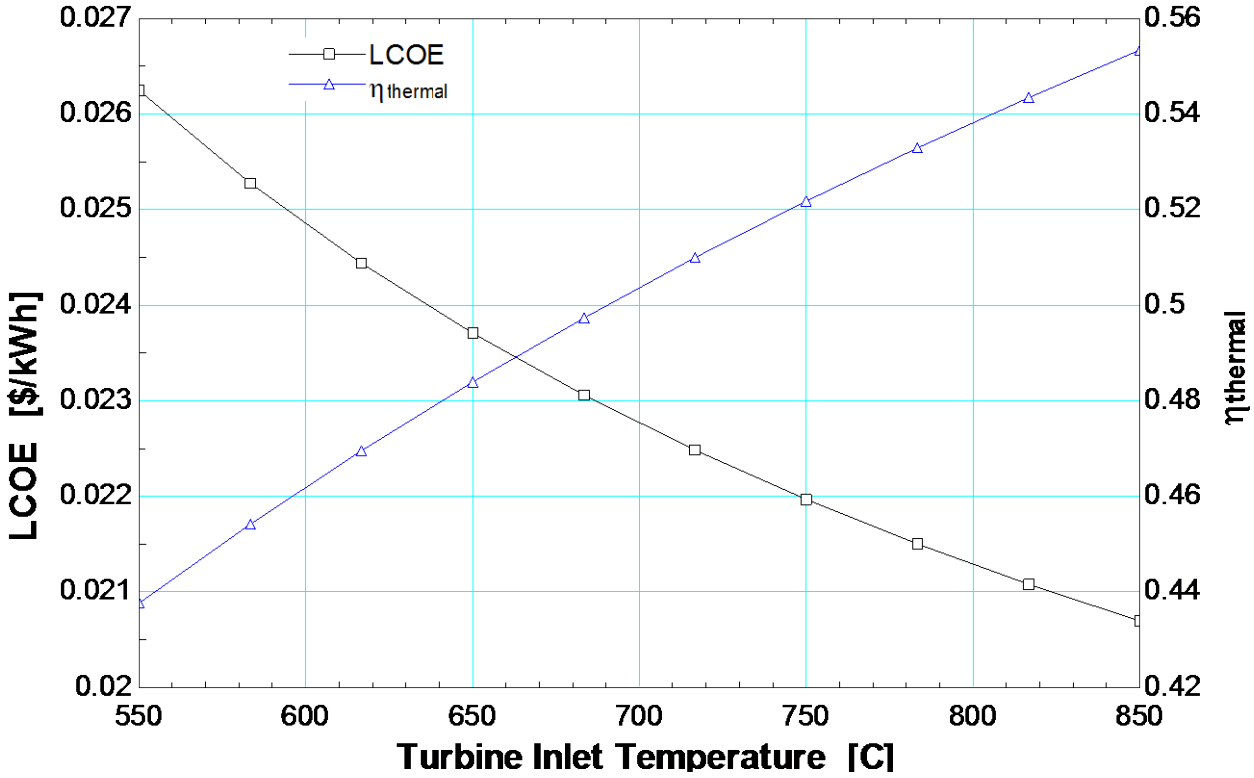

Figure 31 LCoE and thermal efficiency as a function of Turbine Inlet Temperature

At a certain point increasing the TIT will become uneconomical because of the high temperature materials needed to construct the primary heat exchanger and the turbine. An upper limit was set at 720°C for the TIT as this is the limit described in the DOE's SunShot initiative. Without having the temperature sensitivity of cost in the model it would be unfair to assume the TIT could be increased significantly above 720°C.

The effectiveness of the regenerator has a dramatic effect on the thermal efficiency and cost of the cycle. At high effectiveness more heat is recovered, leading to higher thermal efficiency. However, higher effectiveness also causes an increase in carryover. A plot showing LCoE and thermal efficiency as a function of regenerator effectiveness (both high temperature and low temperature regenerator are set to the same effectiveness) is shown in Figure 32.

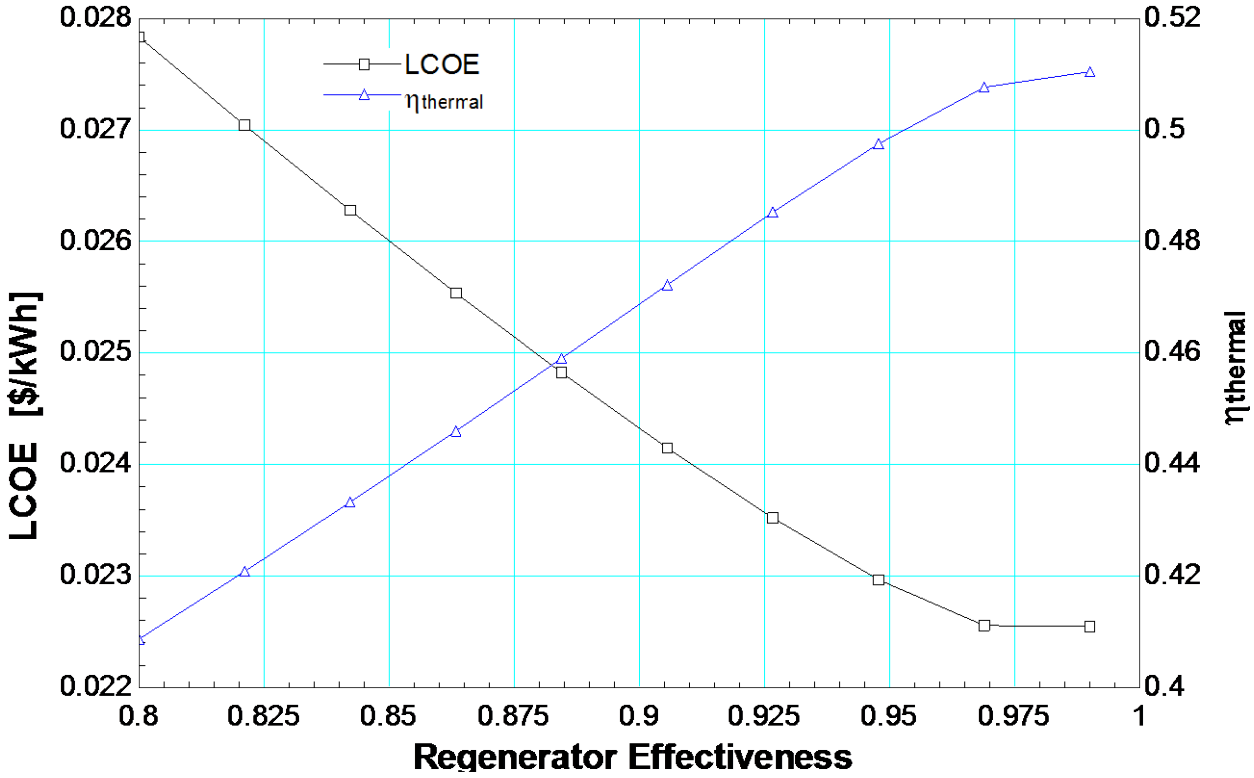

Figure 32 LCoE and thermal efficiency as a function of regenerator effectiveness (both regenerators set to same effectiveness)

At low effectiveness the thermal efficiency is low which in turn lowers the LCoE of the cycle. At approximately 97% effectiveness the LCoE does not decrease with higher effectiveness because the additional cost of the regenerator is too great, and the additional carryover begins to cause the thermal efficiency to level off. Not shown in Figure 32 is the optimal effectiveness of the high and low temperature regenerator when optimized separately. Since CO_2 is denser at lower temperatures, more carryover is seen in the low temperature regenerator. An optimal design will slightly reduce the effectiveness of the low temperature regenerator in order make it smaller and therefore reduce this effect while having a higher effectiveness for the high temperature regenerator. Optimization of each regenerator effectiveness separately is shown in the Optimized Results section.

The compressor inlet pressure is very important to the efficiency of the cycle. Near the critical point the density of the CO_2 increases greatly which cuts down on compressor power, however further

from the critical point the thermal efficiency of the cycle can change drastically. Figure 33 shows the LCoE and thermal efficiency as a function of compressor inlet pressure.

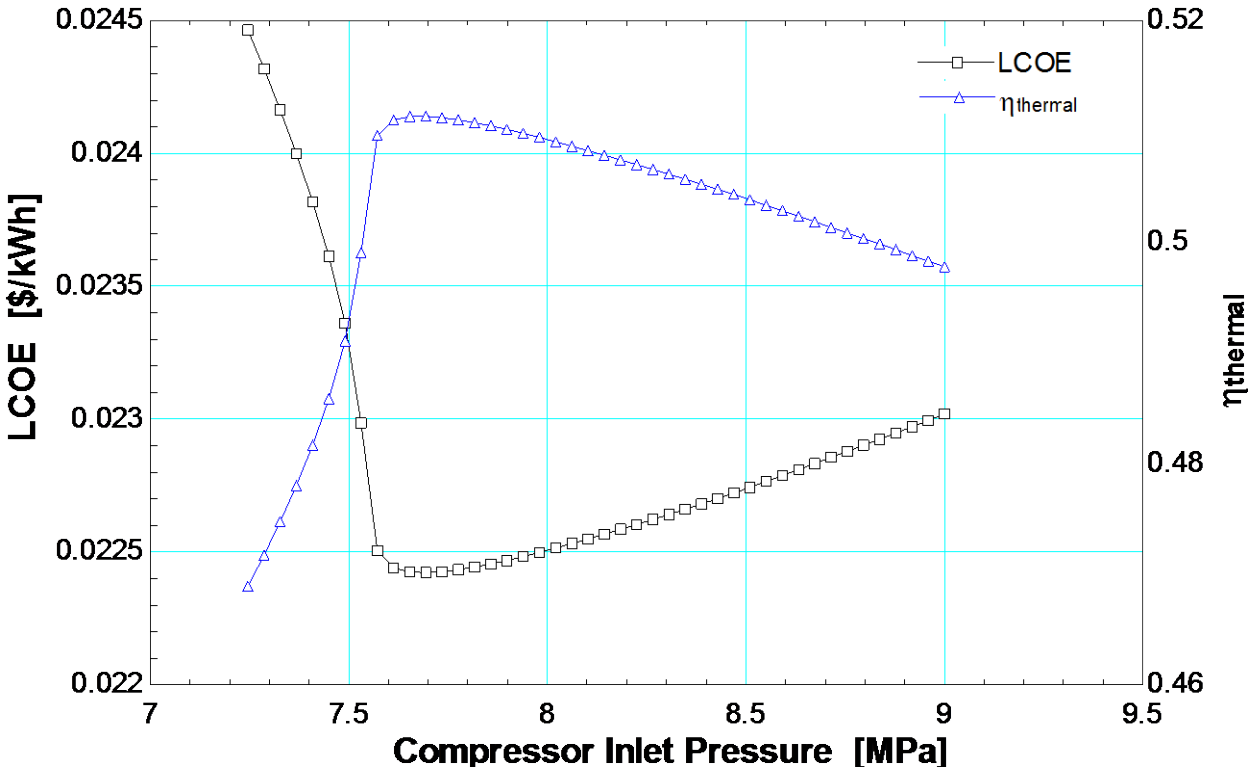

Figure 33 LCoE and cycle thermal efficiency as a function of compressor inlet pressure

The pseudo-critical point is near 7.7 MPa for this case and as a result the thermal efficiency is highest here. At lower pressures the work required for the compressors is too high, resulting in low efficiency. At too high of pressures, the work out from the turbine decreases, which also hurts efficiency. Compressor inlet pressure needs to be optimized as the compressor inlet temperature changes in order to determine the optimal operating condition.

The recompression fraction is used to define the amount of flow that goes through the recompressor as compared to the main compressor. By tuning the amount of flow going through each compressor the cycle can be optimized [26]. Fluid being compressed by the main compressor will be

cooler (because it has gone through the precooler) and will therefore have a lower specific work needed for compression. However, fluid passing through the recompressor will come out warmer, lowering the amount of recuperation needed in the cycle. The recompressor also works to change the capacitance rates in the regenerators. By controlling the amount of flow through each blow of the regenerator, more heat can be recovered from the cycle making it more efficient. A plot showing the LCoE and thermal efficiency as a function of recompression fraction is shown in Figure 34.

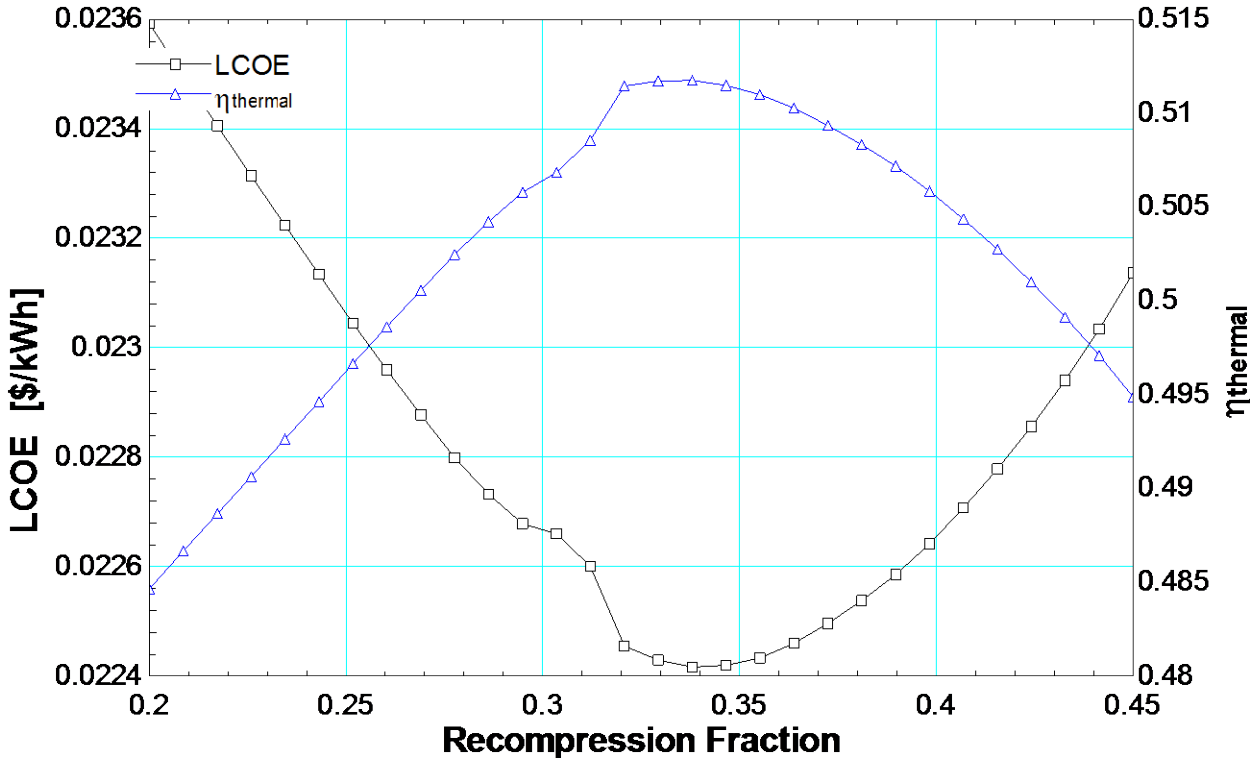

Figure 34 LCoE and thermal efficiency as a function of recompression fraction for 10MW cycle

At low recompression fraction the low temperature regenerator is unbalanced, leading to a lower cycle efficiency. As the recompression fraction increases the low temperature regenerator becomes more balanced until it reaches a maximum heat recovery around a recompression fraction of 0.34. At this point the regenerator is most balanced, so as the recompression fraction continues to increase it only leads to more unbalance in the low temperature regenerator. Additionally, with more mass going

through the recompressor (which requires more work since the fluid is warmer) the total compressor work also increases, driving down thermal efficiency.

Pressure drop in the beds can also affect performance. The system model is set up to size the bed for a specified pressure drop by adjusting the bed aspect ratio. Figure 35 shows the LCoE and thermal efficiency as a function of pressure drop.

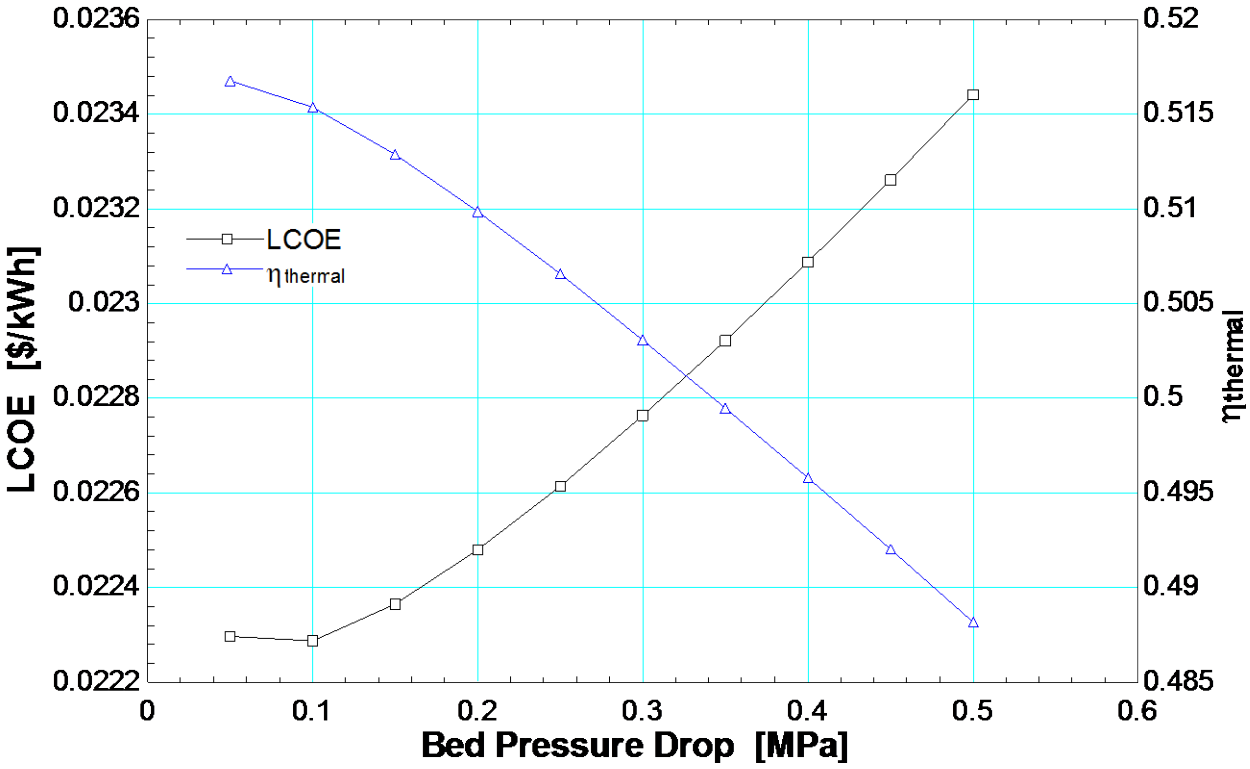

Figure 35 LCoE and thermal efficiency as a function of bed pressure drop

At low pressure drop the thermal efficiency is higher, but the cost is also higher (due to the thicker wall needed for the low aspect ratio bed). At higher pressure drops the thermal efficiency drops off because of work lost due to pressure drop. An optimal value occurs near 0.1 MPa where the bed costs are low, and the thermal efficiency has not been degraded too greatly by pressure drop.

Bed packing material can drastically affect the performance of the regenerator. An ideal bed would have a very small void volume, low pressure drop, high heat capacity, and low axial conduction. A

study of different material for the bed was conducted in order to determine which material would result in the best regenerator cost and performance. The packing material needs to be low cost and have a high volumetric specific heat capacity. A high volumetric specific heat capacity means that a smaller pressure vessel can be used because less volume is needed to store the same amount of energy, which reduces cost. For solid materials the volumetric heat capacity changes much less than the mass specific capacity does, with the variations coming from differences in the size of the atoms [95]. The volumetric heat capacity for several materials compatible with CO_2 are shown in Table 10.

Table 10 Volumetric specific heat capacity of potential regenerator packing materials. Data taken from [17].

Material	**Volumetric Specific Heat Capacity (kJ/m^3-K)**
304 Stainless	4415
316 Stainless	4380
Inconel 718	3828
Aluminum	2786
Titanium	2672
Uranium	2846
Zirconium	2110
Gold	2736
Aluminum Oxide	4426
Silicon Carbide	3872
Titanium dioxide	3651
Soda Lime Glass	2226
Borosilicate Glass	1847

Table 10 shows that stainless steel actually has one of the best volumetric heat capacities, even compared with very dense metals such as gold or uranium. Some ceramics also have favorable properties, high heat capacity and low cost. 304 stainless seems is the best option since it has the highest volumetric heat capacity, has relatively low cost, can be easily formed into many shapes, and is compatible with CO_2 at the regenerator cycle conditions (max 565°C and 25 MPa).

The geometry of the packing material can also be optimized. Ideally the bed would have zero void volume, no axial conduction and no pressure drop. Of course, this is impossible, a packed bed of spheres was finally chosen because of its relatively small void volume, low axial conduction, and predictable pressure drop. Some other options that were explored but not used were cylinders, foams, and pins. Cylinders of stainless steel could cut down on the void volume in the regenerator if two sizes were used, however they would also allow significant axial conduction which could degrade the temperature profile in the bed reducing the effectiveness. Metal or ceramic foams could be custom tailored to the regenerator, but uncertainties in pressure drop and void volume correlations meant it would have been a poor choice for modeling and experimental testing. It is possible that with more research, foams could provide an improvement to performance. Another option are stainless steel pins, which are think shavings of stainless steel. The pins provide a void fraction of 15%, but with no pressure drop or heat transfer correlations it is impossible to use them in an experiment to verify a model. Future work can be done to determine if a performance increase can be gained by switching to pins.

A normal regenerator system would have only two beds, one experiencing the HtCB and the other experiencing the CtHB. However, when the beds go through carryover, there is no flow through the cycle, which results in unsteady flow through the turbomachinery. However, valve operating times are on the order of 3-5 seconds which is long enough to cause significant pressure fluctuations. The solution to this is two-fold, first by using buffer volumes some of the fluctuations can be damped out, and second by dividing the two bed system into four. With four beds there are two ways to size the beds. The first would be to divide the total packed bed mass from the two bed system equally into four beds, which will be called the divided system. In this scenario all 4 beds have flow through them at the same time, however when switchover occurs two of the beds are taken offline and the other two beds must make up for the entire mass flow of the cycle, which increases pressure drop. The second way to size the system is to take the two bed system and double it, essentially creating two separate systems,

this will be called the doubled system. Under this method only two of the beds would have flow through them at a time, while the other two beds went through switchover. In the doubled system the beds never have an increased pressure drop condition because they are already sized for the full flow. The doubled system is significantly more expensive than the divided system since twice as much mass is needed for the bed and the valves must be sized for the full flow. Deciding which system to use depends heavily on the valves used and their corresponding cost. FlowServe was a partner on the project and was able to size valves for each of the conditions provided. FlowServe chose y-pattern globe valves for their reliability (the valves must withstand millions of cycles) and fast actuation time. Four valve/bed configurations were sized and costed, a low pressure drop (30 kPa) and high pressure drop (90 kPa) option for both the divided and doubled system. A valve size was provided that would approximately fit the pressure drop constraint, the actual pressure drop was calculated according to the operating conditions and valve Cv [96]. These costs and calculated valve pressure drops were fed into the 10MW model and used to determine the LCoE and thermal efficiency for each configuration, and an optimization was run to minimize LCoE with effectiveness, pressure drop, compressor inlet pressure, and recompression fraction being optimization variables. The results of the comparison are shown in Table 11.

Table 11 Model results for four different valve options

	Option 1	Option 2	Option 3	Option 4
Compressor Inlet Pressure (MPa)	7.75	7.75	7.95	7.75
Recompression Fraction	35.3	32	34	35.3
Low Temp Recuperator Effectiveness (%)	96.5	95.4	96.1	96.8
High Temp Recuperator Effectiveness (%)	98.2	98.2	98.7	98.2
LCoE ($/kWh)	0.02256	0.02238	0.0245	0.02393
Thermal Efficiency (%)	51.0	50.2	49.3	48.8
Low Temp HX Cost (k$)	203	215	261	285
High Temp HX Cost (k$)	209	210	290	318
Valve Cost (k$)	1492	1164	2348	1660

There is a significant difference between options 1-2 (divided) and 3-4 (doubled) where the cost of the valves is significantly increased, and the thermal efficiency is significantly decreased. For the doubled system the valves need to be significantly larger to achieve the same pressure drop, increasing costs. The drop in efficiency comes from the increased carryover as a result of the larger beds in the doubled system. Since it was determined that the fluctuations caused by the increased pressure drop would not cause significant problems with operation, the divided case was chosen. Option 1 was chosen over option 2 because of the increase in efficiency with a marginal increase in cost. When looking at the system with heat costs included, a 0.8% increase in thermal efficiency will more than pay for the extra 350k$ in costs.

Another advantage of using a four bed system is the ability to cut the amount of carryover in half. When switchover occurs one bed is filled with high pressure CO_2 which is conventionally expanded back to the inlet of the compressor while the other bed is pressurized with CO_2 from the compressor discharge. However, if instead the high pressure bed is used to prefill the low pressure bed, the amount of mass that is returned to the compressor without passing through the turbine is cut in half. A diagram of this option is shown in Figure 36.

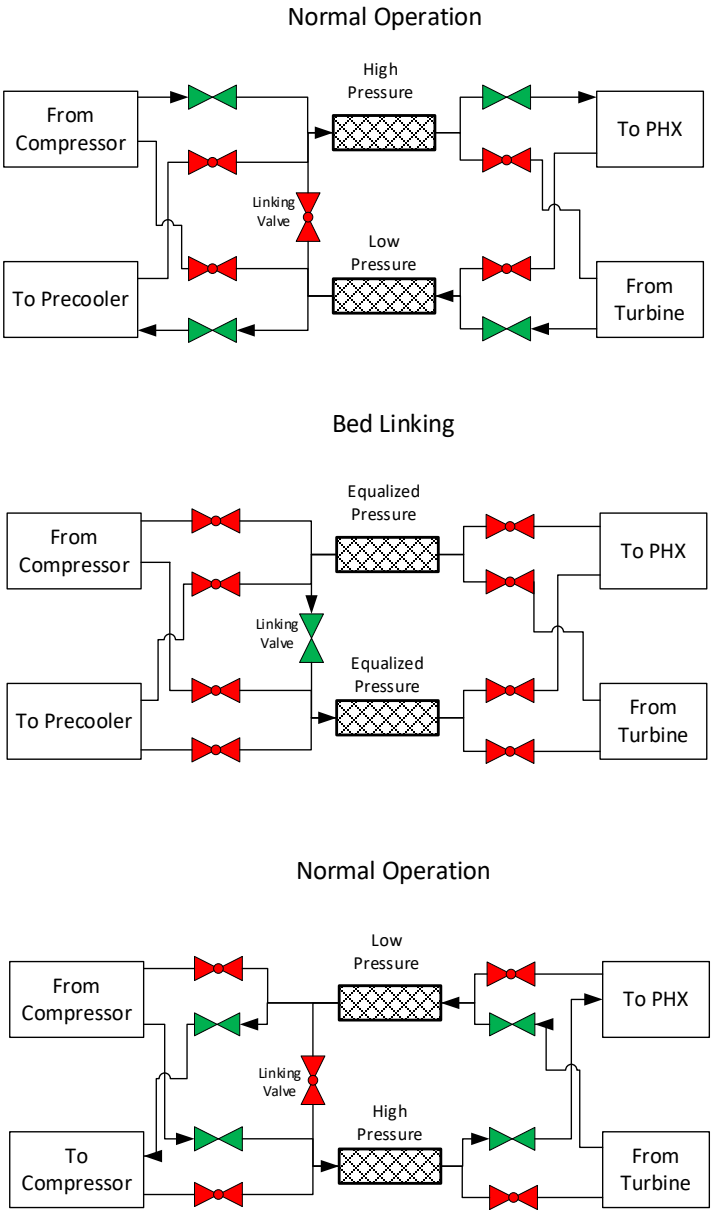

Figure 36 Bed linking valve operation

Four beds are needed for continuous flow while the equilibration process occurs. The bed linking valve can be much smaller than the flow valves and is therefore much less expensive (15k$). Cutting the carryover in half increases the thermal efficiency by 2.2%. For all cases shown it was assumed that a bed

linking valve was employed to reduce the carryover since a large increase in thermal efficiency can be achieved at low cost.

Optimized Results

As discussed above, the goal of the optimization is to have the smallest possible LCoE. Optimizing the regenerator system is more difficult than simply optimizing each of the parameters separately. The monotonic parameters have been set at a reasonable limit. For the non-monotonic parameters, an optimization needs to be run on all variables simultaneously in order to capture the interaction between the variables. EES has several built in optimizers that do a good job at determining the optimal design point [17]. The DIRECT algorithm was used for the optimization, the optimized parameters and results are shown in Table 12.

Table 12 Optimized parameter for 10MW regenerator system

Monotonic Parameters		Non-Monotonic Parameters	
Compressor Discharge Pressure	25 MPa	**Low Temp Regenerator Effectiveness**	97.2%
Compressor Inlet Temperature	32°C	**High Temp Regenerator Effectiveness**	98.8%
Bed Switching Time	45 s	**Compressor Inlet Pressure**	7.87 MPa
Bed Sphere Size	3 mm	**Recompression Fraction**	34.4%
Void Fraction	0.37	**Low Temp Regenerator Pressure Drop**	0.175 MPa
Turbine Inlet Temperature	720°C	**High Temp Regenerator Pressure Drop**	0.175 MPa

Regenerator effectiveness is slightly higher for the high temperature regenerator than the low temperature regenerator because the effect of carryover is larger at low temperature. Additionally, the cycle optimizes to have low pressure drop in the beds which increase effectiveness at a small increase to cost.

An optimization was also conducted for the recuperator system. In this case only the compressor inlet pressure, recompression fraction, and recuperator effectivenesses were optimized. The compressor inlet pressure and recompression fraction behave similar to the regenerator system where an optimum can be found. The recuperator effectiveness plot looks significantly different from the regenerator system because of the lack of carryover and very different costs. A plot showing LCoE and thermal efficiency as a function of recuperator effectiveness is shown in Figure 37.

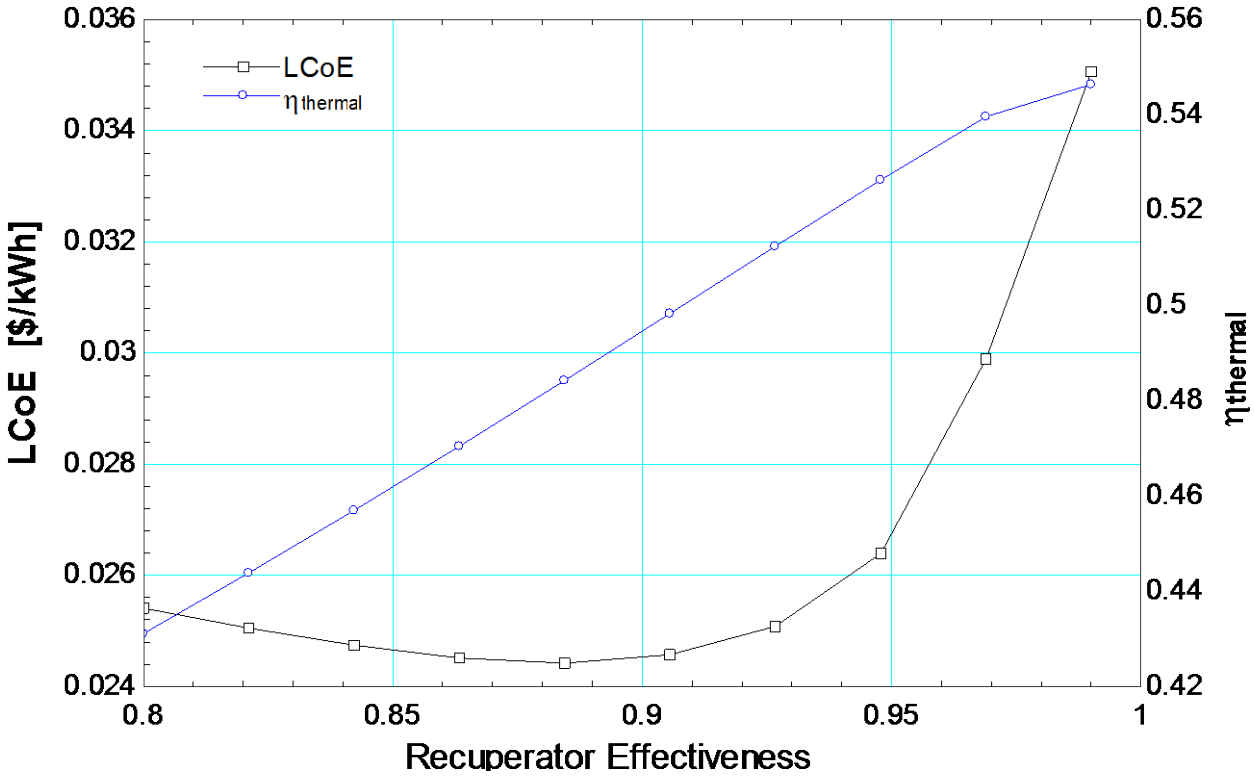

Figure 37 LCoE vs recuperator effectiveness for RCBC at 10MW scale

Figure 37 shows that as recuperator effectiveness increases so does thermal efficiency of the cycle. However, the same trend is observed for LCoE, meaning that the increase in thermal efficiency is not being offset by a larger increase in heat exchanger cost. A minimum value of LCoE is clearly seen at 87%-89% effectiveness.

The recuperator model does not calculate pressure drops so the pressure drop through the recuperator was set to the optimal value of the regenerator system (which assumes that a recuperator could be designed to meet the same condition). Optimizing for LCoE of the recuperated cycle results in rather low thermal efficiency because of the high cost of the recuperators. A low thermal efficiency will lead to lower power output, and when the power block is integrated with a heat source, the total LCoE of the system will suffer. This is particularly important when the heat source cost is high, as is seen in CSP plants. A second optimization can be done with respect to thermal efficiency. For CSP plants and others with high costs it is beneficial to have a higher thermal efficiency as it means the capital costs can be dispersed over a larger amount of electricity produced. Another way to choose a recuperator efficiency is to look at a plot of price index vs recuperator effectiveness shown in Figure 38.

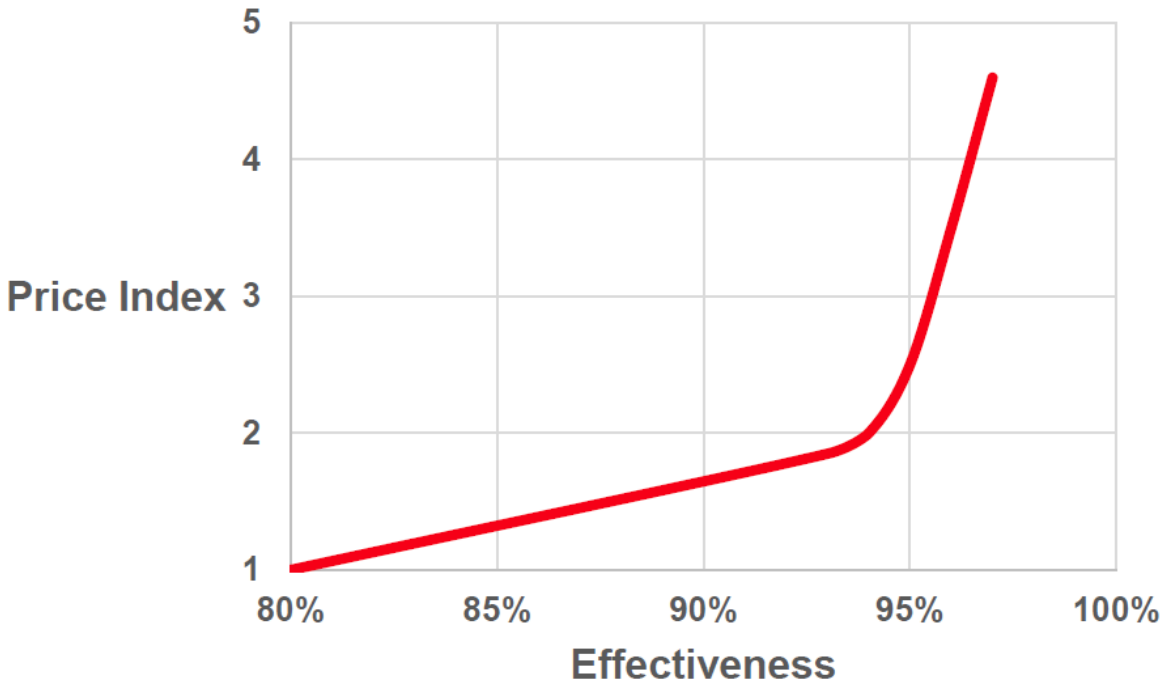

Figure 38 Price index of PCHE recuperator vs effectiveness, taken from [90]

Figure 38 shows that above 94% effectiveness the cost curve hits a knee where price increases rapidly. A third “optimal” point can be taken where the recuperators have 94% effectiveness. The lower cost

regenerators tend to optimize to the highest efficiency since there is little additional cost associated with going to higher effectiveness. The outputs from the 10MW model for the three recuperator optimizations and regenerator optimization are shown in Table 13.

Table 13 Resulting outputs from system model at 10MW for recuperator and regenerator systems

	Recuperators			Regenerator
Objective Function	**LCoE**	**94% Effectiveness**	**Efficiency**	**LCoE**
Compressor Inlet Pressure (MPa)	7.60	7.65	7.62	7.75
Recompression Fraction	28.0	39.0	35.5	35.3
Low Temp Heat Exchanger Effectiveness (%)	86.6	94.0	99.0	96.5
High Temp Heat Exchanger Effectiveness (%)	87.3	94.0	99.0	98.2
LCoE ($/kWh)	0.02406	0.02504	0.04191	0.02256
Thermal Efficiency (%)	48.5	51.1	55.1	51.0
Low Temp HX Cost (k$)	1041	1432	10950	203
High Temp HX Cost (k$)	1043	1891	3718	209
Valve Cost (k$)	-	-	-	1492
Total HX Cost (k$)	2084	3323	14668	1904

Table 13 shows that the regenerator system has a lower LCoE than all of the recuperator systems. There is a 6.2% reduction in LCoE from the LCoE optimized recuperator system to the optimized regenerator system due to the higher efficiency (2.5% increase) at minimal cost decrease (180 k$). The recuperator system operating with 94% effective recuperators is more representative of an installed system since it has significantly higher thermal efficiency than the LCoE optimized system (2.6% increase). The 94% effectiveness system has a very similar thermal efficiency to the regenerator system but the costs for the regenerators are significantly less, leading to a 9.9% reduction in LCoE. The final comparison between the efficiency optimized recuperator system and the regenerator system has significant differences in both thermal efficiency and LCoE. The recuperator system has a much larger thermal efficiency (4.1% increase) but is also much more expensive leading to a 46.2% reduction in LCoE if using the regenerator system.

One problem with this analysis method is it does not consider anything outside of the power block in the LCoE. A better method would be looking at the LCoE of the entire system, for this project that would also take into account the solar field and any thermal storage. Adding the solar field results in a significant complication to the calculations as now the plant operating strategy matters significantly. For instance, a peaker plant may have a very low amount of storage and be designed use all of its energy in a matter of hours. In this case it may be more economical to have a lower cost, lower efficiency, higher capacity cycle where a regenerator would be more beneficial. On the other hand, a base load plant may be more sensitive to thermal efficiency where recuperators may be beneficial. As part of the project funded by DOE, NREL implemented the regenerator model into the System Advisor Model (SAM) where it can be integrated with different solar field capacities and different amount of storage to determine what the advantages would be. Optimization of the regenerator cycle beyond the simple cycle costs and efficiencies was beyond this scope of work, this is an area for future work.

Optimized cycle layouts

So far only a cycle with regenerators or recuperators has been considered, but it is possible that using both in one cycle can provide significant advantages. As previously discussed, carryover in regenerators is higher at low temperatures where the density is higher. By using a recuperator for the low temperature heat exchanger much of the carryover can be avoided while keeping some of the cost savings of the regenerator. As before, an optimization is conducted to determine the optimal parameters for this mixed cycle. Again, the cycle was optimized for three cases; minimizing LCoE, minimizing LCoE with low temperature recuperator set to 94% effectiveness, and maximizing effectiveness.

Table 14 Optimized results for mixed cycle with low temperature recuperator and high temperature regenerator

	Mixed		
Objective Function	LCoE	94% Effectiveness	Efficiency
Compressor Inlet Pressure (MPa)	7.56	7.57	7.67
Recompression Fraction	37.0	37.0	35.3
Low Temp Recuperator Effectiveness (%)	86.0	94.0	99.0
High Temp Recuperator Effectiveness (%)	97.7	94.6	98.3
LCoE ($/kWh)	0.02357	0.02432	0.03075
Thermal Efficiency (%)	50.7	49.4	53.8
Low Temp HX Cost (k$)	1171	1418	6187
High Temp HX Cost (k$)	174	162	187
Valve Cost (k$)	1018	1018	1018
Total Cost (k$)	2363	2598	7392

Optimizing for LCoE results in an almost identical LCoE to the regenerator system, however at the cost of 0.3% loss of thermal efficiency. Much like the recuperated system, when optimizing for LCoE the recuperator is driven to low effectiveness because of its high cost. Constraining the recuperator to 94% effectiveness gives a result similar to the regenerator system, with a 1.6% decrease in efficiency and 9.1% increase in LCoE. Finally, optimizing for maximum effectiveness allows the mixed cycle to reach 53.8% effectiveness a decrease of 1.3% from the maximum effectiveness of the recuperated cycle at a savings of 26.6% of LCoE compared to the recuperator cycle. Again, a more detailed analysis with the heat source is needed to determine which cycle configuration should be chosen.

In all cases the regenerators come in at a lower cost and lower LCoE. While the LCoE results presented here are interesting, the real important result is there is now a cycle model that can be integrated with different heat sources and be used to quickly determine the optimal test parameters. Future work on the project has focused on implementing the cycle model into SAM so it can be used with more powerful heat source and economic tools.

Regenerator test facility

The regenerator and cycle model show an economic case for switching to regenerators; however, this case rests on a regenerator model not tested at sCO_2 conditions. It is important to validate the model against measured performance in order to demonstrate that the model is still valid even at high temperature, high pressure, and fast switching times. Additionally, a proof of concept regenerator operating at prototypical sCO_2 cycle conditions demonstrate that this concept is practical, and all the major effects are accounted for in the model. An existing CO_2 recuperator test facility was modified to operate with regenerators. The system includes a compressor, two auxiliary heat exchangers, and two heaters. In addition, there is a data acquisition and control system to make accurate measurements of regenerator performance and control the flow of CO_2 through the regenerator beds. The test facility with all the components is shown in Figure 39

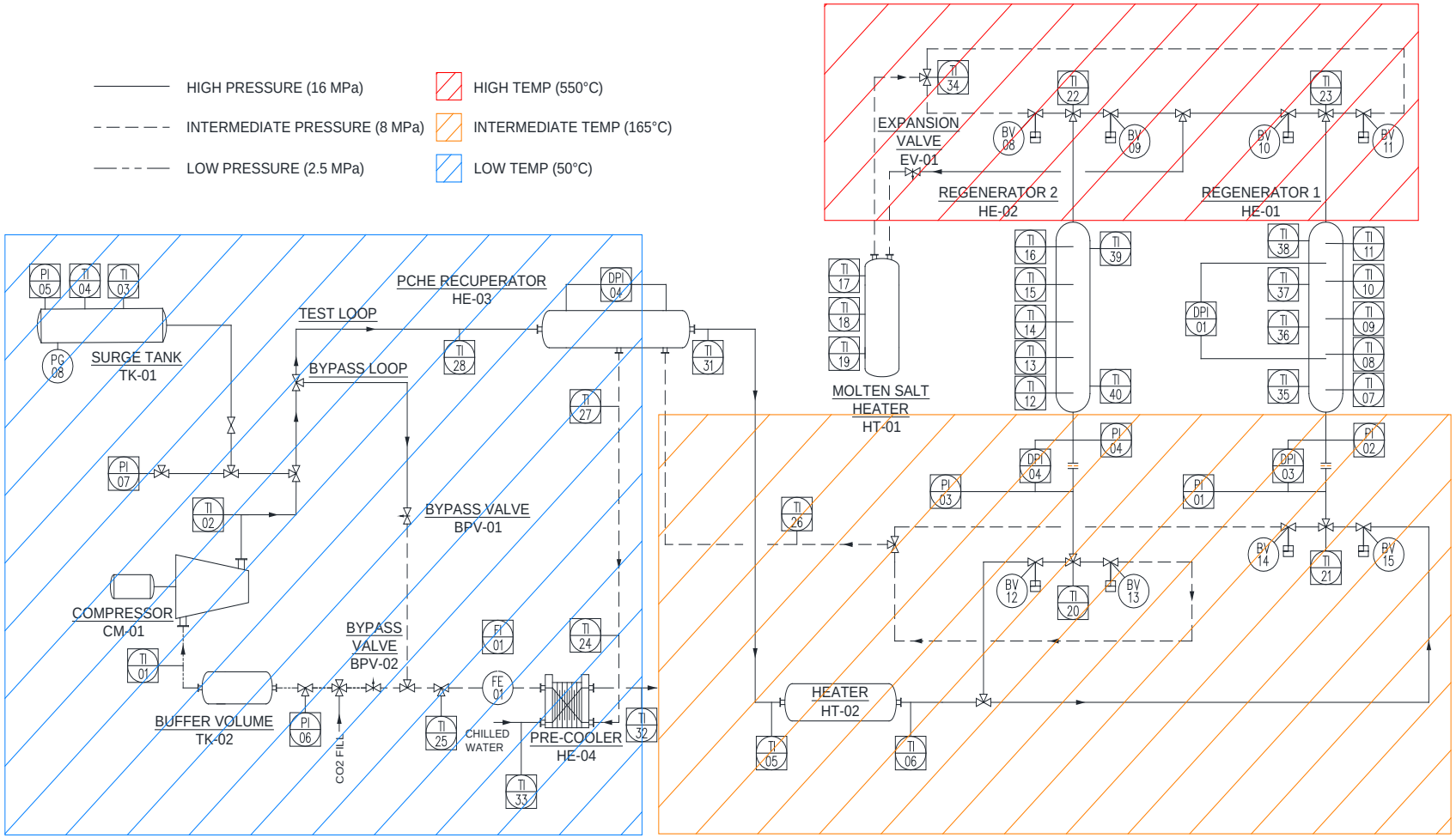

Figure 39 Diagram of test facility shown with temperature zones

Each of the components in the test facility will be discussed in this section. The approximate maximum temperature each component sees is also shown in Figure 39 because the temperature dictates what the maximum operating pressure can be. The regenerators for the experimental test facility were designed to be as large as possible given the constraints associated with the available auxiliary equipment. The limiting factor for the heat transfer in the regenerator is how much heat can be added in the primary heater. The electrical service available is limited to 70A at 208V, giving a maximum power of 14.5kW. Realistically, 11kW is the maximum rate at which heat can be added to the CO_2 when considering losses and limiting the output of the heaters to ensure the element does not burn out. Because of the unbalanced capacitance rates for each blow of the regenerator bed (due to the pressure difference) even for a perfect regenerator some heat is needed to maintain a constant inlet temperature. This limits the maximum heat transfer in the regenerator to about 10kW at sCO_2 cycle conditions (560°C and 25 MPa). Some pictures of the constructed test facility are shown in Figure 40.

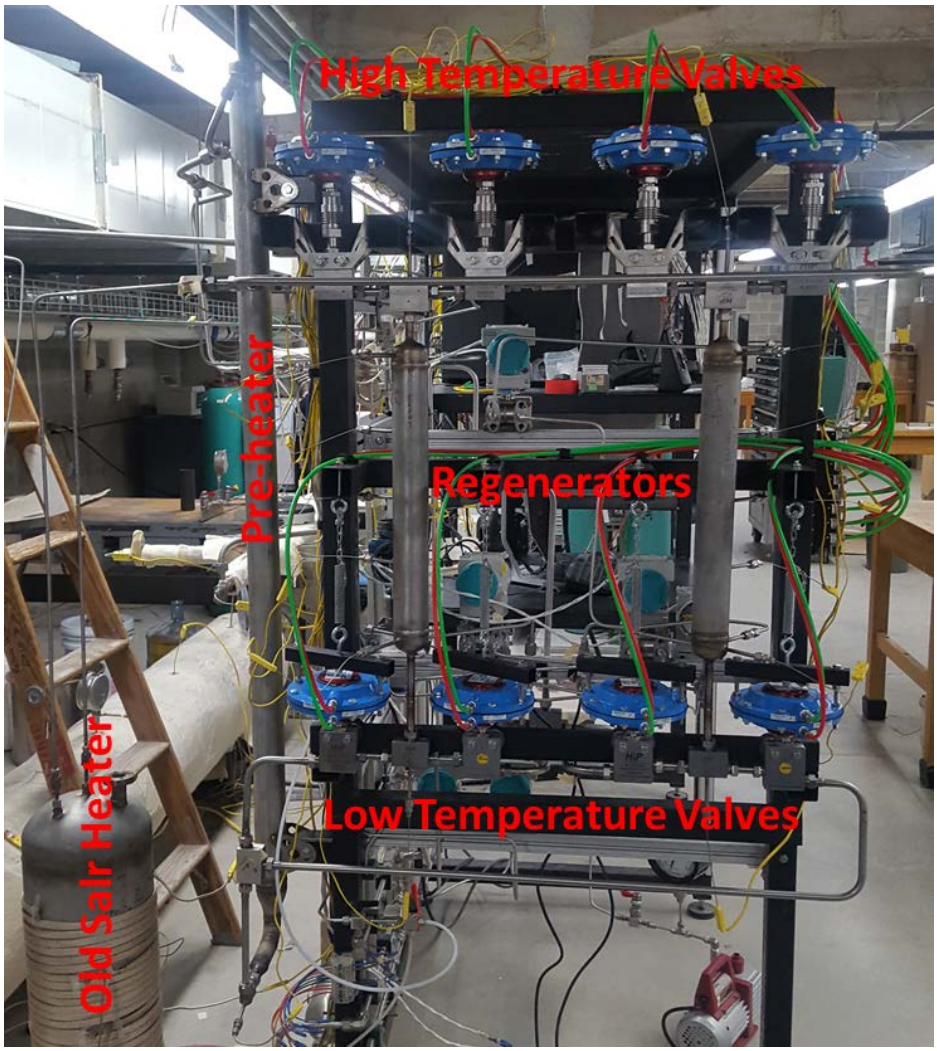

(a)

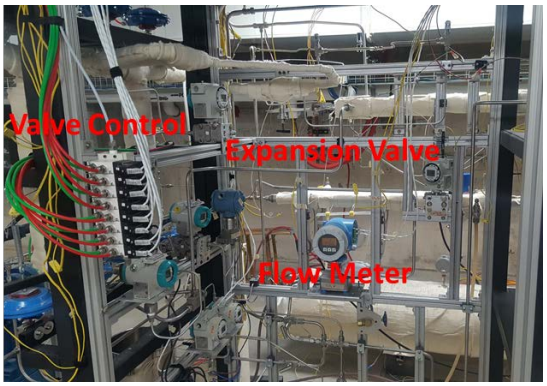

(b)

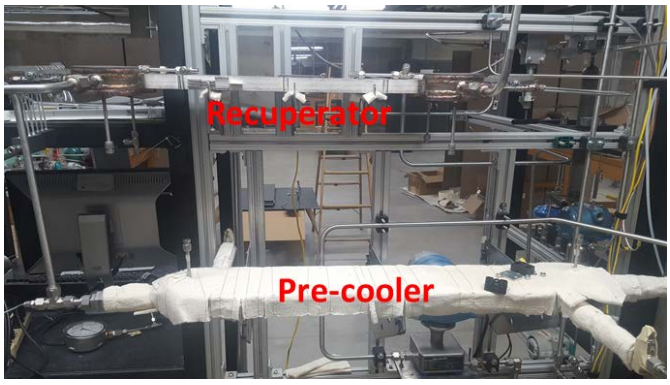

(c)

Figure 40 Images of regenerator experimental test facility. (a) regenerators, (b) control valves and measurement devices, (c) auxiliary heat exchangers

Compressor

The compressor is a positive displacement pump with two heads made by HydroPac. It was modified from a gas compressing pump to be used with CO_2, which involved changing the seals to be compatible with CO_2. Initially the compressor had an inlet pressure range of 300-1200 psi and a maximum outlet pressure of 2400 psi. An actual sCO_2 cycle would have an outlet pressure near 3600 psi. To increase the maximum outlet pressure of the pump new cylinder heads were ordered that have a smaller diameter. These heads are rated to 3600 psi outlet, however they come at the expense of reduced mass flow. The 2400 psi heads have a maximum flow rate of 1.6kg/s while the 3600 psi heads have a maximum flow rate of 1kg/s, this is still much greater than the mass flow through the test section (typically 0.03kg/s) so most of the flow will be bypassed. Initial testing was done on the uninsulated regenerator using the 2400 psi heads, the heads were switched and used to test to the full 3600 psi on the insulated regenerators.

There were some issues with the compressor that needed to be addressed. Leakage past the seals in the compressor caused the CO_2 level in the room to rise drastically. Much like a car engine, the pistons use seal rings to seal the CO_2 into the cylinders. These rings failed, and the heads were taken off of the compressor so the damage could be inspected. There was significant damage to some of the seals, and quite a bit of oil contamination on the back side of the cylinders as shown in Figure 41.

Figure 41 Hydropac piston showing wear marks causing leakage

After the seals were replaced the leakage stopped, however after several more hours of operation the leakage started again. Instead of replacing the seals again, the area behind the cylinders was simply vented out of the room for safety. Leakage was still present, but no longer leaking into the room triggering the alarm and causing a danger to personnel, a CO_2 bottle was used to continuously replenish any CO_2 lost in the compressor in order to maintain a relatively constant operating pressures. Since the leakage was not out of the test section the flow measurements made were still accurate.

The heads of the compressor are driven by a hydraulic system. The compressor is controlled by sending a 0-5Vdc signal to the control box, which subsequently controls how far the proportional hydraulic valve opens on the hydraulic system. There are two limit switches at each end of the compressor stroke which causes the reciprocating action. At low voltages the pump did not operate

well, as it would have trouble tripping the limit switches. Additionally, the switches had to be carefully adjusted to ensure trouble free operation. The switching relay failed occasionally, causing the piston to be stuck on one side of the stroke. Having a stuck piston could cause damage to the pump and ruin any data taken, so the relay was replaced. The new relay still gets stuck occasionally but vibrating the control box causes it to get unstuck. An improvement would be using a solid-state relay that can withstand the high number of cycles that the relay experiences.

The compressor heads are fed with chilled water from the building chilled (10°C) water. The jackets of the cylinder are water cooled, as well as the discharge of one of the cylinders. The water removes some of the heat of compression and therefore prevents the seals from being damaged. The amount of cooling done by the water can be important for maintaining the pressure in the cycle which is discussed in the Surge tank section.

Pre-cooler

The pre-cooler (HE-04) is located on the test loop directly before the Coriolis flow meter. The pre-cooler is used to cool the fluid before it reaches the Coriolis flow meter and compressor. The water source for the precooler is the building chilled water which is supplied at 10°C. The pre-cooler is a PCHE which has been repurposed for this project. The water flow rate can be controlled with a valve on the water supply which can be useful if higher inlet temperatures to the compressor are needed. The capacitance rate of the water is close to that of the CO_2 leading to rather large temperature changes in the cooling water. Cooling before the Coriolis flow meter is especially important because the flow meter will not operate if the flow is two-phase through the measurement section. If the pre-cooler is not able to sufficiently cool the fluid, then it will be two-phase at this location. This is usually not a problem at higher pressures, where the saturation temperature is high, however at lower pressure this is a concern.

Recuperator

The second heat exchanger in the test facility is a PCHE recuperator which is used to preheat the fluid coming from the compressor. To test at conditions consistent with those in a 10MW power plant, significant heat is needed to raise the temperature of the CO_2 from ~50°C at the exit of the compressor to the ~165°C needed at the inlet of the regenerator. There is not enough power in the pre-heater alone to do this, so the recuperator is used to recover some of the energy from the flow returning from the regenerators. Using the recuperator saves reduces the required heating and cooling power needed by between 5 and 10kW.

Pre-heater

The pre-heater is used after the recuperator to bring the CO_2 up to the desired inlet temperature (165°C). A radiative heat transfer cartridge heater is used with a tube in tube heat exchanger design. The cartridge can provide a maximum of 6kW of heat, but at full load the element can burn out quickly. A more practical limit to pre-heater power is 4.5kW. The tube in tube design means that if the cartridge fails it can easily be replaced with a new one. The heater is covered by one layer of kaowool and one layer of pyrogel to prevent heat loss. The heater is controlled by a SCR using a PID controller based on the exit temperature of the fluid. The system is designed to shut off if the temperature of the fluid exceeds 200°C, and the heater is interlocked to only run if there is flow measured through the test section.

Salt heater

The salt heater is the primary heat exchanger in the cycle, it is used to provide the heat needed at the high temperature inlet of the regenerators. Due to the unbalance in the capacitance rate of each blow, even a perfect regenerator will require a significant amount of heat input to maintain temperature. A salt heater is needed due to the transient nature of the regenerator as seen in Figure 42.

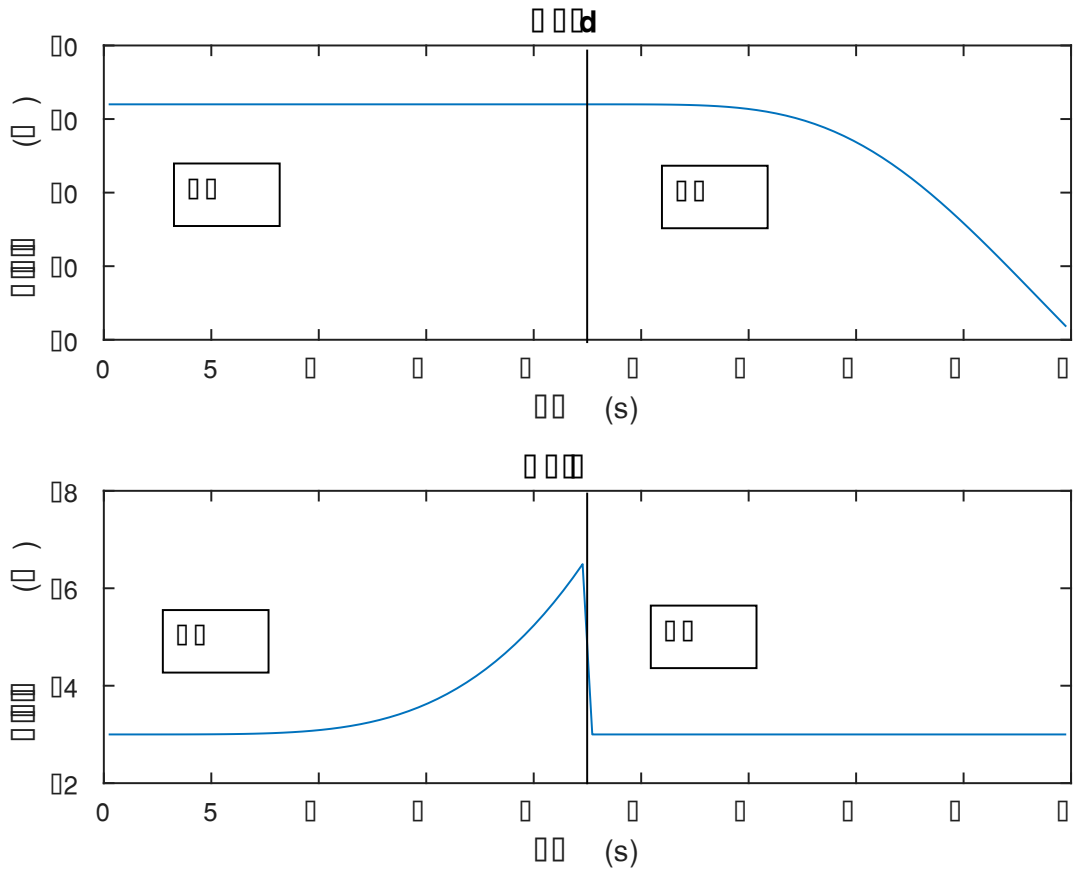

Figure 42 Temperature profiles at the inlet and exit of representative regenerator, data taken from regenerator numerical model

The temperature exiting the regenerator falls drastically at the end of the cycle (hot end CtHB), however, the CO_2 temperature entering during the HtCB on the high temperature side needs to be as constant as possible to ensure the experiment is operating under the same conditions as those assumed in the model and anticipated in practice. The molten salt is a thermal buffer that can maintain a relatively constant temperature at the exit regardless of the inlet temperature. A mixture of lithium, potassium, and sodium nitrate salts were used in the salt heater. The mixture has a relatively low melting temperature of around 100°C and is stable up to 600°C. This temperature span can cover all of the tests needed for testing the regenerators. The initial salt heater was designed to hold 100 pounds of

salt, 6kW of heat was applied using heater tapes wrapped on the outside of the vessel. CO_2 was passed through 40 feet of ¼" tubing coiled inside of the vessel. This design is shown in Figure 43.

Figure 43 Initial salt heater showing vent tube on top, and five heater tapes providing the heat

The heat was provided by 5 tape heaters controlled in 2 zones with on-off relays. The temperature of the salt was measured in 3 locations with thermocouples welded onto the exterior of the shell. The shell

is an 8” sch 10 pipe, the top cap has pass throughs for the inlet and outlet of the CO_2. There is also a vent on the cap that is used in case of a leak to direct the molten salt flow into a catch pail. A secondary vent goes to the building exhaust to vent any gasses coming off of the salt. Nitrate salts are very hydrophilic, meaning they pull moisture out of the air. When the salt is heated this water is removed and is vented into the building air exhaust. The exterior of the heater is insulated with one layer of kaowool and two layers of pyrogel insulation. One of the problems with this heater is it was not able to provide enough heat to reach sufficiently high temperatures. The thermal losses from the heater and the lines limited the maximum temperature that the heater could reach to about 350°C. The ¼” tubing also created a significant pressure drop through the heater. The high pressure drop made it difficult to get enough flow through the test section.

Because of these problems a new salt heater was made with higher heat input and larger diameter tubing. The new heater is an Inconel serpentine with 208V driving current. The power is controlled by a SCR that can vary the amount of time voltage is applied to the heater, thereby affecting the power output of the heater. There are two Inconel band heaters wrapped around the shell each which has a resistance of 2.1 ohm, they are connected in series for a total of 4.2 ohm. Using 208V, the maximum power the heater can provide is 10.3kW. To fit the Inconel heater the shell was made with a 12” sch 10 pipe, this resulted in a much larger heater holding 300lbs of salt. The CO_2 coil was also remade using 40ft of ½” tubing which greatly cut down the pressure drop through the heater allowing for better control of the mass flow through the system. These improvements allowed the system to reach 550°C with some power to spare. The improved salt heater is shown in Figure 44.

Figure 44 New salt heater with larger heaters and ½" tubing

Valves

There are two loops in the system, the bypass loop that handles most of the flow from the compressor and the test loop. The bypass loop has two valves used to control the pressure in the different areas of the cycle, BPV-01 and BPV-02 as seen in Figure 39. These valves create a high, middle, and low pressure zone in the test facility. The high and middle pressure sections are used in the regenerators, while the low pressure is only used to feed the compressor. The low pressure feeding the compressor does two things, first it provides a convenient place to feed in CO_2 from the bottle. Since the CO_2 comes in liquid bottles, the maximum pressure it can reach is the saturation pressure of CO_2 at the

bottle temperature. At room temperature the saturation pressure of CO_2 (~800psi) is significantly less than the low side pressure required for regenerators (1200psi). By running the low side at 300psi there is a significant difference in pressure between the bottle and the system making it easy to fill the system. When quickly emptying a CO_2 bottle the heat of vaporization lowers the temperature of the bottle drastically, which brings down the saturation pressure. Two 200W bottle heaters are used to heat the bottle and therefore fill faster. Second, the low pressure section also keeps the pressure differential large across the compressor. It is important to have a large pressure differential across the compressor because it keeps the exit temperature from the compressor high which is important for system pressure as will be discussed in the Surge tank section. By adjusting BPV-01 and BPV-02 the three pressure zones can be set to the desired pressure and maintained.

A third control valve is located in the test section to regulate mass flow (EV-01). This valve is located on the high temperature side of the regenerators and is designed to expand the CO_2 going through the regenerators from the high pressure to the middle pressure of the cycle. Locating the valve before the salt heater means the CO_2 in the salt heater will be at low pressure, reducing the chance of the line breaking in the heater. Because the compressor has such a high flow rate, most of the flow is bypassed and changing the amount of flow through the test section does not have a noticeable impact on system pressures which makes controlling pressure and mass flow independent and simple.

Eight valves are needed to control the flow of CO_2 through the regenerator beds. FlowServe specified Y pattern globe valves for the valves, however these valves had a very large lead time and would have pushed back testing by months. The FlowServe valves will be tested at a later date at Sandia National Labs; instead HIgh Pressure equipment (HIP) medium pressure valves were used. These valves were fairly inexpensive and were equipped with a dual acting air actuator. On the high temperature side of the regenerator an extended bonnet was used to keep the packing within temperature specs. It was important the valves actuate quickly to cut down on the time it takes to switch the beds between high

and low pressure. The valve actuation time was measured to be about 0.4s for the high temperature valves with the extended bonnet and slightly shorter for the low temperature valves.

The order in which the valves are switched is important because it can drastically affect how the cycle performs. For example, if BV-14 and BV-15 (both valves on the low temperature side of the regenerator) are switched at the same time there will be some flow that bypasses the regenerator entirely and goes directly from the compressor discharge to the compressor inlet. This extra bypassed mass will cause the mass flow rate to read higher than it should, causing a measurement error. The valve switching order is shown in Figure 45.

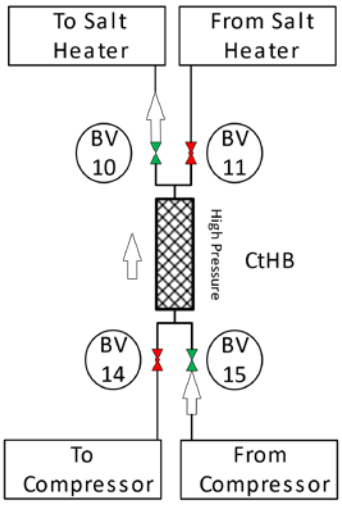

(a)

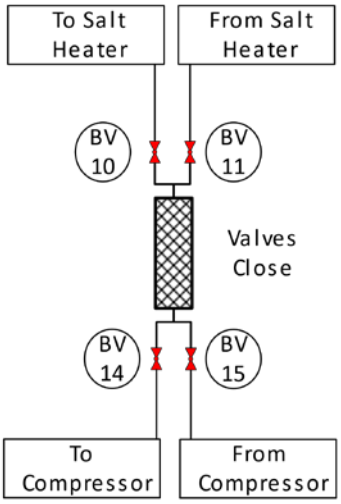

(b)

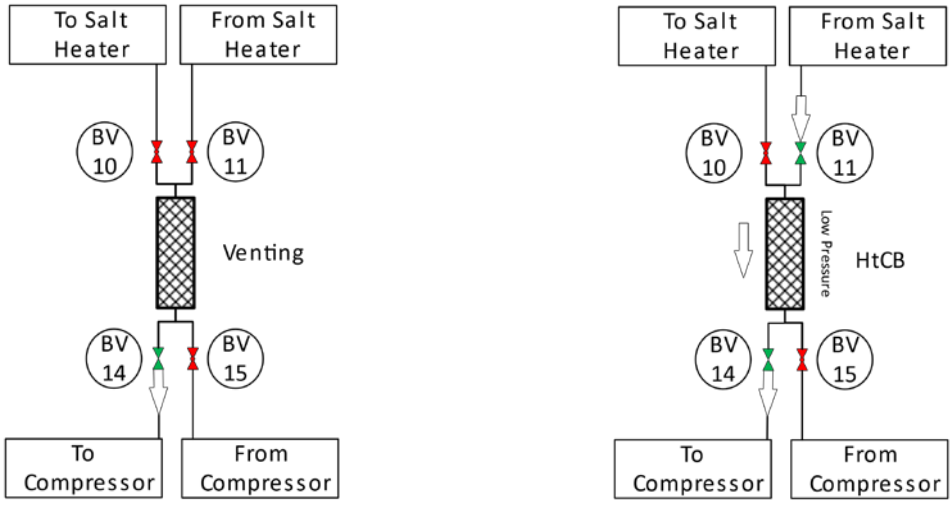

Figure 45 Valve actuation order for switching regenerator bed 1 from CtHB to HtCB; (a) CtHB, (b) close all valves, (c) vent bed to low pressure, (d) HtCB

Figure 45 shows the steps for regenerator 1 going from the CtHB to the HtCB. First, all the valves are closed in Figure 45 (b), which prevents any chance at flow bypassing the regenerator bed and returning directly to the compressor. Second in Figure 45 (c), BV-14 is opened to allow the high pressure in the bed to return to the compressor. Finally, in Figure 45 (d) the cycle returns to normal operation in the HtCB. For each step, the control software allows 0.6s seconds for the valves to actuate which is 50% longer than the actuation time of the valve, allowing the valve to fully seat before moving to the next step. To go from HtCB back to CtHB the same strategy is employed, first closing all valves, next pressurizing by opening BV-15, and finally by opening BV-10 to initiate the CtHB. The bed linking valve is not employed at this small scale because there are only two beds which is insufficient to maintain steady flow while also going through the extended switchover operation.

During experimental testing there were some issues with leakage in the valves. The valve leaked in two spots, where the bonnet attaches to the body of the valve, and past the seat of the valve. The bonnet of the HIP valves is threaded into the body and sealed using a metal to metal 316 seal ring.

Thermal and pressure cycling in the valve can cause the threads holding the bonnet to the body to loosen and eventually leak. The valves were disassembled, and new seals were installed. It was found that these threads would loosen every 10 hours of operation and would need to be retightened; a welded bonnet would solve this problem. The leakage past the seat was likely a result of particles in the CO_2 since only one valve was damaged in this way. A picture of the damaged stem is shown in Figure 46.

Figure 46 Stem of damaged HIP valve showing scratch causing leakage

Since the seat was also damaged, the body of this valve was also replaced. It is likely that a particle of grinding dust from the tube fitting process caused the leak in the valve. This experience reinforces the fact that care must be taken to ensure that dust does not enter the system and cause issues in the valves.

There are also three relief valves installed on the system in case of an over pressure scenario. These are Swagelok spring relief valves set to break at approximately 2600 psi. There is one relief valve at the discharge of the compressor, one right before the expansion valve (EV-01), and one on the compressor discharge surge tank.

Surge tanks

There are two surge tanks in the system, one each at the inlet and discharge of the compressor. The main purpose of these tanks is to dampen out the pulsation caused by the long cycle time of the piston pump (one stroke takes approximately 3 seconds). At the inlet to the compressor a 3" sch 80 pipe 30" long is used. The discharge tank is much longer and made from a 12" sch 160 pipe 7.5' long. The discharge surge tank also provides the means to fill the system to high pressure. CO_2 could not be simply added through bottles because the maximum pressure that could be achieved is the saturation temperature of CO_2 at room temperature around 900 psi. Additionally, CO_2 could not be added by running the compressor because the CO_2 would cool as a result of being converted from liquid to gas. The lower the temperature the lower the vapor pressure and the less CO_2 makes it into the system. It would take hours of running the compressor to reach the desired operating pressure which would cause unwanted wear and result in a significant amount of leakage from the compressor. Liquid CO_2 is added to the discharge surge tank and heated to 50°C, increasing the pressure in the tank. Using the known volume of the tank and the desired pressure, the weight of CO_2 needed to reach the operating pressure could be calculated and added. One problem with this method is maintaining the tank at high pressure once the system starts and flow from the compressor starts entering and exiting the regenerator on every stroke (a result of the surge tank doing its job buffering the flow). If the flow exiting the compressor is too cold it can cause the temperature in the surge tank to drop and thus the pressure to decrease. The heating power available on the surge tank (4 kW) is not sufficient to make up for the heat loss from the cold compressor flow. The solution is to decrease the inlet pressure to the compressor

which makes it transfer more energy to the CO_2 during compression, raising the outlet temperature significantly. The lower pressure is achieved by using the second expansion valve BPV-02 and is the reason why a low pressure zone is needed.

Tubing

Most of the flow tubing is designed using ½" standard wall tubing. Because of the high pressures and temperatures in the system the wall thickness needs to be chosen carefully to ensure safe operation. The pressure ratings for tubing is taken from [97] which lists the working pressure as a function of outer diameter and wall thickness. There is also a derating factor as a function of temperature for 316 tubing, which is listed in Table 15.

Table 15 Derating factor vs maximum temperature for 316 seamless stainless steel tubing. From [97]

Temperature	Derating Factor
93°C (200°F)	1.00
204°C (400°F)	0.96
315°C (600°F)	0.85
426°C (800°F)	0.79
537°C (1000°F)	0.76

There are three different temperature zones in the test facility and how hot each section gets will determine the size of tubing needed. The cold zone will have a maximum temperature of below 93°C, the medium zone will not get any hotter than 204°C, and the hot zone will have a maximum temperature of 537°C due to the rating of the valves (1000°F). To ensure a small pressure drop, the thinnest wall tubing that is rated for the pressure will be used. The maximum pressure possible is 3600 psi, which is the maximum discharge pressure of the compressor with its upgraded heads. The relief valves are set to open at this pressure. The cold section will use 0.049" wall, the medium section 0.063" wall, and the hot section 0.083" wall.

The connections for the low and medium temperature sections will be Swagelok tube fittings since they perform well in this temperature range. Because of the changing temperature profile, as shown in Figure 42, Swagelok fittings will not be used in the high temperature section. The rapid temperature transients can cause Swagelok fittings to loosen over time and leak. Instead cone and threaded connections will be used. Cone and threaded fittings have a cone and backwards threads cut into the tube. The gland is fed onto the tube followed by a collar, threaded into the reverse threads on the tube. The cone is then set into the seat of the fitting and the gland clamps it in place by applying force to the collar. A diagram of the fitting is shown in Figure 47.

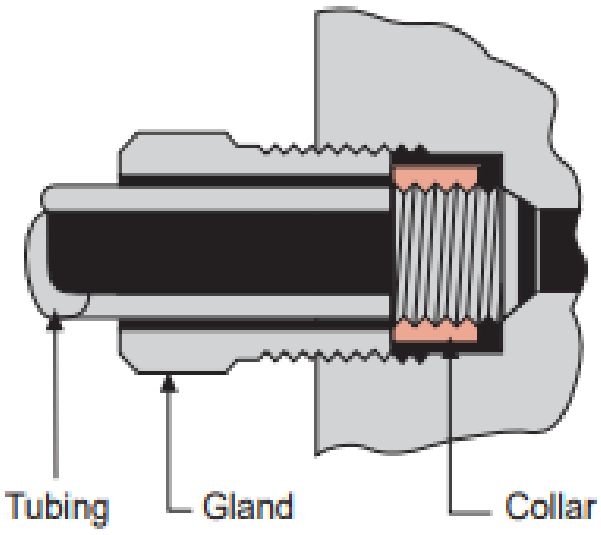

Figure 47 Cone and thread fitting from [98].

There is no ½" size for cone and thread fittings, so the 9/16" size was used instead. This tubing is rated to much higher pressure (20,000 psi), and as a result the wall is very thick (0.250"). The wall thickness makes it very difficult to bend, and very expensive so instead of using it for long runs, ½" tubing was used and a short 2" section of 9/16" was welded to the ends. Another benefit of this method of

construction was the 2” sections could be cut from pre-manufactured tubes, so the cone and thread would already be in place, which would otherwise be a time consuming procedure.

Initially, the cone and threaded fittings worked well, but as higher temperature runs were conducted, leakage started to occur from some of the fittings. The leakage was so sever in some cases that it blew a hole through the insulation and drastically raised the level of CO_2 in the room.

Figure 48 Hole in insulation because of leakage from the high temperature tee

It was unclear what was causing this, the first time it occurred; the insulation was removed, and the fittings were retightened which solved the problem for a short while. It was hypothesized that the vibration from rapidly changing the pressure in the regenerator could be causing the glands to loosen over time. However, further observation showed that the leakage occurred at the same point in the cycle - at the end of the CtHB, when the temperature of the CO_2 passing through the fitting is dropping quickly. After the CtHB would end, the leakage would immediately stop. It seemed that the tubing was contracting faster than the fitting when the cold fluid was passing through and causing a leak. Figure 47 shows that this is not unreasonable, the tube has a much larger area exposed to the CO_2 and a much smaller mass than the fitting. To solve this problem, ¼” tubing was added inside of the 9/16” tubing. An

annular region filled with stagnant CO_2 exists between the two tubes and this region was used to increase the resistance to heat transfer from the CO_2 to the tube wall. A simple 1-D resistance model indicated that the liner would increase the resistance to heat transfer by 20-40x, depending on the conditions. To get the spacing correct for the liner tube a 5/16” x 0.020” tubing was used. On one side of the tube, the ¼” liner tube would be welded directly to the 9/16” tube creating a seal. The cone could then be recut over the top of the weld. The other end of the ¼” tube would be welded to the 5/16” locator tube and slid into the 9/16” tube. This allowed for CO_2 to flow into and out of the annular gap depending on the pressure but did not allow flow through the annular gap. An example of this construction is shown in Figure 49.

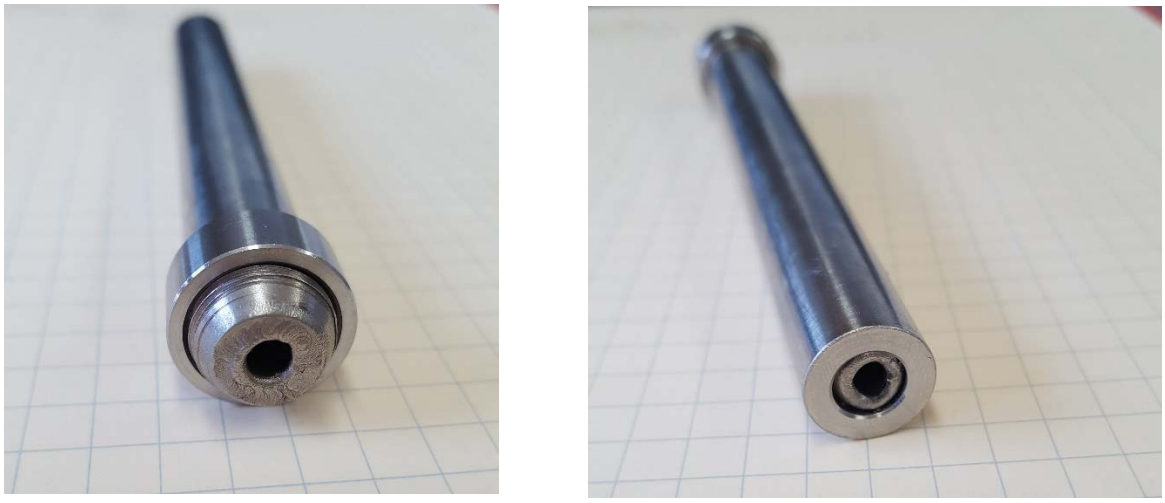

(a) (b)

Figure 49 9/16" tubing with 1/4" liner tube installed; (a) welded shut, (b) open to flow

Liner tubes were added to the three connections on the high temperature tee, highlighted in Figure 50.

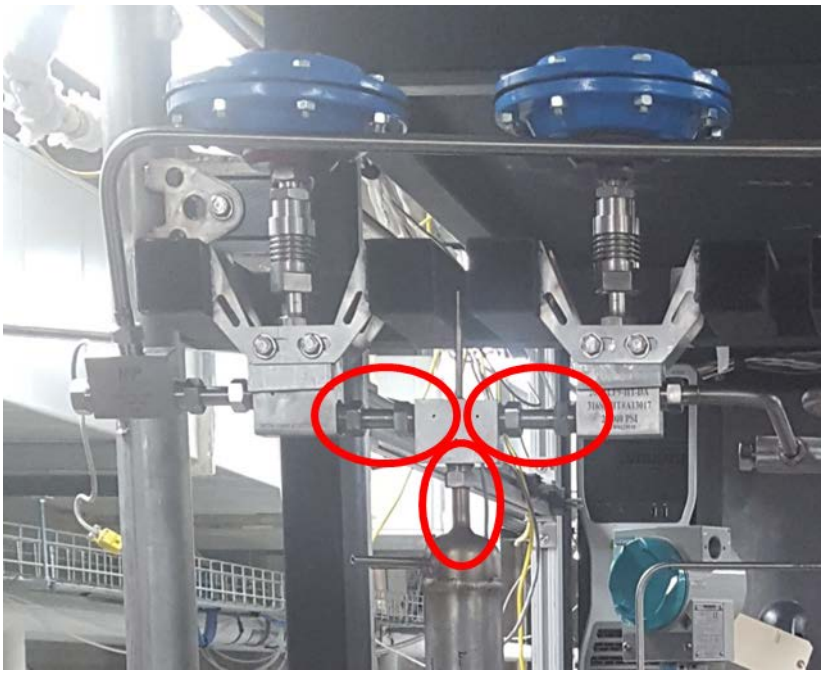

Figure 50 Top T showing locations of liner tubes in 9/16" HIP tubing

In addition to adding the liner tubes to one of the tees, the other tee was replaced by a tee that was completely welded together, eliminating the joints the previously leaked. The welded tee is shown in Figure 51.

Figure 51 Welded tee on uninsulated regenerator bed

The high temperature tests were run again using this new construction method and there was some leakage observed initially, but after 3-4 cycles the system sealed and did not leak again. Leakage occurred when the system was first starting up, meaning there were likely larger temperature transients that caused rapid changes in the fittings, and when a more steady state was reached the fittings were able to fully seal. To get a quantitative measurement of how effective the liner tube is, a TC was welded to one of the tubes, as seen in Figure 51. This TC showed a very small change in temperature throughout the cycle, showing that the tubing wall is well insulated to the fluid passing through which experiences

changes on the order of 200°C. The temperature of the wall for three cycles of a cycle operating at 550°C salt temperature is shown in Figure 52.

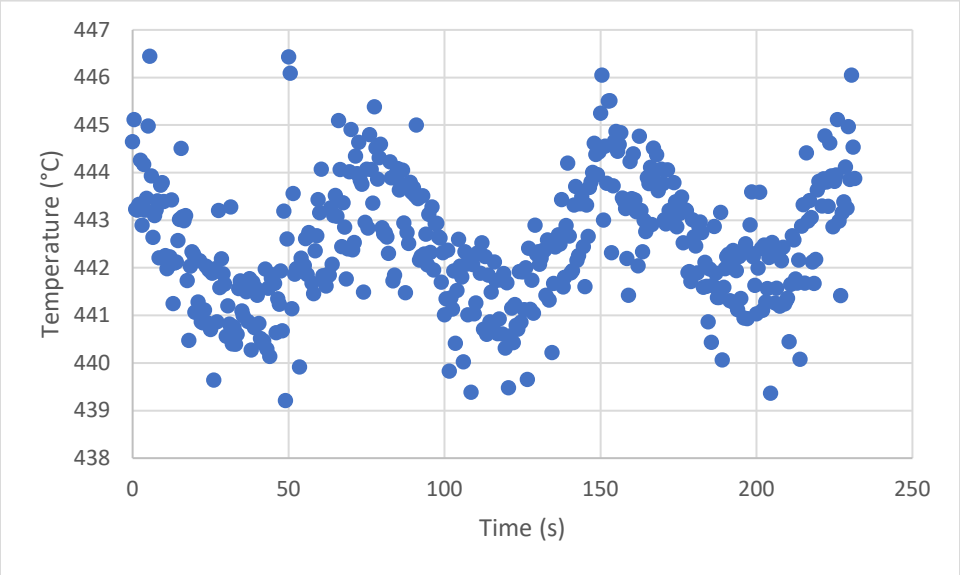

Figure 52 Temperature of thermocouple welded to outside of welded T for 3 cycles operating at 550°C salt temperature

Experimental Regenerator Design

The experimental test facility was used to test two different iterations of regenerators. First, the uninsulated regenerators were tested; these regenerators had instrumentation to measure the temperature in the bed as well as pressure drop. Second, insulated regenerators were tested which more closely match the design that would be used in the 10MW cycle; these regenerators did not have embedded, in-bed temperature sensors installed. The uninsulated test regenerators were designed to match the 10MW high temperature regenerator conditions as closely as possible. Both the uninsulated and insulated regenerator beds were designed to have an *NTU* and C_m that are similar to the high temperature regenerator in the 10MW cycle which results in the regenerators having a similar effectiveness. Matching *NTU* and Reynolds number required some runs to be done at much higher flow rates than design (0.06 kg/s vs 0.03 kg/s). After initial testing it became clear that the heater was not

able to maintain a constant temperature at such a high mass flow rate. As a result, the *NTU* was significantly lower than expected, leading to lower effectiveness which will be discussed more in the Test Results section. A difference in Reynolds number is not critical because the heat transfer and pressure drop correlations used in the model are valid for the range of operating conditions at which the regenerator was tested.

The uninsulated regenerator was constructed from a 2” sch 80 pipe. The pressure rating for the pipe at 538°C (1000°F) is 21.8MPa (3160 psi) which is less than needed for the 10MW cycle but greater than the maximum allowable discharge pressure from the compressor with its original heads. To achieve high efficiency with approximately 10kW of heat transfer, the length of the bed was sized to 0.445m (17.5in). Constructing an uninsulated regenerator allowed for initial data to be obtained and the concept verified while insulation selection was conducted. Additionally, because of the lack of insulation ThermoCouples (TCs) could be inserted directly into the bed, providing the spatial temperature profile of the bed as well as accurate pressure drop readings. All the instrumentation for one bed is shown in Figure 53.

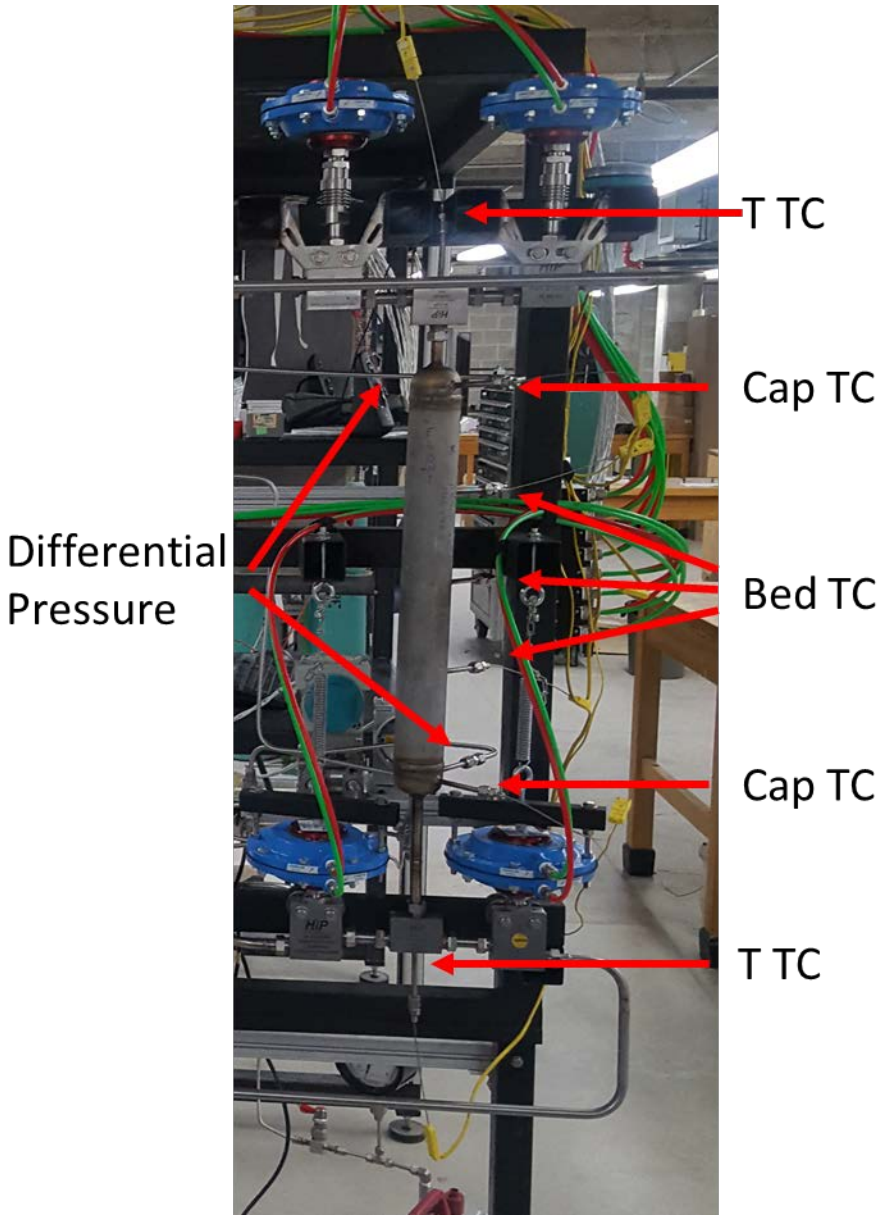

Figure 53 Location of instrumentation of one regenerator bed, wall TCs are not shown.

In each end cap there is a K-type TC, and an additional TC in each tee-connector. Three TCs are evenly spaced down the length of the bed to allow for measurements of the bed temperature during operation. The original design called for an orifice flow meter at the cold side of each bed which would be used to measure the carryover in the bed. The orifice flow meter was a square edge flow restriction with an inner diameter of 5/32" that produces a pressure drop of 2-7 psi depending on the flow conditions. The

orifice was instrumented with a slow response, highly accurate pressure sensor on one side, and a quick response, low accuracy pressure sensor on the other. A highly accurate differential pressure sensor measures the pressure difference between each side of the orifice. The mass flow through the regenerators is measured very accurately by a Coriolis flow meter. The orifice could not measure mass flow through the regenerators as accurately as the Coriolis flow meter and was to be used primarily to measure the carryover in the bed. Carryover in the bed occurs very quickly (less than 1 second), which cannot be measured with any accuracy using the orifice flow meter. The data acquisition system only takes pressure data every 0.25 seconds and the pressure sensors simply do not respond fast enough for an accurate reading. As a result, the orifice flow meters could not be used to measure carryover and were found to be inferior to the Coriolis flowmeter for measuring the steady state mass flow; they were eventually abandoned. The bed also has a high accuracy differential pressure sensor tapped into each end cap which measures the pressure drop across the bed. The absolute pressure in the bed is measured by the high accuracy pressure sensor that is on the bed side of the orifice. The model numbers and associated uncertainty of each device is listed in Table 16.

Table 16 Instrumentation range and accuracy for regenerator test facility

Type	Manufacture	Span	Accuracy	Serial Number
All Thermocouples	Omega		±2.2°C	Type K
PT-01	Rosemount	0-2000 psi		3051S1CG5A2B11A1A
PT-02	Omega	0-5000 psi	±1.0%	071715D117
PT-03	Siemens	0-3000 psi	≤0.1%	7MF4033-1GA10-1AC8-2
PT-04	Omega	0-5000 psi	±1.0%	071715D117
PT-05		0-6000 psi		0101454 DOM 0114
PT-06	Siemens	0-1500 psi	≤0.1%	7MF4032-1GA10-1NC1-Z
PT-07	Siemens	0-3000 psi	≤0.1%	7MF4032-1GA10-1NC1-Z
DP-01	Siemens	-7-7 psi	≤0.1%	7MF4532-1GA30-1NC1-Z
DP-02	Siemens	0-20 psi	≤0.1%	7MF4432-1HA62-1NC1-Z
DP-03	Siemens	-15-7 psi	≤0.1%	7MF4553-1GA32-1AC8-Z
DP-04	Siemens	-15-7 psi	≤0.1%	7MF4532-1GB30-1NC1-Z
FI-01	Endress-Hauser	0-1000 kg/hr	±0.5%	EC137D020000

The insulated regenerator design differed from the uninsulated regenerator in a few ways. Because of the layer of insulation needed, it was impossible to add TCs to the bed. Additionally, because the pressure taps could not be located in the heads to the regenerator, no differential pressure measurements were taken for the insulated beds. Since the orifice flow meter proved to be not useful for the uninsulated regenerators, these were omitted for the insulated regenerators. For the insulated case the TCs were inserted down the header tubes and were located ¾” above the bed, in the same location as the corresponding TC in the uninsulated regenerator.

Regenerator Construction

The regenerator construction begins with machining the end caps and the main body with holes for the pressure and thermocouple taps as shown in Figure 54.

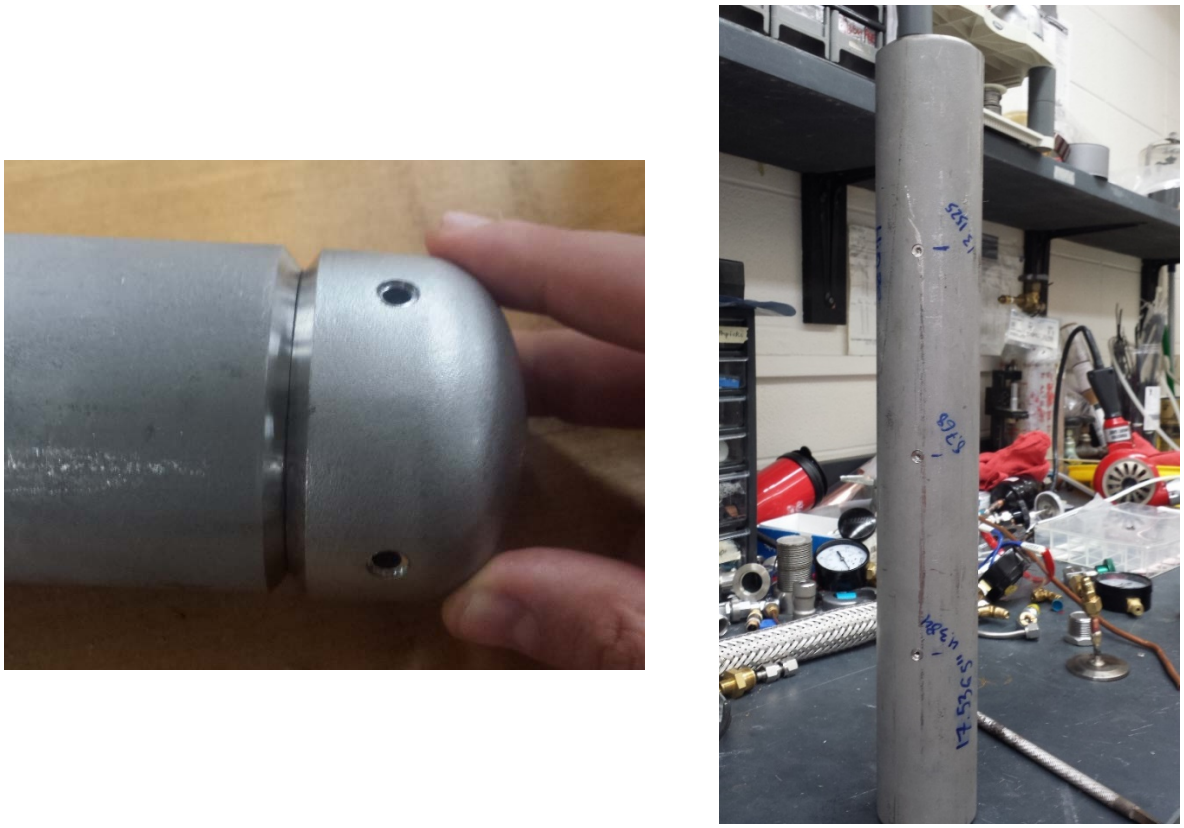

(a) (b)

Figure 54 Initial Machining of uninsulated regenerator bed

The bottom cap and screen are welded on and the bed is held vertically while the spheres are fed in. As the level of spheres reaches the bed TC taps, the TCs are fed into the center of the bed and swaged down. About 500g of spheres was fed in at a time and a hammer was used to vibrate the bed to ensure tight packing. Once the bed was full the top screen and cap were welded on, sealing the spheres inside the bed. Images of the bed construction process are shown in Figure 55.

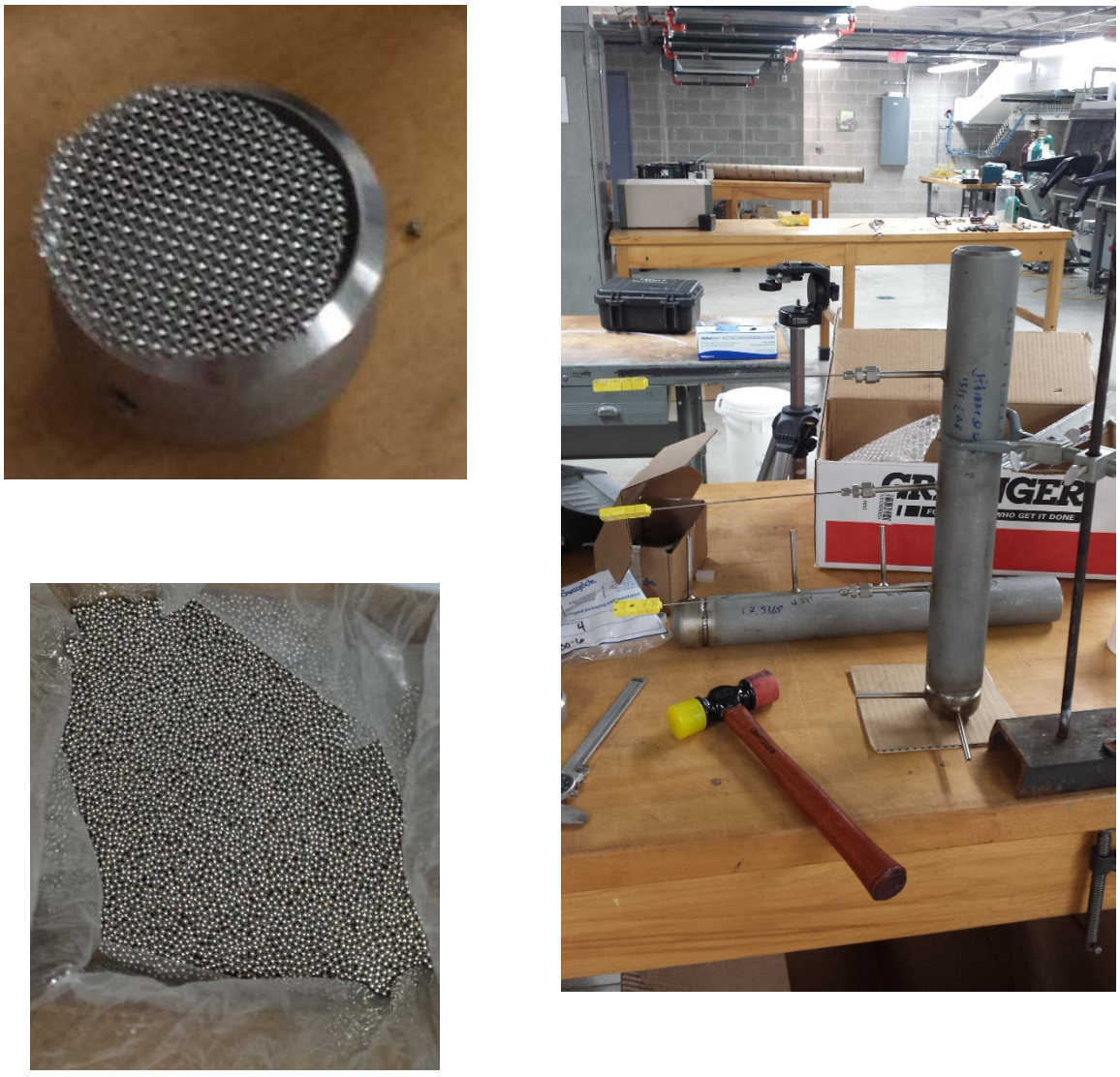

(a) (b)

Figure 55 Regenerator construction; (a) end cap with screen, (b) stand for filling with spheres with manual sphere vibrator

All of the components were weighed before and after filling with spheres, and this measurement together with the measured length and diameter of the bed allowed an accurate calculation of the void fraction in each bed. The spheres were 1/8" 304 stainless steel spheres. Since the spheres are not pressure bearing, a less expensive 304 stainless steel can be used compared to 316 stainless. 304 exhibits negligible corrosion at the temperatures and pressures the regenerator will be operated. For bed 1 the void fraction was 0.373, and bed 2 had a void fraction of 0.375. Randomly packed spheres

have a maximum void fraction of approximately 0.37 meaning that the spheres were packed tightly. After the bed was welded closed the 9/16” taps were welded on each side.

Insulated Regenerator Construction

The insulated regenerator needed considerable care in design because the difference in the expansion between the hot inner bed and cool outer shell. The first change to the design was to use a thin walled vacuum tube as the liner for the bed. The corrugations on the vacuum tube were initially too small to fit between the corrugations so the tube was stretched. A lifting ring was welded to the top and a brace welded at the bottom and an engine hoist was used to stretch the tubing to the desired length. Transitioning from the thin walled vacuum tubing to the end cap was another challenge. Initially the design called for sandwiching the thin walled tube between two 1/18” stainless rings and welding the face closed which would seal the tube. One bed was constructed in this manner, after the bed was welded shut it was tested for leaks, and a leak was discovered. Analysis of the failure showed that the weld did not penetrate down to the thin walled tubing below. Instead of welding on caps to the vacuum tube at UW, vacuum tubes were purchased with 2” sch 40 tubes already welded on. It was easy to simply weld caps onto the ends of the 2” tubing. To avoid issues with leakage from the fittings as described in the tubing section, all of the inlet and exit tubes from the bed were lined with ¼” tubing. The inner bed was constructed in the same manner as the uninsulated beds described above. Two locating brackets were welded on to each end that locate the bed in the center of the outer shell and were welded to the outer shell to hold the bed in place. Next the end caps were added to the outer shell and welded into place. The locating brackets fix the location of the caps in the bed, and as a result graphite seals were used at the interface between the outer shell and the inlet tubes, allowing the inlet tubes to expand differentially from the outer shell. A diagram of the insulated regenerator design is shown in Figure 56.

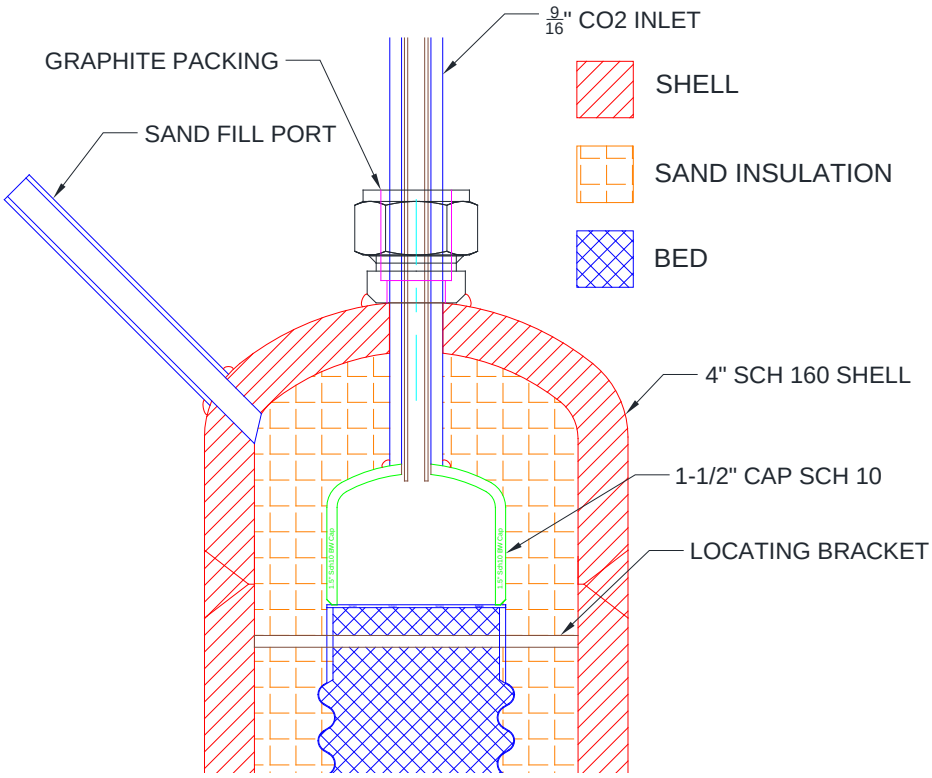

Figure 56 Diagram of insulated regenerator design showing high temperature end of regenerator

The graphite seals are essential to allow the tubing between the packed bed and the top fitting to expand at a different rate than the outer shell. The graphite seals were created by modifying a ¾" Swagelok compression fitting by removing the ferrules and replacing them with a custom machined backing ring that compresses the graphite braided packing into the fitting. The design is shown in Figure 57.

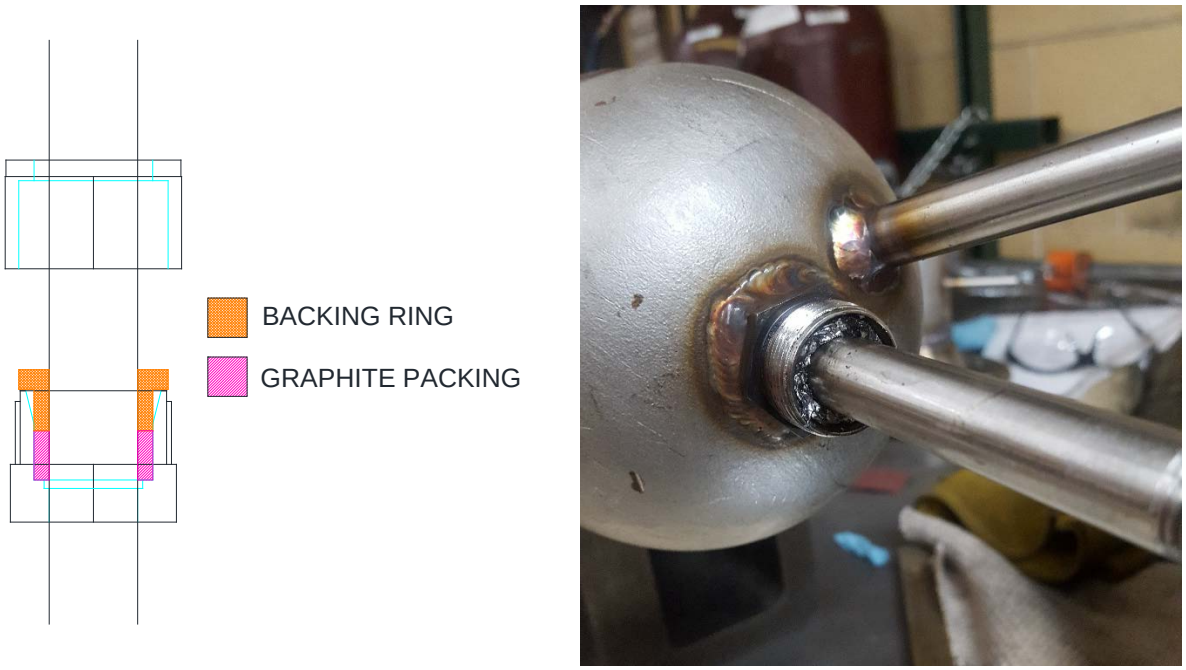

(a) (b)

Figure 57 (a) Diagram of graphite packed seal, (b) Graphite seal installed on regenerator tube

The cap of the Swagelok fitting is compressed tightly on the graphite, forming a seal. Figure 58 shows pictures of the construction of the insulated regenerator.

(a) (b)

(c)

(d)

(e)

Figure 58 Pictures showing construction process of insulated regenerator; (a) packed bed with locating bracket, (b) constructed bed inside of outer shell, (c) completed packed bed, (d) Packed bed inside of outer tube with end caps being welded on, (e) Hammer drill being used to pack the sand into the bed

Once constructed the regenerator tubes were pressure tested. Using a hydraulic pump, the packed bed and the outer shell were both pressurized at the same time to a pressure of 6050 psi which is approximately 1.5 times the 1000°F rating of the outer shell (4200 psi). Usually, the pressure vessels are tested to 1.5 times the room temperature rating of the vessel (in this case 7950 psi), however the beds were not tested at higher pressures because there was concern that the graphite seals could not withstand the higher pressure. The packed bed and outer shell were pressurized at the same time to ensure there would be no stress on the thin walled tubing used to contain the packed bed. A picture of the pressure testing process setup is shown in Figure 59.

Figure 59 Pressure testing the outer shell of the insulated regenerators

Both shells passed the pressure test with some minimal leakage past the graphite seals. However, with the design of these regenerators, if there is fluid pressure in the sand chamber the regenerator has already failed, and some leakage can be tolerated. Once the chamber was drained and dried it was filled with the CeramCast sand through the sand fill port. Initially the sand was poured into the gap and vibrated with a hammer by striking the outside of the regenerator. Once the sand reached the top of the fill port the bed was tipped to ensure the gap was fully filled. Sand was continuously added until no more sand would go into the bed, which took several hours. To speed up this process on

the second bed a hammer drill was used with a buffer plate of aluminum hose clamped to the bed as shown in Figure 58 (e). The hammer drill was set to impact only and proved effective at vibrating the regenerator bed. It was important to ensure there were no voids in the sand because a void would allow the inner bed to cyclically expand and contract which could cause failure of the bed.

After the sand was added an additional pressure test was conducted where the inner bed was pressurized. This test was designed to demonstrate the ability of the sand to transmit the pressure from the inner bed to the outer shell. The sand fill port was filled with a stainless steel mesh to prevent sand from being forced out from the insulation gap. A pressure gage was added to the fill port so that any leak could be immediately detected. The inner bed was pressurized to 4400 psi which is 1.5 times the maximum operating pressure of 3600 psi. After, the beds were cycled between 0 and 4000 psi 10 times. Both beds passed the test and were ready to be installed on the test facility.

Dimensions and fill weights of both stainless steel spheres and sand are shown in Table 17. Since the insulated beds are significantly heavier than the uninsulated beds, due to the larger thicker tubing needed for high pressure and the insulation gap, springs were used to support the bed. Mounting the bed on springs allows for thermal expansion of the regenerator bed without adding excessive stress to the tubing.

Table 17 Dimensions of insulated beds

	Bed 1	**Bed 2**
Bed Diameter (in)	1.86	1.86
Bed Length (in)	19.19	19.19
Bed Fill Weight (g)	4274.1	4284.3
Sand Fill Weight (g)	4901.2	N/A

During testing one of the liners in the insulated regenerator broke and CO_2 leaked from the bed into the sand insulation. The system was designed to handle this possibility and the beds were isolated

to prevent further leakage. In addition, all of the heaters were turned off and the pump stopped. The leak was too great to continue testing and allowing the sand to be pressurized would have allowed the opportunity for sand to make its way into the system where it could damage other components. The bed was removed and cut apart in order to inspect the failure. Inspection revealed a crack approximately 1/8” long running parallel to the welded seam near the high temperature side of the bed, near the heat affected zone of the weld. A picture of the crack is shown in Figure 60.

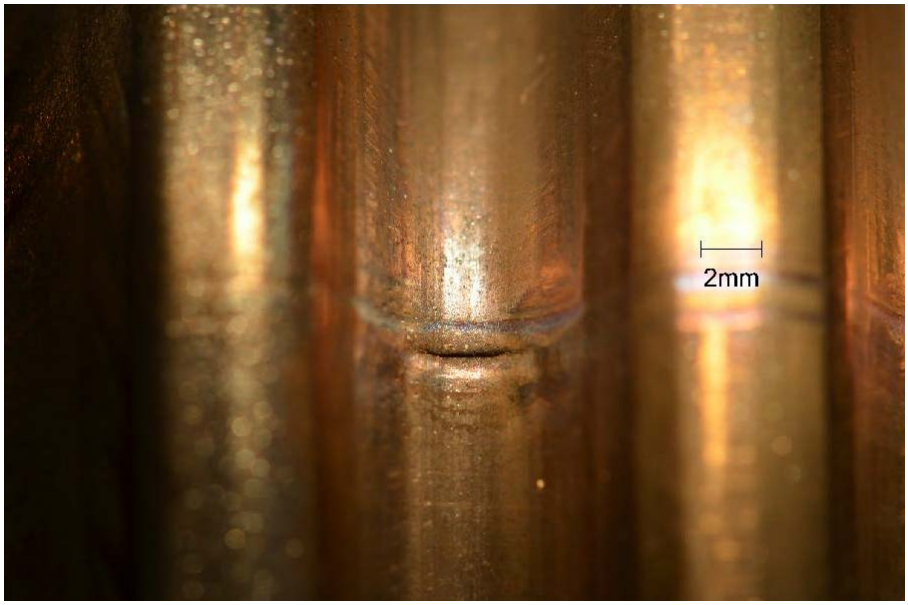

Figure 60 Crack in insulated bed liner near hot end of regenerator bed

It was impossible to repair the liner, so instead an uninsulated bed was created that could be used to collect the remainder of the data. Since data is only taken on one bed, using one uninsulated bed does not result in a loss of information. In the future three recommendations were made to prevent breakage of the liner.

1. Better packing of sand

Sand in this bed was packed using vibrations from hammering on the outer shell, which is not as effective as using the hammer drill that was used on the other bed. Poor sand packing could have allowed excessive strain in the shell which could have caused the failure.

2. Less stretching of the bed

Significant stretching was done to the bed which could have damaged the liner before testing started. Less initial stretching should keep the liner in a lower strain condition making the design more robust.

3. Smaller sand gap

Keeping a smaller gap between the outer wall and the inner liner will mean less sand to compress and lower strain on the thin walled liner.

Test Results

There were 26 uninsulated test runs that resulted in good data. The initial tests were conducted at lower temperatures and pressures to ensure the system could handle the conditions. The kinks were worked out, and the final test runs were operated at supercritical pressures and high temperature. The temperature, pressure and mass flow conditions for all the uninsulated runs are shown in Table 18.

Table 18 Test conditions for uninsulated regenerators

Run	Hot Temp (°C)	Cold Temp (°C)	High Pressure	Low Pressure	CtHB Mass Flow (kg/s)	HtCB Mass Flow (kg/s)	Switching Time (s)	Eff. Exp.	Eff. Model	NTU	C_m
1	253.2	70.5	7.80	3.39	0.0288	0.0291	170	0.844	0.813	18.2	0.79
2	217.1	69.4	7.41	2.75	0.0293	0.0296	161	0.868	0.844	17.8	0.83
3	222.6	68.8	7.67	4.55	0.0263	0.0266	161	0.863	0.862	18.2	0.89
4	110.7	67.0	8.96	4.95	0.0391	0.0401	80	0.935	0.931	14.3	0.98
5	326.7	40.3	6.44	4.96	0.0332	0.0329	120	0.871	0.874	17.4	0.97
6	221.9	65.5	7.08	4.90	0.0200	0.0204	45	0.991	0.973	20.2	4.18
7	401.0	74.6	6.44	4.97	0.0335	0.0331	90	0.907	0.927	18.9	1.35
8	503.2	165.2	7.02	5.20	0.0286	0.0284	90	0.912	0.939	21.3	1.61
9	307.9	51.2	8.55	5.88	0.0294	0.0295	100	0.961	0.939	17.4	1.23
10	383.1	81.8	14.46	8.69	0.0315	0.0302	100	0.890	0.949	17.7	1.14
11	480.6	149.3	14.89	9.11	0.0313	0.0305	100	0.943	0.940	20.0	1.26
12	487.5	148.4	14.92	9.13	0.0302	0.0300	80	0.959	0.953	20.3	1.61
13	489.2	147.3	14.98	9.17	0.0296	0.0290	60	0.980	0.969	20.6	2.20
14	240.6	72.4	9.01	8.50	0.0283	0.0278	140	0.837	0.831	17.3	0.89
15	241.8	72.2	9.99	9.30	0.0305	0.0300	120	0.848	0.847	16.6	0.93
16	243.6	71.6	9.69	8.81	0.0297	0.0293	100	0.901	0.905	16.9	1.16
17	245.9	70.9	9.52	8.66	0.0285	0.0283	70	0.946	0.939	17.3	1.73
18	246.7	70.6	9.44	8.58	0.0279	0.0277	50	0.968	0.952	17.6	2.48
19	247.6	70.4	9.40	8.55	0.0263	0.0265	30	0.976	0.955	18.3	4.36
20	244.0	72.7	10.03	9.36	0.0158	0.0152	280	0.821	0.781	20.2	0.77
21	240.7	72.2	10.18	9.50	0.0162	0.0157	240	0.847	0.838	19.9	0.87
22	237.6	71.6	10.27	9.58	0.0162	0.0157	200	0.886	0.898	19.8	1.03
23	236.4	71.2	10.30	9.61	0.0163	0.0159	140	0.940	0.942	19.7	1.46

24	234.2	70.0	9.76	8.76	0.0154	0.0150	100	0.982	0.966	20.4	2.22
25	233.0	69.5	9.46	8.52	0.0146	0.0144	60	0.993	0.971	21.0	3.91
26	231.9	69.3	9.32	8.41	0.0142	0.0141	40	0.999	0.972	21.5	6.04

The insulated regenerator was designed to have a significantly higher NTU than the uninsulated design. The higher NTU allows higher effectiveness to be achieved at shorter switching times. This was accomplished in two ways, first the sphere size was reduced, from 1/8” in the uninsulated case to 3/32” in the insulated case. The smaller spheres increase the volume specific surface area as well as increases the heat transfer coefficient, both of which result in a higher NTU. The diameter of the packed bed for the insulated case was also decreased which increases the mass flux through the bed, further increasing the heat transfer coefficient. At the 10MW size the regenerator is designed to have an NTU of about 33, whereas the uninsulated regenerator has an NTU of around 18 for normal mass flow rates and 22 at higher mass flow rates. Looking back to Figure 12 it is clear that this difference in NTU can cause a significant reduction to the effectiveness of the regenerator. The insulated regenerator fixes this issue and more closely matches the NTU and C_m of the 10MW cycle. The test conditions for the insulated regenerator runs are shown in Table 19.

Table 19 Test conditions for insulated regenerators

Run	Hot Temp (°C)	Cold Temp (°C)	High Pressure (MPa)	Low Pressure (MPa)	CtHB Mass Flow (kg/s)	HtCB Mass Flow (kg/s)	Switching Time (s)	Eff. Exp.	Eff. Model	NTU	C_m
1	326.6	163.5	8.38	7.51	0.0291	0.0294	75	0.967	0.953	31.2	1.85
2	327.9	163.3	8.44	7.56	0.0296	0.0299	90	0.954	0.945	30.9	1.52
3	328.6	163.4	8.42	7.55	0.0290	0.0291	60	0.975	0.963	31.5	2.33
4	421.5	164.6	8.81	7.90	0.0284	0.0286	90	0.954	0.949	32.3	1.60
5	421.4	164.0	8.66	7.76	0.0276	0.0278	75	0.964	0.956	32.7	1.98
6	422.7	163.8	8.52	7.64	0.0264	0.0268	60	0.974	0.965	33.3	2.58
7	515.1	165.0	8.46	7.60	0.0256	0.0255	90	0.963	0.959	34.3	1.80
8	515.7	164.4	8.35	7.48	0.0251	0.0253	75	0.970	0.961	34.6	2.19
9	516.6	165.0	8.24	7.41	0.0244	0.0242	60	0.982	0.971	35.2	2.85
10	315.1	117.7	14.70	8.66	0.0319	0.0331	90	0.976	0.958	28.2	1.26
11	318.2	114.5	14.46	8.57	0.0311	0.0318	75	0.989	0.975	28.5	1.57
12	318.3	110.7	14.34	8.55	0.0314	0.0320	60	1.001	0.984	28.4	1.93
13	413.0	118.6	15.26	8.24	0.0312	0.0324	90	0.972	0.960	29.6	1.34
14	414.4	118.5	15.37	8.33	0.0315	0.0325	75	0.984	0.972	29.6	1.59
15	415.5	116.9	15.36	8.35	0.0318	0.0324	60	0.997	0.982	29.7	1.98
16	514.1	164.8	13.81	9.39	0.0307	0.0313	90	0.975	0.951	32.0	1.44
17	515.7	163.6	15.43	8.42	0.0306	0.0313	75	0.967	0.966	32.1	1.73
18	515.5	163.8	15.58	8.65	0.0305	0.0318	60	0.956	0.965	32.2	2.14
19	300.9	126.5	23.67	8.89	0.0353	0.0354	90	1.013	0.973	27.0	1.09
20	297.6	121.1	23.68	8.59	0.0389	0.0400	75	1.025	0.978	26.0	1.16
21	301.6	121.5	23.71	8.28	0.0324	0.0333	60	1.032	0.996	27.7	1.75
22	401.9	157.1	23.32	9.33	0.0334	0.0363	90	1.003	0.947	29.3	1.20
23	404.8	157.2	23.21	9.12	0.0306	0.0332	75	1.012	0.970	30.2	1.57
24	405.1	158.2	23.76	7.95	0.0282	0.0304	60	1.018	0.985	31.2	2.16

Corrections

Data taken by the data acquisition system needs to be corrected in two ways due to errors in measurement. Due to the transient nature of the regenerator operation the Thermocouple (TC) reading must be corrected for the time constant of the TC. Additionally, due to the vertical orientation of the regenerator beds the pressure drop in the bed needs to be corrected for the static pressure as a result in difference in density inside and outside of the regenerator bed.

The TCs do not respond instantly to a change in temperature which is not a problem for steady state measurements, however the transients from the regenerator system are on the order of seconds which is similar to the time constant of the TC. The 1/16" TCs were the smallest sized TCs that could be used in the system and had the smallest time constant. The time constant of the TC can be measured by inducing a step change in temperature and seeing how long it takes for the TC to respond. When the bed switches from the HtCB to the CtHB there is a step change in temperature at the cold end of the regenerator. The time constant is how long it takes for the TC to experience a 63% change in reading, in this case it was measured to be 0.75s. A simple first order lumped capacitance model was used to correct the temperatures of the TCs. The equations used for the correction are given in (1.19).

$$T_{c,i} = \tau\left(\frac{T_i - T_{i-1}}{\Delta t}\right) + T_i \tag{1.19}$$

where τ is the time constant of the TC, T_i is the measured temperature at time i, T_{i-1} is the measured temperature at time i-1, and Δt is the difference in time between measurements. The result of correcting for the time constant is shown in Figure 61.

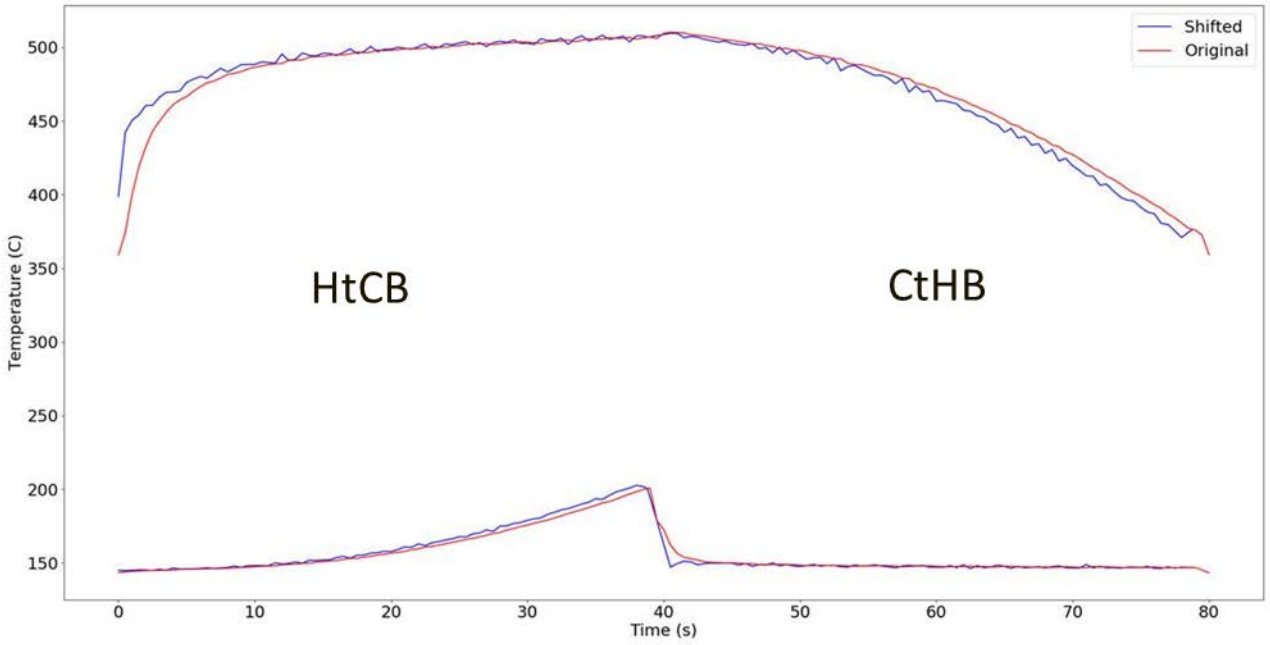

Figure 61 Measured and corrected temperature profiles of an example test run

On the HtCB the temperatures are shifted up slightly for both sides of the regenerator while the CtHB does the opposite. These corrections are most pronounced on the high temperature side where the temperature change is much larger. Correcting for the TC time constant changes the measured effectiveness by about 1%.

Pressure drop through the bed also needs to be taken into account. The taps for measuring differential pressure are about 19 inches different in height from each other. Static pressure due to the difference in pressure can be calculated using equation (1.20).

$$dP_{header} = \rho\, g\, \Delta h \tag{1.20}$$

Where ρ is the density of the fluid in the vertical section of the leads, g is the gravitational constant, and Δh is the difference in height between the tap locations. If the density in the pressure tap headers was the same as those in the bed, this would not be an issue. However, the bed is significantly hotter and thus less dense than the headers. Since the headers are far away from the regenerators, the

temperature will be close to room temperature. Thermocouples were attached to the headers to monitor the temperature during a run. The cycle was run with a high and low side temperature of 250°C and 70°C respectively. The headers remained constant at 25°C throughout the cycle. Changing the temperature even slightly can drastically affect the correction especially near the critical point as shown in Figure 62.

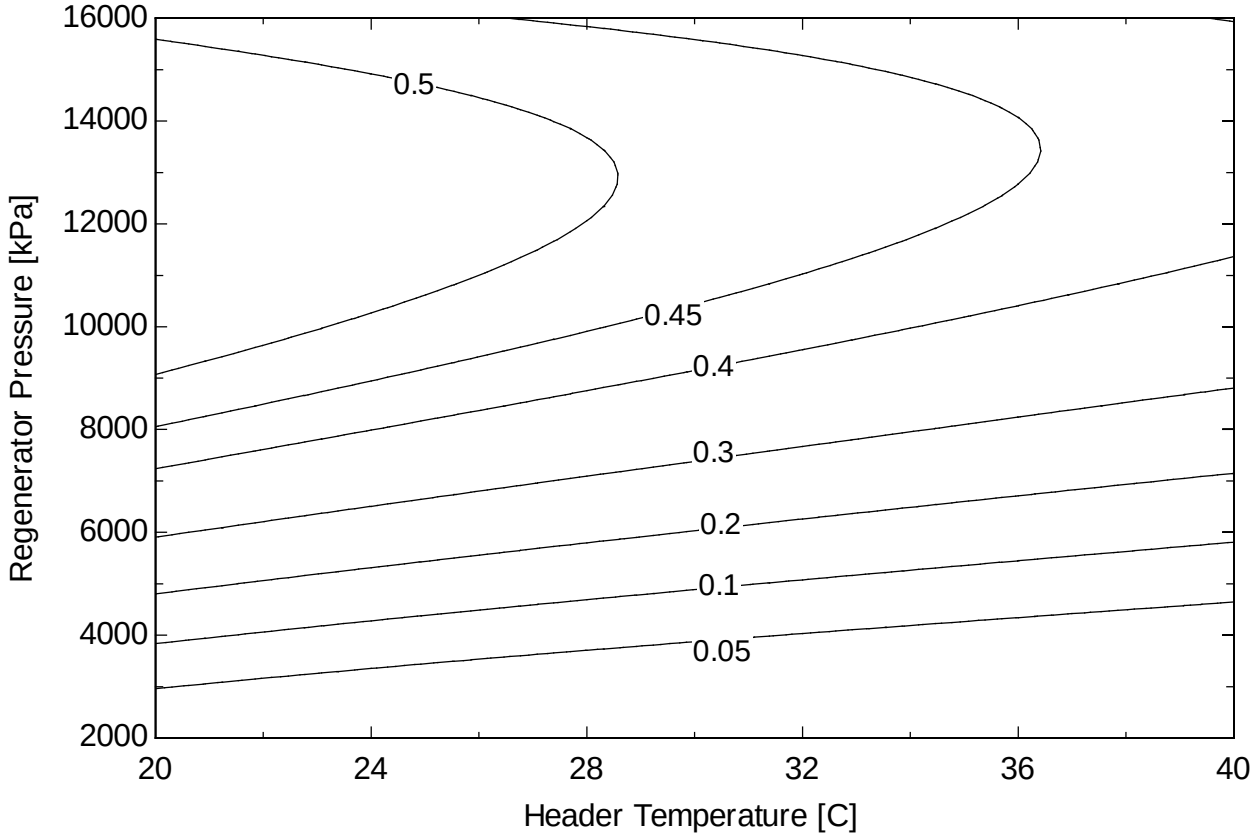

Figure 62 Differential pressure measurement correction is psi as a function of pressure in the regenerator and temperature in the differential pressure measurement headers

The static pressure correction is usually on the order of 0.3 psi which is on the same order of magnitude of the measured pressure drop of 0.5-1.5psi. The correction for dP is calculated from the contribution of the headers as shown in equation (1.20) and subtracting out the effect of the bed which is calculated by integrating the density over the height of the bed shown in equation (1.21).

$$dP_{bed} = g\int_{0}^{L} \rho(T(x), P)\, dx \tag{1.21}$$

where ρ(T(x),P) is the density of the fluid at pressure P and temperature T(x) which is the temperature at location x. T(x) is determined using a linear interpolation of the temperature data in the bed. L is the total length of the bed and g is the gravitational constant. Combining these two corrections with the measurement for pressure drop gives the actual pressure drop in the bed shown in equation (1.22).

$$dP_{act} = dP_{measure} - dP_{header} + dP_{bed} \tag{1.22}$$

Since there is mass flow in both directions, the differential pressure measurement can be either positive or negative. Either way the correction always contributes to pressure drop in the same way. All pressure drops are reported as the absolute value of the corrected pressure drop.

Effectiveness Calculation

Once steady state is reached, data is taken for 20-30 minutes which corresponds to 10-20 cycles depending on the switching time. As mentioned before the temperatures are recorded every 0.5s and the pressure and mass flow recorded every 0.25s. To calculate effectiveness the amount of heat transferred in one cycle (Q) is needed. The important part of the cycle is the CtHB where the energy is recovered by the fluid from the bed. The following calculations shown were done by Logan Rapp, for a more detailed write-up please see his thesis [99]. Using the measured temperature and pressure at the inlet and exit of the bed the enthalpy can be calculated using FIT [89]. Using the enthalpy and mass flow from the Coriolis flow meter Q can be calculated according to equation (1.23).

$$Q = \int_{CtHB_{start}}^{CtHB_{end}} \dot{m}\left(h_{out} - h_{in}\right) dt \tag{1.23}$$

Where $\dot{m}$ is the mass flow, h_{out} is the exit enthalpy, and h_{in} is the inlet enthalpy. A trapezoidal method is used for integration. A heat transfer rate can be calculated according to equation (1.24).

$$\dot{Q} = \frac{2Q}{P_0} \tag{1.24}$$

Where P_0 is the total cycle time. To compare the regenerators directly to recuperators, the effectiveness calculation for both must be analogous. The effectiveness calculation is shown in equation (1.25).

$$\varepsilon = \frac{\dot{Q}}{\dot{Q}_{\max}} \tag{1.25}$$

$\dot{Q}_{max}$ is the maximum possible heat transfer from a perfectly effective recuperator operating at the same inlet conditions as the regenerator. The hot inlet temperature is determined by taking the mass flow average of the inlet temperature for the HtCB and the cold inlet is determined by taking the mass flow average of the inlet temperature during the CtHB. The pressure is calculated in the same manner as temperature. The mass flow must be carefully chosen to account for the switchover time. If the average mass flow during the CtHB and HtCB was used, more flow would be going through the recuperator than the regenerator, artificially inflating $\dot{Q}_{max}$. The corrected mass flow for the CtHB is shown in equation (1.26), the process is identical for the HtCB.

$$\dot{m}_{CtHB,cor} = \frac{(P_0 / 2)\,\dot{m}_{CtHB}}{(P_0 / 2) + P_{switch}} \tag{1.26}$$

Where P_{switch} is the length of time to accomplish the switching sequence outlined above. The same EES routine used in the 10MW model is used to calculate $\dot{Q}_{max}$ for the experimental data.

The effectiveness of each cycle during the steady state data is calculated since every cycle will have a slightly different value. Each cycle has an error that corresponds to the uncertainty of the effectiveness calculation due to the accuracy of the instruments. The uncertainty is calculated from the

accuracy values listed in Table 16 using a Monte Carlo method. The Monte Carlo method calculates the effectiveness for many different runs and for each run the input parameters are varied randomly. The randomness is controlled by a gaussian distribution where the standard deviation is the uncertainty of that measurement. The uncertainty in effectiveness is around 1.2% due to instrument accuracy. The standard deviation of the effectiveness for each run is much smaller than the uncertainty in the model. A more detailed report on calculating uncertainty is available in [99].

Since there are many different runs at the same conditions, the average effectiveness can be calculated. The calculation for average effectiveness for all of the runs is shown in equation (1.27).

$$\varepsilon_{avg} = \frac{\sum Q}{\sum Q_{\max}} \tag{1.27}$$

Calculating the average effectiveness this way takes into account any correlation between effectiveness and heat transfer. If the effectiveness for each run were averaged, the result would not be the same if every run did not have the same Q_{max}. A single value is also needed for the average uncertainty. This value needs to take into account both the uncertainty in the measurements, and the standard deviation of effectiveness between the runs. This is done by taking the root mean square of the uncertainty of the effectiveness measurement and the standard deviation of all runs as shown in equation (1.28).

$$U = \sqrt{U_{measure}^2 + \sigma^2} \tag{1.28}$$

$U_{measure}$ is the uncertainty of the measurements and σ is the standard deviation on the effectiveness between the runs.

Temporal experimental test data needs to be turned into a single point that can be used in the effectiveness-NTU-C_m model. The same inputs that are used for calculating $\dot{Q}_{max}$ are used as inputs to

the effectiveness-NTU-C_m model. A comparison between the model and the experimental results is shown in Figure 63 for the uninsulated regenerators and Figure 64 for insulated regenerators.

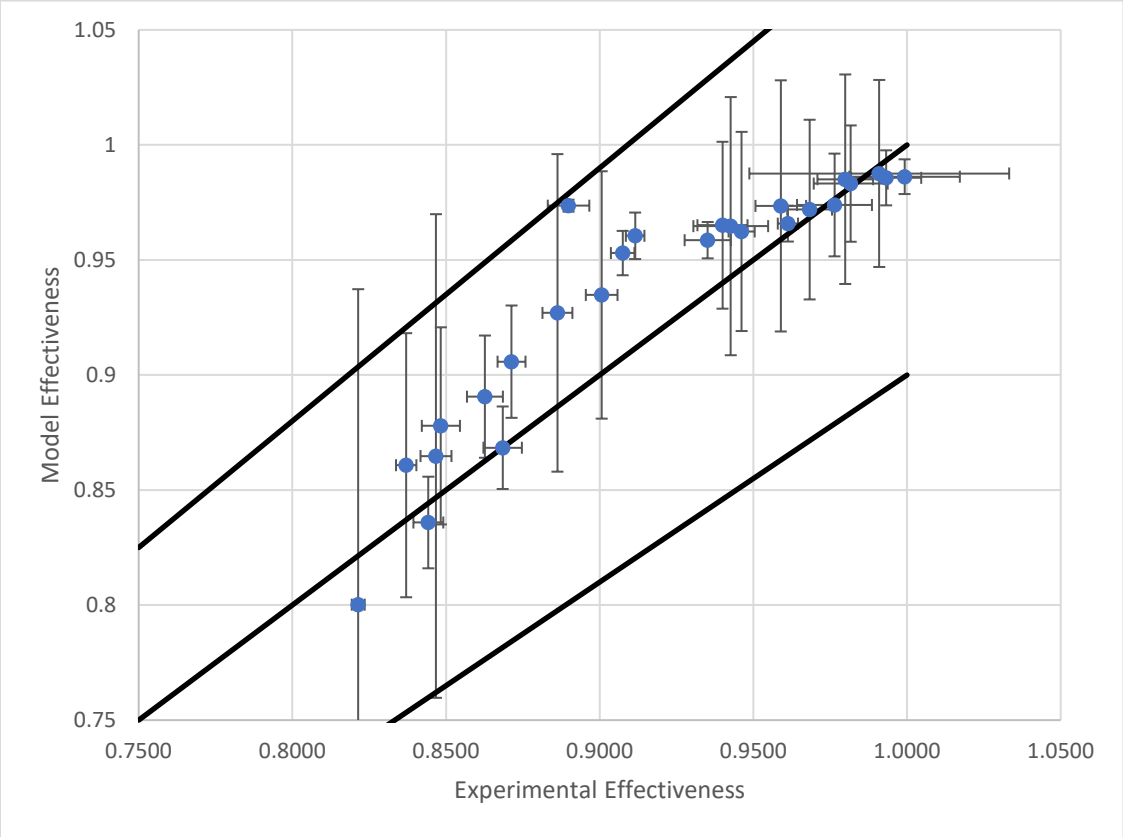

Figure 63 Model effectiveness vs Experimental effectiveness for uninsulated regenerator with 10% error lines

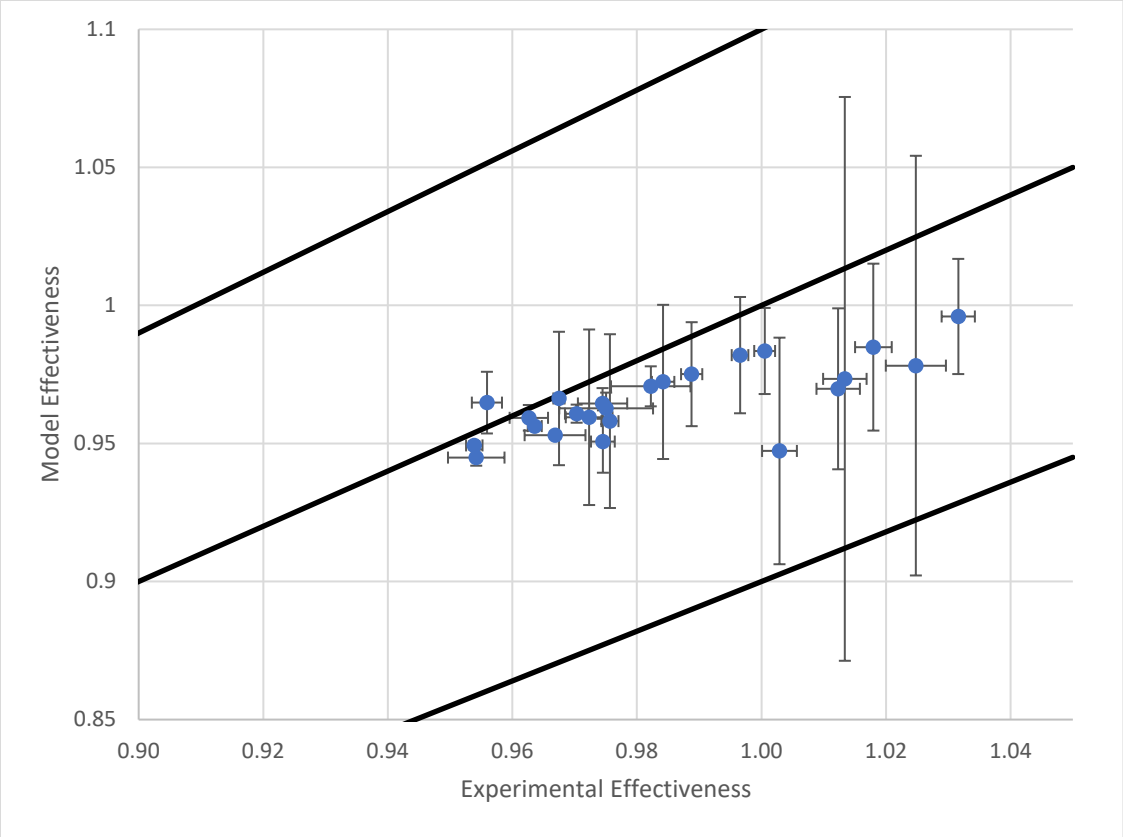

Figure 64 Model effectiveness vs Experimental effectiveness for insulated regenerator with 10% error lines

Overall the model did a good job at predicting effectiveness with an average error of only 1.8%. At low effectiveness the model slightly overpredicts the regenerator performance, while at higher effectiveness the model matches much better for the uninsulated case. The insulated case always underpredicts regenerator performance. Having the model slightly under predict performance means the model is conservative which is preferential to it overpredicting performance. One of the reasons for the mismatch between the model and experimental data for the uninsulated case is the participation of the wall. The model does not take into account the participation of the wall which could result in a larger matrix capacity ratio than expected. Once this was hypothesized, thermocouples were welded to the outside of the shell and temperature was measured. The thermocouples were evenly spaced along the length of the bed. The temperature averaged over many runs is shown in Figure 65.

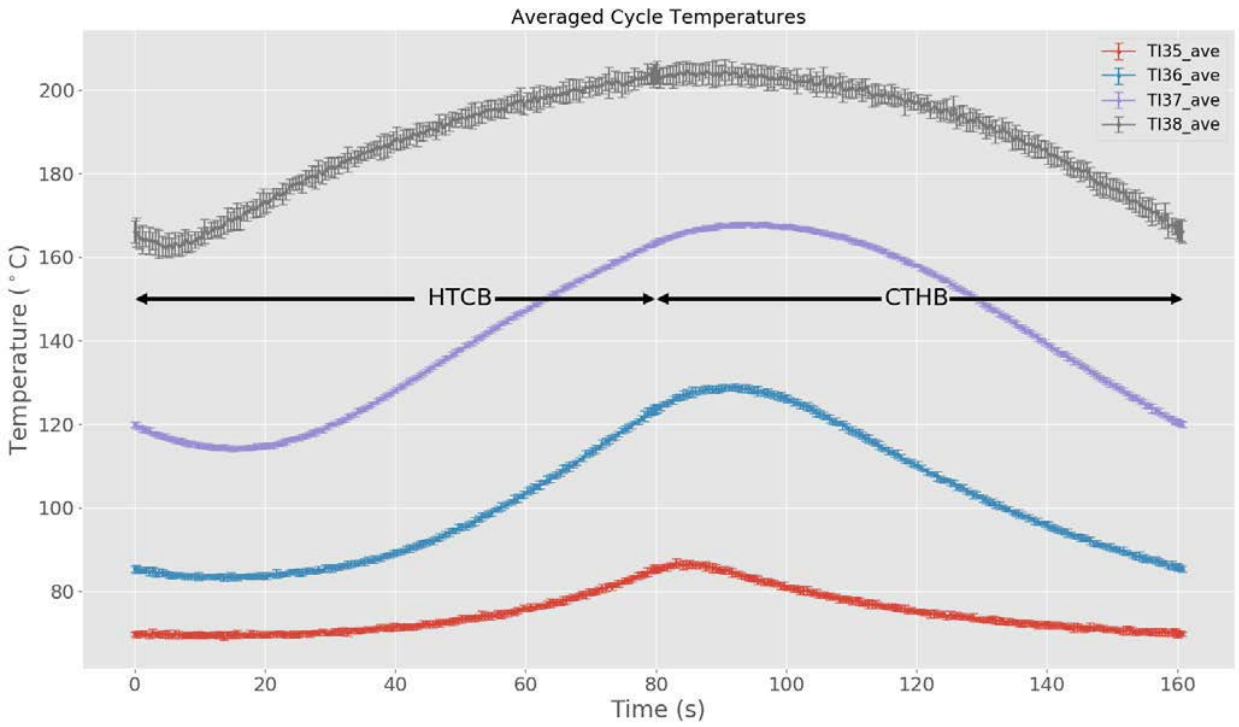

Figure 65 Wall Temperature profiles for run at 250°C, from [99]

It is clear that the wall temperature changes drastically throughout one cycle, in some cases up to 50°C. This is much less drastic than the temperature change of the bed, however it is still important because both the bed and wall weigh about 4kg. A simple model was created with four zones that were weighted based on the location of the thermocouples. The amount of energy stored and released from the wall for one cycle can be calculated according to equation (1.29).

$$Q = \sum_{i=1}^{4} m_i \, c \left(T_{i,\max} - T_{i,\min} \right) \tag{1.29}$$

Where *i* is the index of each TC, m_i is the mass of each section, and *c* is the specific heat capacity of the wall material. For the case shown, the amount of heat released from the bed is about 30 percent of the total heat transfer as measured using equation (1.23). This means that the wall could be having a significant impact on the experimental results. It is important to calculate the diffusive time constant of the wall to see if the wall will respond quickly to the change in temperature, or in other words, how

good is it at storing and releasing heat. A short time constant means that the wall will be uniform temperature at the temperature of the inner wall, while a long time constant means there will be a large difference between the inner and outer wall temperature. The diffusive time constant is calculated according to equation (1.30).

$$\tau_{diff} = \frac{L^2}{4\alpha} \tag{1.30}$$

Where L is the thickness of the wall, and α is the thermal diffusivity of the wall material (316SS). The result is a time constant between 1.5 and 2 seconds depending on the cycle conditions. This is much less than the time it takes to complete one cycle, so the wall can be considered a lumped capacitance. The lumped capacitance time constant also needs to be calculated, which is a measure of the amount of time it takes for heat to get from the fluid into the wall. The equation for calculating the lumped capacitance time constant is shown in (1.31).

$$\tau_{lumped} = \frac{m\,c}{\bar{h}\,A_s} \tag{1.31}$$

Where m is the mass of the wall, c is the specific heat capacity of the wall material, $\bar{h}$ is the average heat transfer coefficient at the wall (it is assumed to be the same as the heat transfer coefficient of the spheres), and A_s is the surface area of the wall. The lumped capacitance time constant is around 30 seconds with slight variation based on the actual operating conditions of the bed. The lumped capacitance time constant is much closer to the cycle time (between 30-200 seconds) and as a result the temperature of the wall will lag significantly behind the temperature of the bed. This lag can be seen in Figure 65 where the peaks do not correspond to the switchover times. So instead of the wall adding to the mass of the bed it is now helping the bed at some times and hurting it in others. Thus, the wall

cannot be treated simply as extra bed mass, instead it is like having a second bed in parallel to the primary packed bed. The effectiveness-NTU-C_m is simply not equipped to handle a situation like that.

What is needed is a one-dimensional transient numerical model that can model both the bed and the wall at the same time. An initial regenerator model was created based on the numerical regenerator model provided in [40]. This model uses matrix decomposition to quickly solve the temperature profiles in the regenerator bed as a function of time. However, this model relies on constant properties which is an ok assumption when the regenerator is operating far from the critical point but falls apart near the critical point where properties vary greatly. Because the properties cannot be determined locally, the heat transfer coefficients cannot be determined locally either which can be important when there is a large temperature difference from one end of the regenerator to the other. In addition, this model does not take into account the mass of CO_2 in the bed, it assumes that there is no void fraction. The mass in the bed is especially important when the regenerator is switching over. Evan Reznicek at Colorado School of Mines (CSM) has developed a numerical model that can calculate local properties and takes into account the mass trapped in the bed. Instead of matrix decomposition, a successive substitution method is used that takes much longer to solve. Using the data from the experiments as an input, he tried to model the bed and the wall at the same time, which resulted in a poor match to experimental results. Initial tests with the numerical model had an acceptable match on effectiveness with the experimental data, but when the wall was added, it actually made the results worse. It was hypothesized that the difference could be attributed to the heat transfer coefficient being different between the bed and wall, due to the larger gaps between the wall and the spheres. The numerical model was ran over a range of wall heat transfer coefficients, and the cases that matched best with effectiveness did not match well with the measured wall temperature profile. Since the 10MW regenerator was designed to have an insulated wall, where there would be little to no wall participation

it was determined that no more resources should be devoted to trying to match the wall temperature profile, when the effectiveness matched well.

The insulated regenerator always underpredicted performance for the regenerator which could be a result of a temperature spike experienced at high pressure differential between the two beds. The temperature spike resulted in an increase in measured effectiveness. In these cases, high pressure differential caused a spike in temperature at the hot side of the regenerator bed as a result of compressing the CO_2 stuck in the bed, Figure 66 shows an example of the temperature spike.

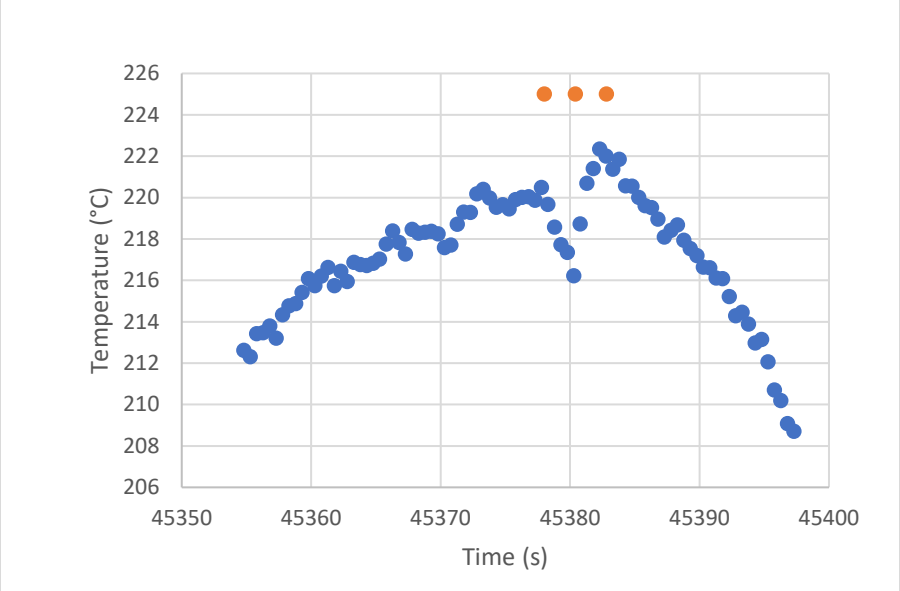

Figure 66 Temperature spike on high temperature TC as a result of compression

Modeling the compression of the fluid in the bed as isentroptic compression proved that a 100-200°C temperature rise was possible simply from compression. In reality, the mixing in the bed limited the temperature rise to between 10-20°C. This temperature rise was not seen in the uninsulated regenerators because of the orifice flow meter which slowed down the pressurization process enough to cause the temperature spike to be minimized by mixing of the fluid in the bed. The temperature spike actually acts to increase the performance of the regenerator by taking work done by the compressor and turning it into heat in the regenerator. Calculations showed that a 1% increase in effectiveness was

possible because of this effect. However, the time constant of the TC needs to be considered as well when reading these results. The temperature spike is temporary, but the TC time constant can cause the effectiveness to be measured larger than it actually is which is the reason for effectiveness greater than one in some cases. Additionally, the temperature spike can introduce considerable uncertainty in the effectiveness calculation which is the reason for the large uncertainty in model effectiveness for some of the runs in Figure 64.

One of the goals of testing the insulated regenerator was determining the effectiveness of the insulation. The insulated regenerators were run at 250°C, 350°C, 450°C, and 550°C and the minimum and maximum wall temperature was recorded at five locations along the length of the bed. A plot showing the results can be seen in Figure 67.

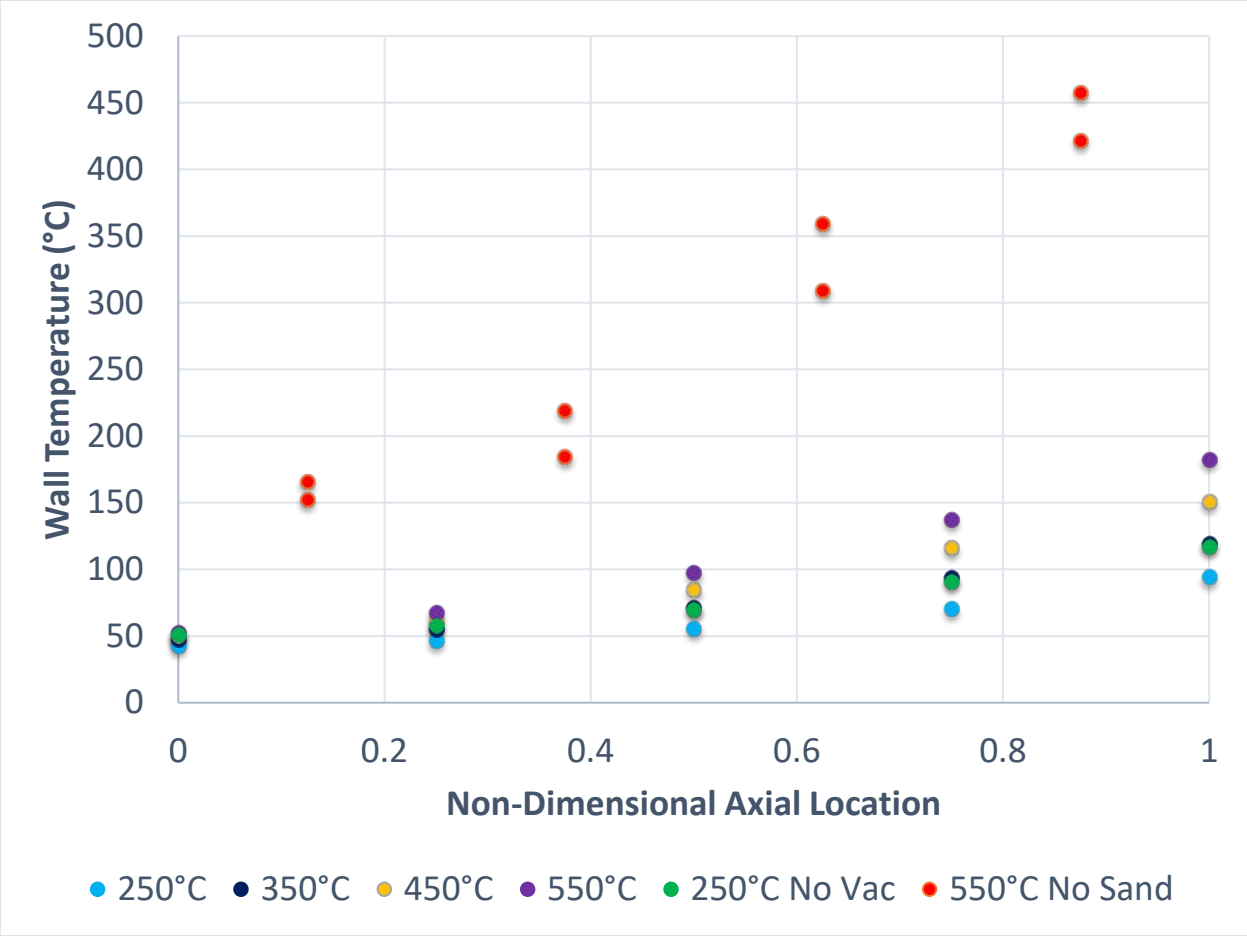

Figure 67 Wall Temperature vs position for insulated and uninsulated runs at different temperatures

Figure 67 shows that even with 550°C fluid inside of the bed, the outer wall of the insulated bed remains below 200°C which is much less than the 375°C required for keeping the allowable stress high in the wall material. It also shows that the sand conductivity decreases from 0.2 W/m-K to 0.1 W/m-K under vacuum which further reduces the amount of insulation needed. Figure 67 also shows that all thermal transients in the wall have been eliminated by using the insulated regenerators. The insulated regenerators passed all tests for wall temperature and thermal performance.

Pressure Drop

Another important parameter to verify is the pressure drop through the bed. The maximum pressure drop through the bed is about 1% of the absolute high side pressure. Even a relatively small

change in pressure drop can result in a significant reduction in power output from the turbine which hurts the efficiency of the cycle. As mentioned above in the corrections section, the low flow rate through the bed creates a very low pressure drop over the bed, in some cases less than 1psi. Several different pressure drop correlations were tried to determine which would best match the experimental data. The Fahien-Schriver correlation had the best match to the experimental data [77]. The model vs experimental pressure drop for the uninsulated tests is shown in Figure 68 and Figure 69. Because of the design of the insulated regenerator, there was no way to accurately measure the pressure drop through the insulated bed.

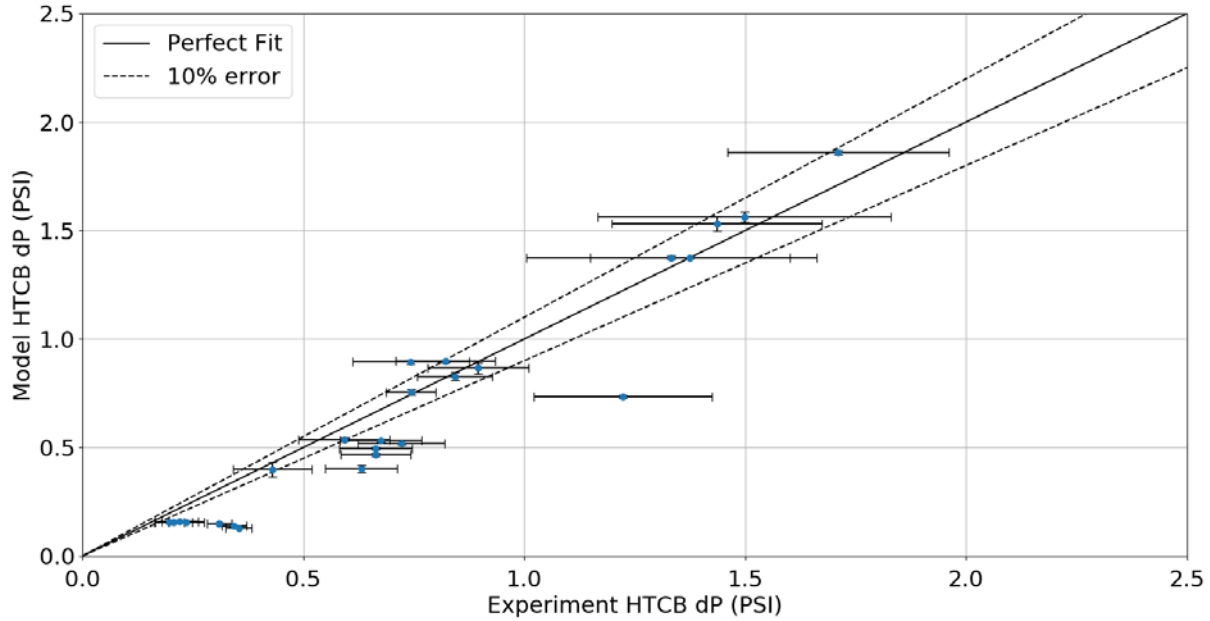

Figure 68 Modeled pressure drop vs experimental pressure drop for HtCB of uninsulated test runs

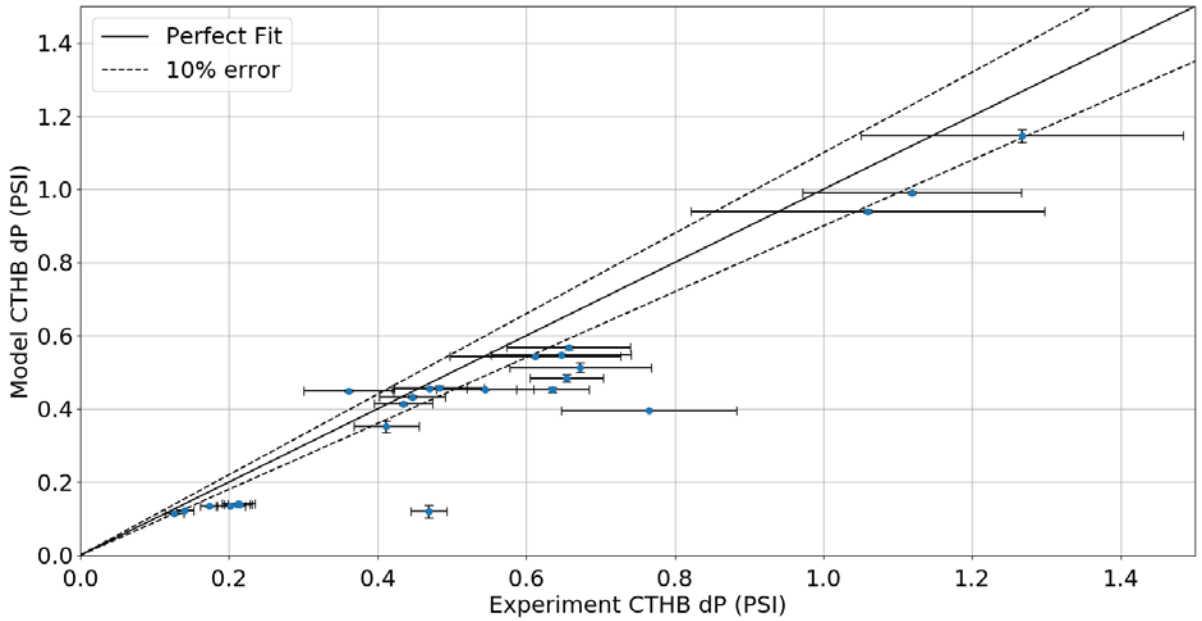

Figure 69 Modeled pressure drop vs experimental pressure drop for CtHB of uninsulated test runs

There is some observed error in the agreement between the modeled and measured pressure drop across the packed bed. In both the HtCB and CtHB, when the experimental pressure drop is less than 1 psi the model under predicts pressure drop. Because the compressor mass flow rate fluctuates every 3 seconds (the time it takes for one stroke of the compressor) the flow is changing by as much as 10 percent for the low flow (low DP) tests. This variation in mass flow results in a variation in pressure drop over the bed and the result are the very large error bars seen in Figure 68 and Figure 69. Another issue is that the pressure drops are on the same order as the corrections needed to correct for the static pressure in the pressure taps. If the beds were designed to have a higher pressure drop, then the measurements would be more accurate because the corrections would be smaller compared to the absolute pressure drop. Since the properties in the bed are well known and pressure drop through a packed bed has been exhaustively researched the mismatch between the experimental data and model is not a large concern [100–102]. To ensure the pressure drop model is conservative, a 20% increase to pressure drop was added to the 10MW model.

Carryover

Carryover is difficult to measure because of the short period of time it occurs over. The valves can be actuated in 0.6s and the large pressure differential between the bed and the lines mean that the mass flow occurs very quickly. This quick spike in flow rate cannot be measured accurately by the Coriolis flow meter or the orifice flow meter. What is well known is the temperature profile in the bed using the 3 TCs located in the bed and the 2 TC in the end caps. The pressure in the regenerators can also be accurately measured using the absolute pressure sensors. The same method that is used to calculate carryover in the model can be used to calculate the actual carryover, however instead of using a linear temperature profile for the bed, instead the actual temperature profile can be used. Again, because of the design of the insulated regenerator the carryover for the insulated case cannot be measured because TCs cannot be inserted into the bed. The actual bed temperature differs quite significantly from the temperature predicted by the model, the actual and predicted profiles are shown in Figure 70.

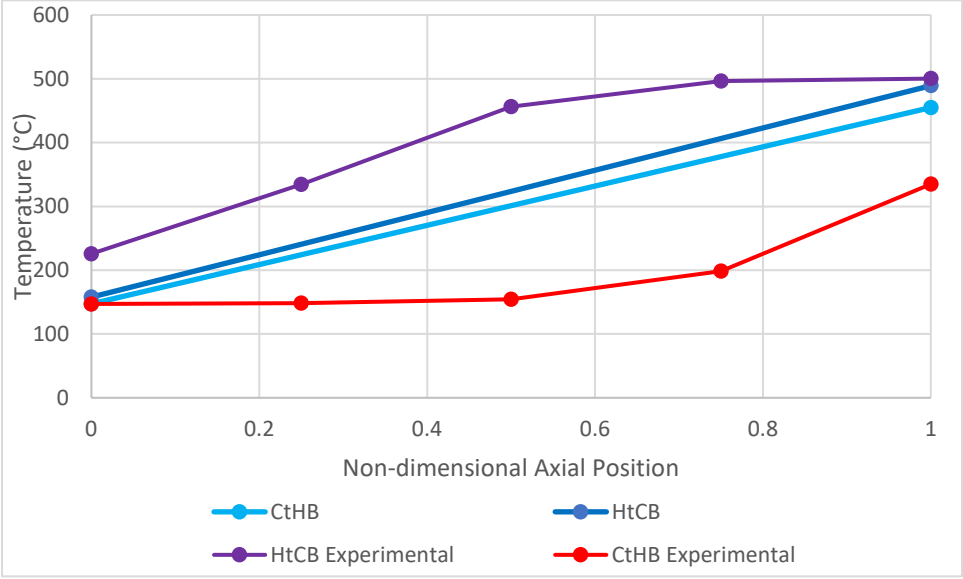

Figure 70 Experimental and model temperature profiles used for calculating carryover of a representative cycle

Since the data does not contain a continuous temperature profile, the bed is instead broken into 5 sections based on the location of the TCs. The location of the TC and the percentage of the total bed volume for each TC is shown in Figure 71.

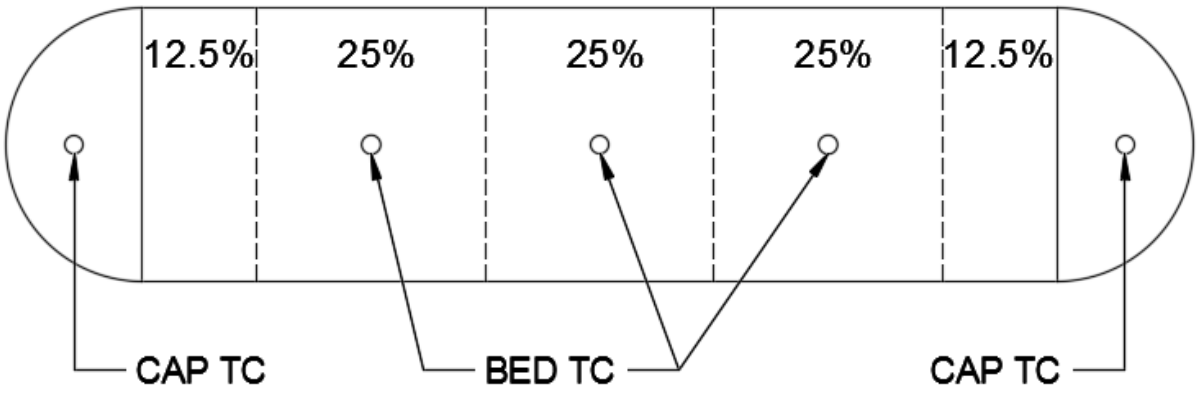

Figure 71 Location of TC in bed and zones used for calculating mass for carryover calculation

The bed is broken into 5 nodes and the temperature is assumed to be constant within each node. The center 3 nodes each account for 25% of the void volume while the two end cap TC account for only 12.5% each. The mass in the bed is calculated continuously throughout the cycle and the carryover is calculated by finding the difference between the maximum and minimum mass in the bed. The model carryover compared to the experimental carryover is shown in Figure 72.

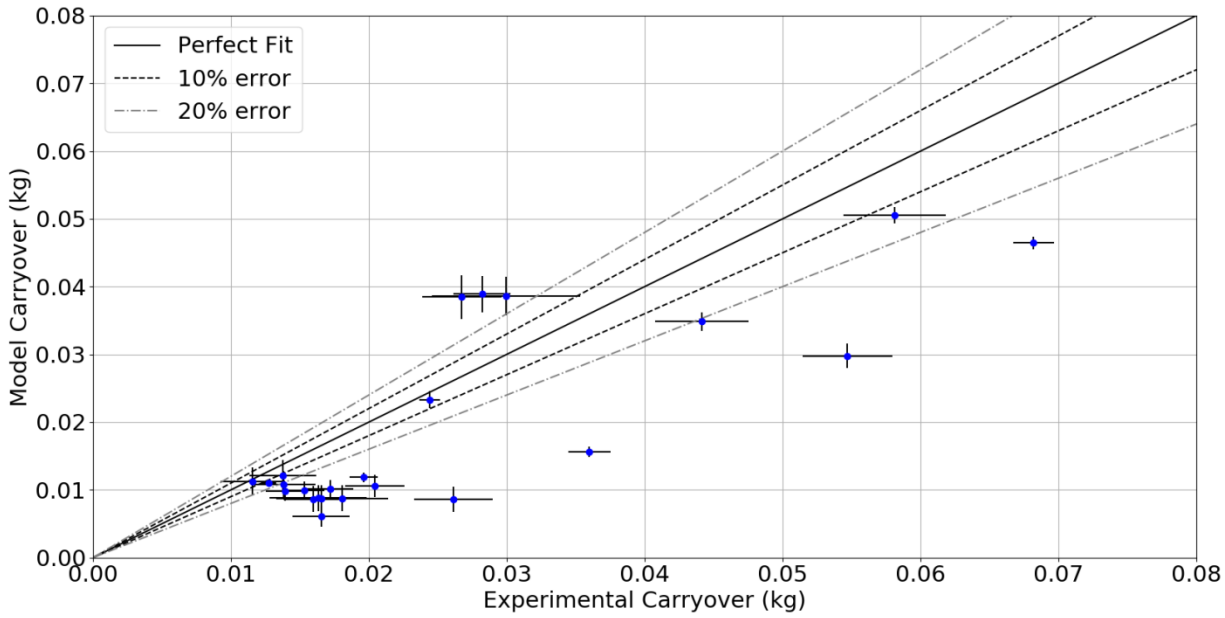

Figure 72 Model carryover vs experimental carryover for all test runs

The plot clearly shows that the model is not doing a good job at predicting carryover mass. One of the problems is the difference between the actual temperature profile and the model temperature profile illustrated in Figure 70. Unfortunately, the effectiveness-NTU-C_m model cannot predict the temperature profile in the bed, so a correction is needed to make the model match the experimental results. Analysis of experimental data showed that there was no simple correlation between the shape of the temperature profile and the operating conditions of the regenerator, so the temperature profile used in the model is assumed to be linear. The temperature profiles for the HtCB and CtHB each only have one free temperature, since the inlet temperature for both are set by the cycle operating conditions. Thus, the cold exit temperature of the HtCB will be increased (lowering the amount of minimum mass in the bed), while the hot exit temperature of the CtHB will be decreased (increasing the amount of maximum mass in the bed) the temperature they are corrected will be the same for both the HtCB and CtHB and will be called dT. EES was used to calculate what dT was needed to get the same amount of carryover as

the experimental data [17]. A corrected temperature profile for the example shown in Figure 70 is shown in Figure 73.

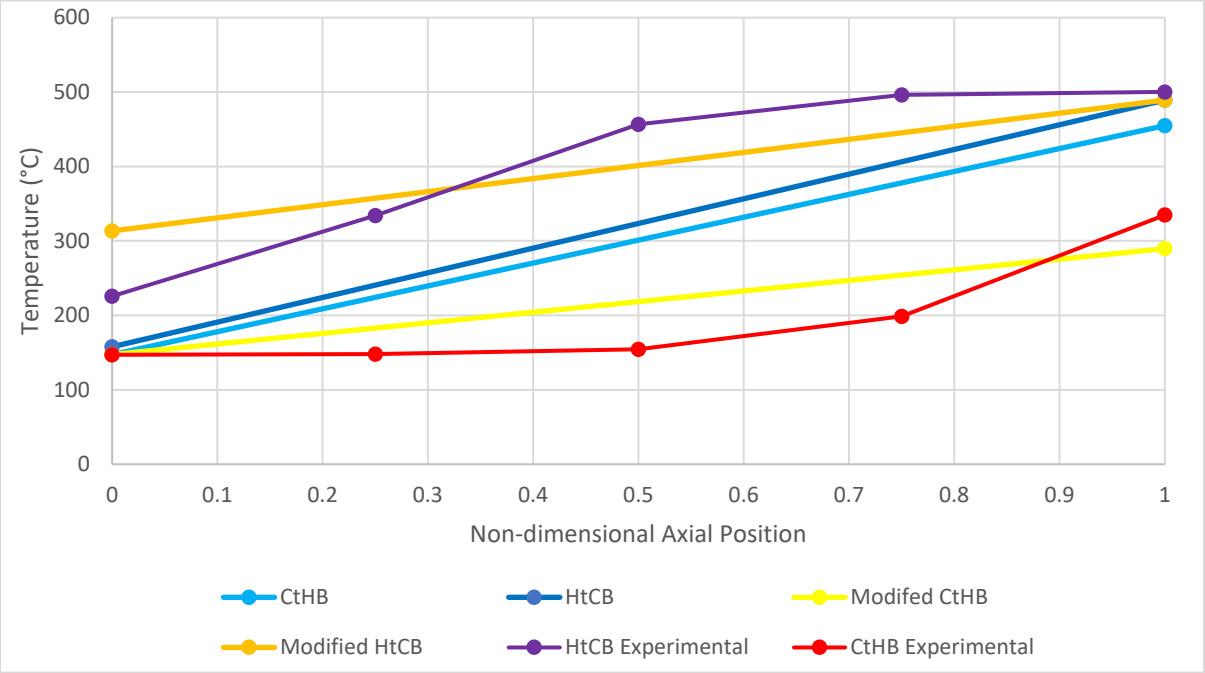

Figure 73 Temperature profile of example run showing temperature profiles at minimum and maximum mass in regenerator as well as corrected temperature profiles

Correcting the temperature profiles make them fit much closer to the experimental temperature profiles. Knowing what the dT needs to be is important, but more importantly an equation is needed for dT, so it can be added to the model. The linear regression tool in EES was used to correlate dT to the inlet temperatures, inlet pressures, and matrix capacity ratio (C_m) [17]. The results are shown in Figure 74.

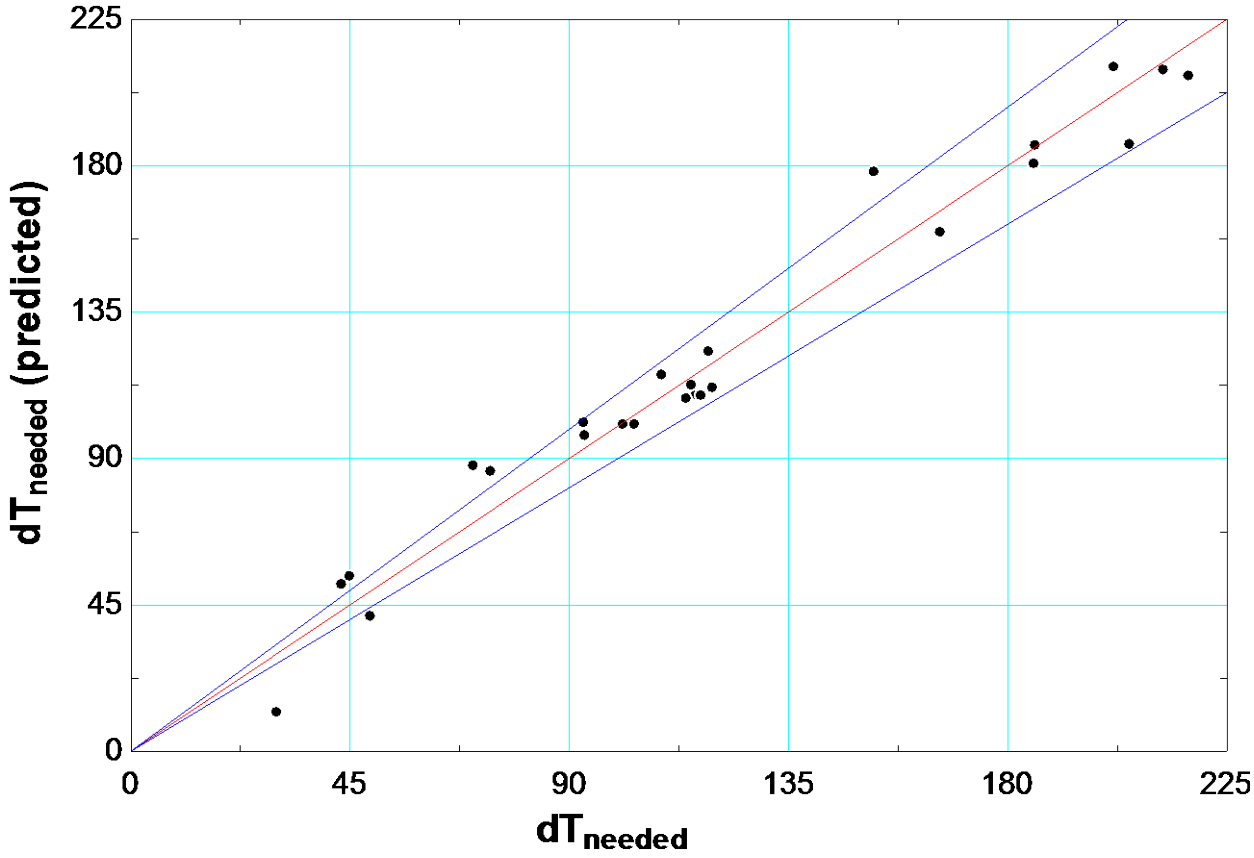

Figure 74 Differential temperature needed to correct carryover

The x axis shows what dT is needed to perfectly match the carryover in the model to the experimental data. The y axis shows what dT the linear regression will return using the inlet parameters (temperature, pressure, and matrix capacity ratio) for each run. Again, lines of 10% error are added. Most of the points are within 10% of the correct value. Using this correction method, the modeled carryover can be recalculated as shown in Figure 75.

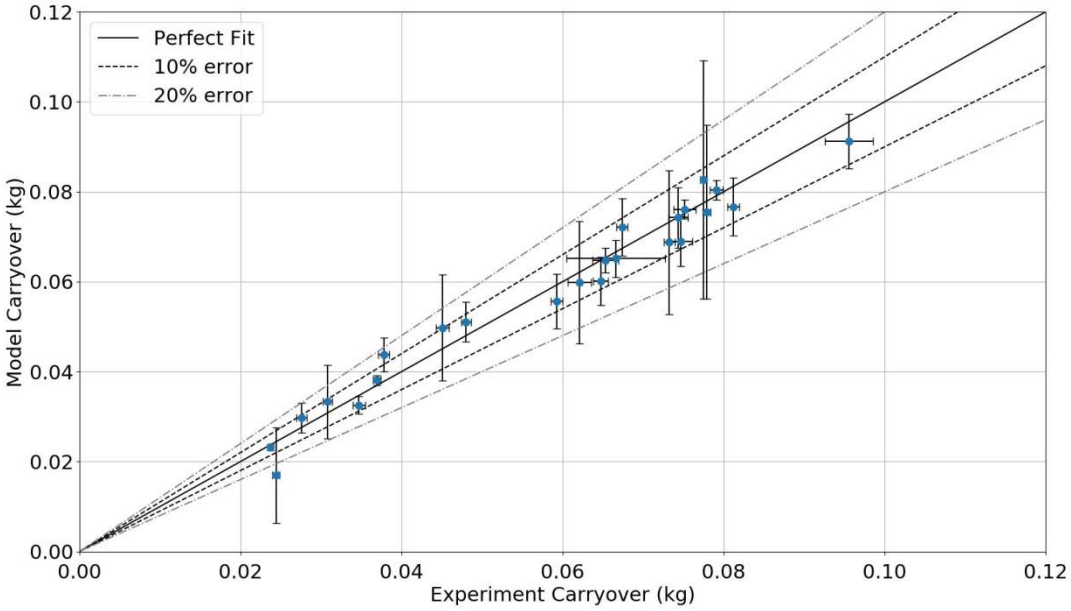

Figure 75 Experimental vs model carryover results with corrected temperature profiles

After correcting the temperatures, the model and experiments match very well, with most points within 10% error and almost all points being within 20% error. Some tests show very high uncertainty in the carryover since the correction factor dT is a function of inlet temperatures, pressures, and matrix capacity ratio. In particular, the cases that have the largest uncertainty also have the largest matrix capacity ratios (greater than 3). An economically designed regenerator will have a matrix capacity ratio of approximately 1.7, so the uncertainty is still reasonable for an optimally designed regenerator. The corrected model shows an average agreement of 8.6% for all the data points collected which is considered to be a good agreement.

Conclusions

This thesis was meant to determine the applicability of using switched bed regenerators for supercritical CO_2 Brayton cycles. A simple analytical regenerator model was created and integrated with a cycle model. An analysis comparing recuperators and regenerators showed that a modest (6.2%) reduction in LCoE could be achieved by switching to regenerators. Greater cost savings are possible

depending on the desired design of the regenerator. The regenerator model was verified using experimental testing, which is the first time regenerators have been tested in sCO_2 conditions. In particular the periodic nature and large pressure differential between hot and cold streams makes this research unique. The model matched the experimental results well for effectiveness. The pressure drop model did not match as well because of issues with measuring very large pressure drops. An increase of 20% was added to pressure drop to ensure a conservative model. Carryover is harder to model because of the non-linear temperature profiles in the bed and the fact that the model inherently cannot determine the temperature profile in the bed. Instead a correction factor was created that can correct the model to accurately predict the carryover. The carryover correction is used in all the model calculations and even with it included a cost savings can be realized. Additionally, the design of the regenerator calls for an insulated regenerator to keep the pressure vessel wall isolated from the hot fluid inside. A 10kW regenerator was created with an insulated wall that performed well in testing, keeping the shell below the allowable temperature. A crack in the insulated regenerator liner provided insight into the failure mechanisms of the insulated regenerator which was used to improve the insulated regenerator design. Overall the regenerator concept seems shows promise for use in the sCO_2 Brayton cycle.

Future Work

There are several things that can be done to continue work on this project. One idea is to use a binary packing of spheres to create a more densely packed bed. A first pass was taken at modifying the model to use a binary packing. Past experiments have shown that a 20% void fraction requires the larger spheres to be seven times larger than the small spheres. Under these conditions the best packing occurs when 70% of the spheres are the larger size [94]. The surface area of the binary mixture was calculated based on the number of each size spheres in the bed. An equivalent sphere size was found by calculating

the sphere size that would give the same specific surface area for a single sphere packing. It was assumed that a binary packed bed and a uniformly packed bed with the same specific surface area would have approximately the same heat transfer coefficients and pressure drops. The equivalent sphere size was set to 3mm, which means that the large sphere size is 4.3mm and the small sphere diameter is 0.6mm. The surface area, heat transfer coefficient, and size of the bed was determined based on the specified effectiveness, the ratio between large spheres and small spheres, and packing fraction. Figure 76 shows LCoE and thermal efficiency as a function of void fraction for a constant equivalent sphere size.

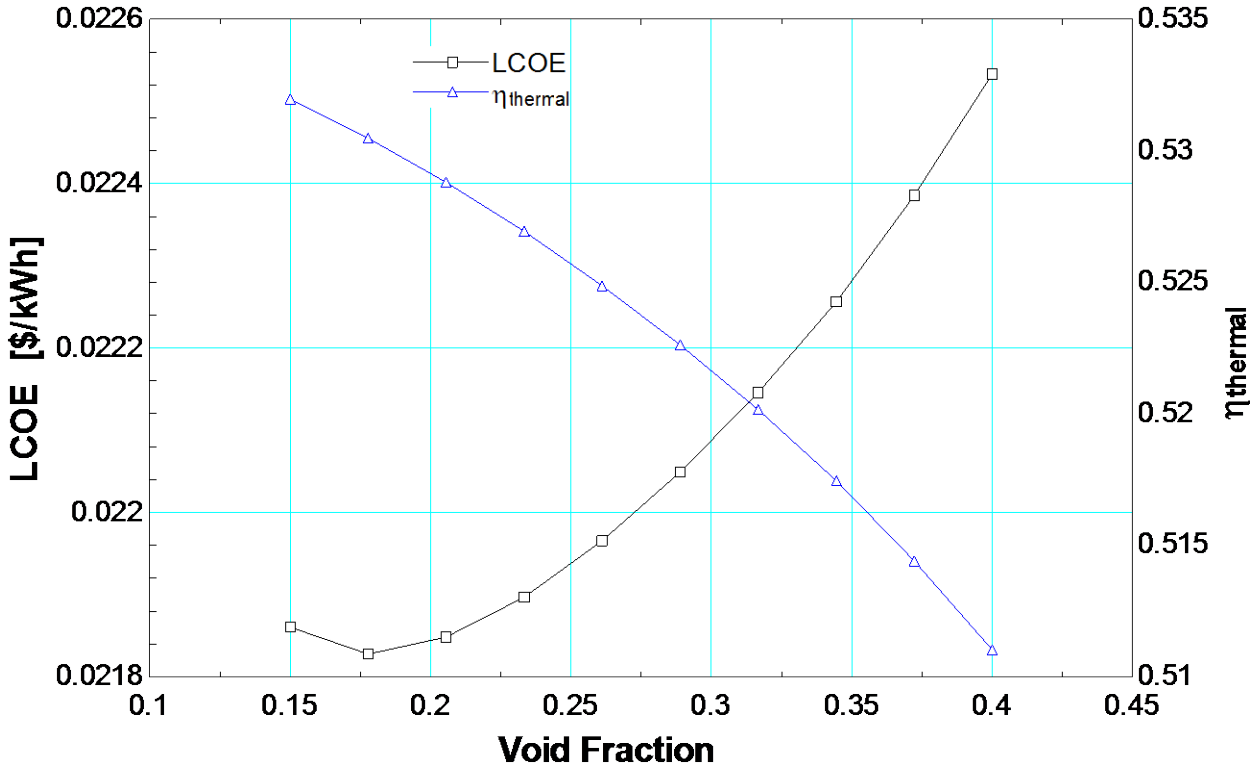

Figure 76 LCoE and Thermal Efficiency as a function of void fraction in the packed bed

A randomly packed bed with single sphere size will have a void fraction of about 0.37 where as an ideally packed bed with single sphere size can have a void fraction of 0.26. Using a binary packing of spheres, the void fraction can be further reduced to approximately 0.2 [94]. As the packing fraction gets lower

the aspect ratio of the bed must be reduced to maintain the same pressure drop. The smaller aspect ratio results in a more expensive pressure vessel because the walls must be thicker. However, the efficiency gain from the decreased carryover outweighs the additional cost of the pressure vessel, and the result is a decrease in LCoE. Only at void fractions of less than 0.2 does LCoE start increasing, which cannot be reached easily with binary packing. One caveat to this is the pressure drop and heat transfer correlation used for the packed bed. The correlation assumes a uniform sphere size so for the binary mixture of spheres it is not valid. A different heat transfer and pressure drop correlation is needed for the binary mixture which could change the results of the optimization. If possible, the regenerator should be constructed with a void fraction of 0.2 corresponding to the binary packed spheres. Due to the uncertainty in heat transfer coefficients and pressure drop correlations the randomly packed bed of spheres will be used because it gives acceptable performance and can be used to easily verify the model. Future work could be focused on developing heat transfer and pressure drop correlations for a binary mixture of spheres which could be used to increase the performance of the regenerators.

The decoupled thermal and pressure boundary is another advantage regenerators have over recuperators. It allows for a significantly higher turbine inlet temperature which greatly increases thermal efficiency as seen in Figure 31. For a normal RCBC operating with recuperators the temperature at the inlet to the high temperature recuperator is shown in Figure 77.

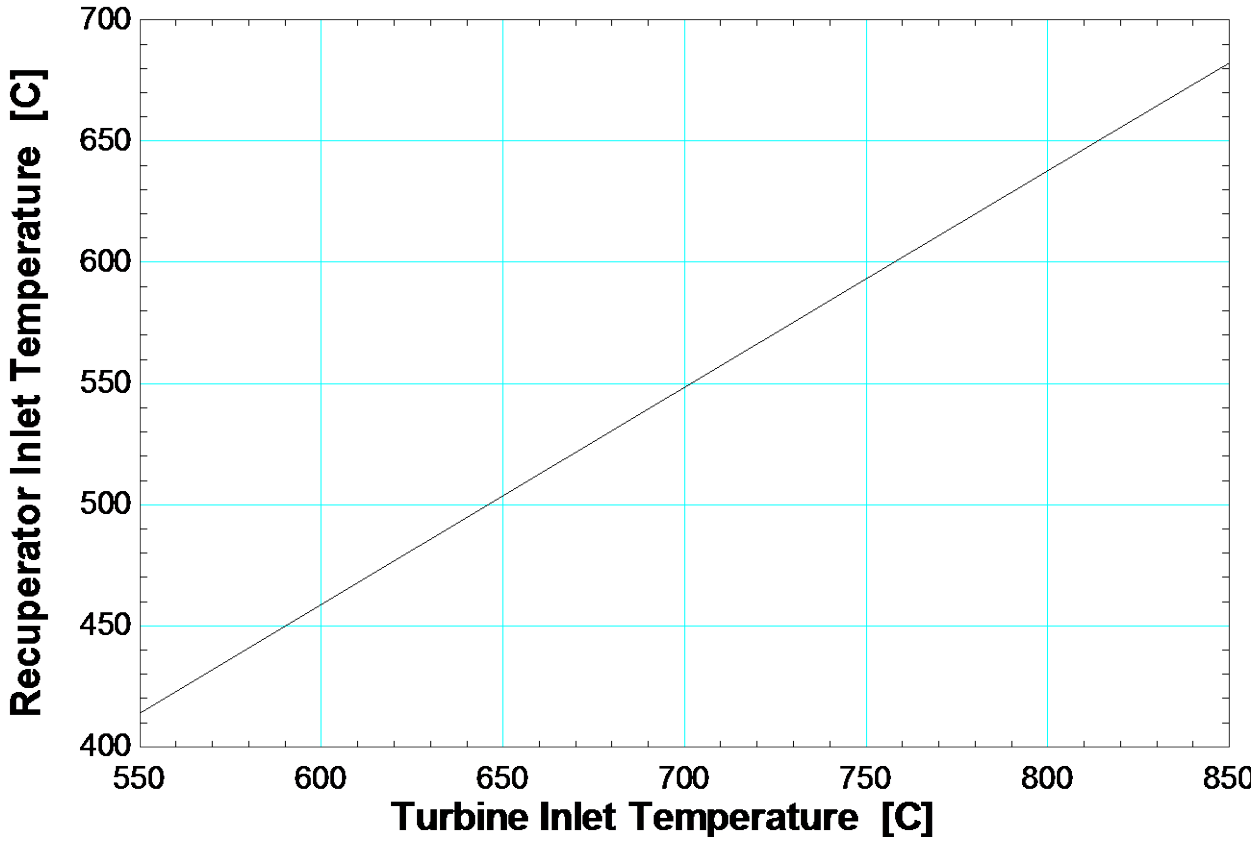

Figure 77 Recuperator Inlet Temperature vs TIT for recuperator cycle operating with 94% effective recuperators

Figure 15 shows that 316, the usual choice for PCHEs, has less than half of the allowable stress at 648°C compared to 538°C and continues to lose strength at higher temperatures. Even at a 720°C TIT the recuperator inlet temperature is above 538°C which means that any further temperature increases will likely result in a nickel alloy being used. To save on the cost of the nickel PCHE, the high temperature recuperator would be split into two parts, a lower temperature section made of 316 and a high temperature section made of a nickel alloy. Nickel alloys are 4-7 times more expensive than 316, which means that even though the nickel PCHE has a much lower conductance it can be very expensive [103]. Replacing the expensive nickel alloy PCHE with a regenerator could be highly cost effective. A rather interesting optimization must also occur. For a high temperature recuperator system the nickel recuperator should be designed as small as possible, meaning it has very high inlet temperatures. A

regenerator needs to have valves operating on the low temperature side, so having the inlet temperatures too hot could lead to very expensive valves being needed. It may be more cost effective to design the regenerator to be larger, so it can operate with a lower inlet temperature to allow for cheaper valves to be used. This optimization would be a good area for future work as it maximizes the benefits of the regenerator (low cost at high temperature operation) while minimizing the negatives (carryover).

The cost comparison between regenerator and recuperators for this thesis is rather simple because of undefined goals for the cycle. Depending on the heat source and desired operating conditions, the optimal cycle configuration, cost, and efficiency can change greatly. It could be possible that regenerators are not always the best option, or that a low temperature recuperator should be coupled with a high temperature regenerator. Modeling several different plant configurations could give a better insight into the best uses for regenerators.

This analysis has shown that valve costs are much greater than the costs for the actual regenerator bed. So, any opportunity to reduce the costs of the valves makes the regenerators even more attractive. One option to reducing valve cost is to use a one way valve on the high temperature side of the regenerator. Then all the control of the flow can be done using the valves on the low temperature side, while significant cost savings can be achieved in the high temperature valves. Experiments are needed to see if one way valves can withstand the number of cycles required of a regenerator system. Additionally, pressure drop will need to be explored to ensure the system is not over encumbered with losses which would reduce thermal efficiency.

Costing for this project was done based on a 10MW plant which is small relative to most power plants which are usually 100MW or greater. Some work was done looking at the feasibility of scaling up the regenerator for a 100MW plant. Initial results showed keeping the four bed configuration was the

most cost effective, however more work is needed. One issue is the maximum valve size (24”) which can result in significant pressure drop at some conditions. Dividing the regenerator system into smaller beds increases the number of valves while also making the valve size smaller. An optimization can be done that looks at the results of splitting the beds into more units as well as allowing for different pressure drops in the bed.

Funding

This material is based upon work supported by the U.S. Department of Energy under Award Number DE-EE0007120.

References

[1] Klein SA, Nellis G. Thermodynamics. New York: Cambridge UP; 2012.

[2] Cheang VT, Hedderwick R a., McGregor C. Benchmarking Supercritical Carbon Dioxide Cycles Against Steam Rankine Cycles for Concentrated Solar Power. Sol Energy 2015;113:199–211. doi:10.1016/j.solener.2014.12.016.

[3] EIA. Updated Capital Cost Estimates for Utility Scale Electricity Generating Plants. 2013.

[4] Haynes International. HAYNES ® 282 ® alloy. n.d.

[5] Weitzel PS. Steam Generator for Advanced Ultra-Supercritical Power Plants 700 to 760C. Proc ASME 2011 Power Conf 2011:1–11. doi:10.1115/POWER2011-55039.

[6] El-Wakil MM. Powerplant Technology. 1st ed. New York: McGraw-Hill; 2013.

[7] Feher EG. The Supercritical Thermodynamic Power Cycle. Energy Convers 1968;8:85–90.

[8] Angelino G. Carbon Dioxide Condensation Cycles For Power Production. Gas Turbine Conf 1968.

[9] Driscoll MJ. Supercritical CO 2 Plant Cost Assessment. Cambridge: 2004.

[10] Engineers AS of M. Section VIII Rules for Construction of Pressure Vessels. In: American Society of Mechanical Engineers B and PVC, editor. ASME Boil. Press. Vessel Code, New York: 2007.

[11] Kiran E, Debenedetti PG, Peters CJ. Supercritical Fluids—Fundamentals and Applications. vol. 336. 2000.

[12] Carlson M. Measurement and Analysis of the Thermal and Hydraulic Performance of Several Printed Circuit Heat Exchanger Channel Geometries. University of Wisconsin - Madison, 2012.

[13] Dostal V. A Supercritical Carbon Dioxide Cycle for Next Generation Nuclear Reactors. Massachusetts Institute of Technology, 2004.

[14] Neises T, Turchi C. A Comparison of Supercritical Carbon Dioxide Power Cycle Configurations With an Emphasis on CSP Applications. Energy Procedia 2014;49:1187–96. doi:10.1016/j.egypro.2014.03.128.

[15] Hoffmann JR, Feher EG. 150 kwe Supercritical Closed Cycle System. J Eng Power 1971;1:70–80.

[16] Fleming D, Conboy T, Rochau G, Holschuh T, Fuller R. Scaling Considerations for a Multi-Megawatt Class Supercritical CO2 Brayton Cycle and Path Forward for Commercialization 2015:1–8.

[17] F-Chart. EES Engineering Equation Solver 2015.

[18] Angelino G. REAL GAS EFFECTS IN CARBON DIOXIDE. Internaitional Gas Turbine Conf. Prod. Show, Cleveland: 1969, p. 1–12.

[19] Gokhstein DP, Verkhivker GP. Future Design of Thermal Power Stations Operating on Carbon Dioxide. Therm Eng 1971:2.

[20] Ho CK, Carlson M, Garg P, Kumar P. Cost and Performance Tradeoffs of Alternative Solar-Driven S-CO2 Brayton Cycle Configurations. Proc. ASME 2015 Power Energy Convers. Conf., 2015, p. 1–10.

[21] Besarati SM, Goswami DY. Analysis of Advanced Supercritical Carbon Dioxide Power Cycles With a Bottoming Cycle for Concentrating Solar Power Applications 2016;136:1–7. doi:10.1115/1.4025700.

[22] Allam RJ, Palmer MR, Brown GW, Fetvedt J, Nomoto H, Itoh M, et al. High efficiency and low cost of electricity generation from fossil fuels while eliminating atmospheric emissions , including carbon dioxide. Energy Procedia 2013;37:1135–49. doi:10.1016/j.egypro.2013.05.211.

[23] Ho CK, Iverson BD. Review of high-temperature central receiver designs for concentrating solar power 2013. doi:10.1016/j.rser.2013.08.099.

[24] Santini L, Accornero C, Cioncolini A. On the adoption of carbon dioxide thermodynamic cycles for nuclear power conversion: A case study applied to Mochovce 3 Nuclear Power Plant. Appl Energy 2016;181:446–63.

[25] Schroder AU. A Study of Power Cycles Using Supercritical Carbon Dioxide as the Working Fluid. University of Cincinnati, 2016.

[26] Dyreby JJ. Modeling the Supercritical Carbon Dioxide Brayton Cycle with Recompression. 2014.

[27] Musgrove GO, Pierres R Le, Nash J. Tutorial : Heat Exchangers for Supercritical CO2 Power Cycle Applications. 2014.

[28] Carlson M, Conboy T, Pasch J, Fleming D. SCALING CONSIDERATIONS FOR SCO2 CYCLE HEAT EXCHANGERS. Proc. ASME Turbo Expo, 2014, p. 1–5.

[29] Carlson MD, Kruizenga AK, Schalamsky C, Fleming DF. Sandia Progress on Advanced Heat Exchangers for SCO2 Brayton Cycles. 4th Int. Symp. - Supercrit. CO2 Power Cycles, 2014, p. 1–10.

[30] Held T. Performance & Cost Targets for sCO2 Heat Exchangers. NETL-EPRI Work. Heat Exch. Supercrit. CO2 Power Cycles, 2015.

[31] Le Pierres R, Southall D, Osborne S. Impact of Mechanical Design Issues on Printed Circuit Heat Exchangers. Proc. sCO2 Power Cycle Symp. 2011, Boulder: 2011.

[32] Mezzo Technologies. Shell and Tube Industrial n.d. https://mezzotech.com/performance-applications/shell-and-tube-industrial/.

[33] Lewinsohn C, Ceramatec JF. Ceramic , Microchannel Heat Exchangers for Supercritical Carbon Dioxide Power Cycles Introduction & Overview. 5th Int. Symp. - Supercrit. CO2 Power Cycles, 2016.

[34] Lipke DW, Zhang Y, Liu Y, Church BC, Sandhage KH. Near net-shape/net-dimension ZrC/W-based composites with complex geometries via rapid prototyping and Displacive Compensation of Porosity. J Eur Ceram Soc 2010;30:2265–77. doi:10.1016/J.JEURCERAMSOC.2010.01.011.

[35] Jarrahbashi D, Kang T, Pidaparti SR, Ranjan D. Computational Analysis of Ceramic Heat Exchangers for Supercritical CO2 Brayton Cycle in CSP Applications at High-Temperatures. 6th Int. Supercrit. CO2 Power Cycles Symp., Pittsburgh, PA: 2018.

[36] Kruizenga A, Anderson M, Fatima R, Corradini M, Towne A, Ranjan D. Heat Transfer of Supercritical Carbon Dioxide in Printed Circuit Heat Exchanger Geometries. J Therm Sci Eng Appl 2011;3:031002. doi:10.1115/1.4004252.

[37] Jentz IW. Modeling , Performance Testing , and ASME BPVC Certification of a s-CO 2 Marbond Channel Heat Exchanger. University of Wisconsin-Madison, 2016.

[38] Aakre SR, Jentz IW, Anderson MH. Nuclear Code Case Development of Printed-Circuit Heat Exchangers with Thermal and Mechanical Performance Testing. 6th Int. Supercrit. CO2 Power Cycles Symp., Pittsburgh, PA: 2018.

[39] Carlson MD, Bell C, Schalansky C, Fleming DF, Rochau G. The Selection, Evaluation and Rating of Compact Heat Exchangers (SEARCH) Software Suite - Code Capabilities and Experimental Comparison. 5th Int. Symp. - Supercrit. CO2 Power Cycles, San Antonio: 2016, p. 1–13.

[40] Nellis G, Klein SA. Heat Transfer. New York: Cambridge University Press; 2009.

[41] Wright S a, Radel RF, Vernon ME, Rochau GE, Pickard PS. Operation and Analysis of a Supercritical CO2 Brayton Cycle. 2010.

[42] Wright SA, Conboy TM, Rochau GE. Break-even Power Transients for two Simple Recuperated S-CO2 Brayton Cycle Test Configurations. 2011 SCO2 Power Cycle Symp., Boulder: 2011.

[43] Conboy T, Wright S, Pasch J, Fleming D, Rochau G, Fuller R. Performance Characteristics of an Operating Supercritical CO2 Brayton Cycle. J Eng Gas Turbines Power 2012;134:111703. doi:10.1115/1.4007199.

[44] Nikitin K, Kato Y, Ngo L. Printed circuit heat exchanger thermal – hydraulic performance in supercritical CO 2 experimental loop. Int J Refrig 2006;29:807–14. doi:10.1016/j.ijrefrig.2005.11.005.

[45] Ngo TL, Kato Y, Nikitin K, Ishizuka T. Heat transfer and pressure drop correlations of microchannel heat exchangers with S-shaped and zigzag fins for carbon dioxide cycles. Exp Therm Fluid Sci 2007;32:560–70. doi:10.1016/j.expthermflusci.2007.06.006.

[46] Tsuzuki N, Utamura M, Ngo TL. Nusselt number correlations for a microchannel heat exchanger hot water supplier with S-shaped fins. Appl Therm Eng 2009;29:3299–308. doi:10.1016/j.applthermaleng.2009.05.004.

[47] Xu X, Ma T, Li L, Zeng M, Chen Y, Huang Y, et al. Optimization of fin arrangement and channel configuration in an airfoil fin PCHE for supercritical CO2 cycle. Appl Therm Eng 2014;70:867–75. doi:10.1016/j.applthermaleng.2014.05.040.

[48] Hyun S, Cheon H, Beom G. Assessment of straight , zigzag , S-shape, and airfoil PCHEs for intermediate heat exchangers of HTGRs and SFRs. Nucl Eng Des 2014;270:334–43. doi:10.1016/j.nucengdes.2014.01.006.

[49] Eok D, Hwan M, Eun J, Kim SO. Numerical investigation on thermal – hydraulic performance of new printed circuit heat exchanger model &. Nucl Eng Des 2008;238:3269–76. doi:10.1016/j.nucengdes.2008.08.002.

[50] Kim IH, No HC, Lee JI, Jeon BG. Thermal hydraulic performance analysis of the printed circuit heat exchanger using a helium test facility and CFD simulations. Nucl Eng Des 2009;239:2399–408. doi:10.1016/j.nucengdes.2009.07.005.

[51] Kim IH, No HC. Thermal hydraulic performance analysis of a printed circuit heat exchanger using a helium e water test loop and numerical simulations. Appl Therm Eng 2011;31:4064–73.

doi:10.1016/j.applthermaleng.2011.08.012.

[52] Kim IH, No HC. Physical model development and optimal design of PCHE for intermediate heat exchangers in HTGRs. Nucl Eng Des 2012;243:243–50. doi:10.1016/j.nucengdes.2011.11.020.

[53] Kim IH, No HC. Thermal – hydraulic physical models for a Printed Circuit Heat Exchanger covering He , He – CO 2 mixture , and water fluids using experimental data and CFD. Exp Therm Fluid Sci 2013;48:213–21.

[54] Kim J, Kim SJ, Kim E, Kim H, Cha JE, Kim SO. Progress in the performance verification of PCHE type Na-CO2 heat exchanger. Trans. Korean Nucl. Soc. Spring Meet., 2012.

[55] Barron R, Nellis G. Cryogenic Heat Transfer. 2nd ed. Taylor and Francis; 2016.

[56] Satoh T, Numazawa T. Cooling Performance of a Small GM Cryocooler with a New Ceramic Magnetic Regenerator Material. Cryocoolers 12, Boston, MA: Springer US; 2003, p. 397–402. doi:10.1007/0-306-47919-2_52.

[57] Nam K, Jeong S. Measurement of Cryogenic Regenerator Characteristics Under Oscillating Flow and Pulsating Pressure. Cryogenics (Guildf) 2003;43:575–81. doi:10.1016/S0011-2275(03)00166-8.

[58] Nagao M, Inaguchi T, Yoshimura H, Yamada T, Iwamoto M. Helium Liquefaction by a Gifford-Mcmahon Cycle Cryocooler 1990:1251–60. doi:10.1007/978-1-4613-0639-9_149.

[59] Matsumoto K, Hasimoto T. Thermodynamic Analysis of Magnetically Active Regenerator From 30 To 70 K With a Brayton-Like Cycle. Cryogenics (Guildf) 1990;30:840–5.

[60] Nam K, Jeong S. Experimental study on the regenerator under actual operating conditions. Microcryocoolers AIP Conf Proc 2002;977. doi:10.1063/1.1472119.

[61] Helvensteijn BPM, Kashani A, Spivak AL, Roach PR, Lee JM, Kittel P. Pressure Drop over Regenerators in Oscillating Flow. Adv. Cryog. Eng., Boston, MA: Springer US; 1998, p. 1619–26. doi:10.1007/978-1-4757-9047-4_203.

[62] Schaefer BR, Bellis L, Ellis MJ, Conrad TJ. Advanced Regenerator Testing in the Raytheon Dual-Use Cryocooler Advanced Regenerator Testing in the Raytheon Dual-Use Cryocooler 2014;5701:4860751–175. doi:10.1063/1.3422351.

[63] Knowles TR. Composite Matrix Regenerator for Stifling Engines. 1997.

[64] Berggren R, Moynihan T. Free-piston Stirling engine experimental program: Part 1. Baseline test summary. Argonne, IL: 1983.

[65] Kwankaomeng S, Silpsakoolsook B, Savangvong P. Investigation on Stability and Performance of a Free-Piston Stirling Engine. Energy Procedia 2014;52:598–609.

[66] Alhusseny A, Turan A, Nasser A. Computational Simulation of the Heat and Fluid Flow through a Rotary Thermal Regenerator Based on a Porous Media Approach. 2015.

[67] Sayama J, Morishita T. Development of a Regenerator for an Automotive Gas Turbine Engine. J Eng Gas Turbines Power 1993;115:424–31. doi:10.1115/1.2906726.

[68] Helms HE. Ceramic Applications in Turbine Engines. Ceram. High-Performance Appl. III, Boston, MA: Springer US; 1983, p. 151–72. doi:10.1007/978-1-4684-3965-6_8.

[69] Korakianitis T, Beier KJ. Investigation of the Part-Load Performance of Two 1.12 MW Regenerative Marine Gas Turbines. J Eng Gas Turbines Power 1994;116:418. doi:10.1115/1.2906837.

[70] McDonald CF. The Role of the Recuperator in High Performance Gas Turbine Applications. Vol. 1A Gen., ASME; 1978, p. V01AT01A046. doi:10.1115/78-GT-46.

[71] Daschner R, Binder S, Mocker M. Pebble Bed Regenerator and Storage System for High Temperature Use. Appl Energy 2013;109:394–401. doi:10.1016/J.APENERGY.2012.10.062.

[72] Gil A, Medrano M, Martorell I, Lá Zaro A, Dolado P, Zalba BN, et al. State of the Art on High Temperature Thermal Energy Storage for Power Generation. Part 1—Concepts, Materials and Modellization n.d. doi:10.1016/j.rser.2009.07.035.

[73] Medrano M, Gil A, Martorell I, Potau X, Cabeza LF. State of the Art on High-Temperature Thermal Energy Storage for Power Generation. Part 2—Case Studies n.d. doi:10.1016/j.rser.2009.07.036.

[74] Reznicek E, Braun R. Simulation of sCO2 Recompression Brayton Cycles with Regenerators. 6th Int. Supercrit. CO2 Power Cycles Symp., Pittsburgh, PA: 2018.

[75] Kays WM, London AL. Compact Heat Exchangers. 3rd ed. New York: McGraw Hill; 1984.

[76] Kaviany M. Principles of Heat Transfer in Porous Media. 2nd ed. New York: Springer-Verlag New York Inc; 1995.

[77] Fahien RW, Schriver CB. Paper presented and Denver meeting of AIChE. In: Fahien RW, editor. Fundam. Transfport Phenom., New York: McGraw Hill; 1983.

[78] Sadeghbeigi R. Fluid Catalytic Cracking Handbook. 3rd ed. New York: Butterworth-Heinemann; 2012.

[79] Halvorsen. Pressure Vessel Shell Fabrication and Tank Shell Manufacturing n.d. http://www.halvorsenusa.com/steel-alloy-plate-fabrication/pressure-vessel-shell-fabrication-and-tank-shell-manufacturing/.

[80] Carter B. Personal Correspondence 2016.

[81] Beer FP, Johnston ERJ, DeWolf JT, Mazurek DF. Mechanics of Materials. 6th ed. New York: McGraw Hill; 2012.

[82] ANSYS Academic Research, Release 16.1 n.d.

[83] Aspen Aerogels INC. Pyrogel XTE. Northborough, MA: 2018.

[84] Zircar Ceramics INC. Alumina Castable Type ZIRALCAST-95. Florida, NY: 2016.

[85] Harbison-Walker Refractories Company. Harbison-Walker Handbook of Refractory Practice. Moon Township, PA: 2005.

[86] Refractories West I. EXPRESS 27 55# Bag High Strength Conventional Castable 2015. http://refwest.com/Express27in55lbbag.aspx (accessed April 4, 2018).

[87] Martinez-Santos J. Analysis and performance of refractory insulation for regenerative heat exchangers on s-CO2 Brayton cycles. University of Wisconsin-Madison, 2017.

[88] Carlson MD, Middleton BM, Ho CK. Techno-Economic Comparison of Solar-Driven SCO2 Brayton Cycles Using Component Cost Models Baselined With Vendor Data and Estimates. Proc. ASME 2017 11th Int. Conf. Energy Sustain., Charlotte: 2017.

[89] Numerics N. Fluid Property Interpolation Tables (FIT) 2017.

[90] Weiland N, Thimsen D. A Practical Look at Assumptions and Constraints for Steady State Modeling of sCO 2 Brayton Power Cycles. 5th Int. sCO2 Symp., 2016, p. 1–14.

[91] Boothroyd Dewhurst Inc. DFMA 2016.

[92] Baior G. Personal Correspondance 2018.

[93] U.S. Department of Energy. SunShot Vision Study. 2010.

[94] Mcgeary RK. Mechanical Packing of Sphereical Particles. vol. 58. Apollo: 1955.

[95] Blackman M. The theory of the specific heat of solids. Reports Prog Phys 1941;8:11–30. doi:10.1088/0034-4885/8/1/303.

[96] Hutchinson JW. ISA Handbook of Control Valves. 2nd ed. Pittsburgh, PA: 1976.

[97] Swagelok. Tubing Data. 2017.

[98] High Pressure Equipment Compant. High Pressure Equipment Full Line Catalog 2016. https://www.highpressure.com/pdfs/FullLineCatalog1214.pdf.

[99] Rapp LM. Experimental Testing of sCO2 Switched Bed Regenerators for Power Applications by. 2017.

[100] Erdim E, Akgiray O, Demir I. A Revisit of Pressure Drop-Flow Rate Correlations for Packed Beds of Spheres. Power Technol 2015;283:488–504.

[101] Hicks RE. Pressure Drop in Packed Beds of Spheres. Ind Eng Chem Fundam 1970;9:500–2. doi:10.1021/i160035a032.

[102] Gnielinski V. G9 Fluid-Particle Heat Transfer in Flow Through Packed Beds of Solids. VDI Heat Atlas, Berlin, Heidelberg: Springer Berlin Heidelberg; 2010, p. 743–4. doi:10.1007/978-3-540-77877-6_42.

[103] Kalra AK. Piping materials for supercritical carbon dioxide Brayton cycle. University of Wisconsin-Madison, 2015.